POLITECNICO DI MILANO
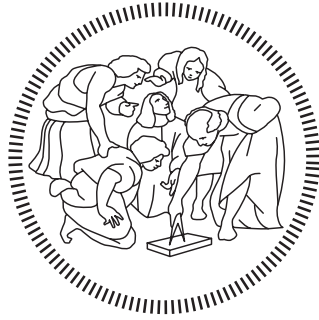
Facoltà di Ingegneria Industriale

Corso di Laurea Magistrale in Ingegneria Aeronautica

Generalized Kolmogorov Equation for Wall-Bounded Flows with Turbulent Drag Reduction

Relatore: Prof. Maurizio QUADRIO
Co-Relatore: Dr.Ing. Davide GATTI

Tesi di Laurea di
Alberto REMIGI
Matr. 836666

Anno Accademico 2015 - 2016

Ai miei genitori

Contents

Abstract

The present work studies how the energetic properties of turbulent flows confined between two plane parallel walls are modified by turbulent skin-friction drag reduction strategies.

A new Direct Numerical Simulation (DNS) database of turbulent channels at low Reynolds numbers - canonical or modified by skin-friction drag reduction strategies - is produced and provides high-fidelity turbulent flow data for the present analysis. The peculiar feature of this new set of DNS simulations is the strategy adopted to drive the flow throughout the channel via the Constant Power Input (CPI) approach, according to which the power provided to the flow via pumping is kept constant. CPI is the enabling strategy, which allows the direct comparison of energy transfer rates among canonical and drag-reduced channels.

The single-point Turbulent Kinetic Energy (TKE) and Mean Kinetic Energy (MKE) budget equations are analysed in order to achieve a detailed description of the control-induced modifications on energy transfer rates. The integral TKE and MKE budget equations, represented compactly in terms of a energy box, are analysed in the search for general trends, i.e. common to different control strategies, regarding the effects of drag reduction upon the way in which turbulent flow transforms and dissipates the power which is provided to it. The more the control strategy is effective (i.e the more it increases the flow rate) the more the peak of production of TKE is weakened. The energy box representation has shown that it is still hard to draw a conclusion about the dissipative behaviour of the control techniques.

The budget equation for the second-order structure function in turbulent channels, the so-called Generalized Kolmogorov Equation (GKE), is exploited in order to inspect the energy fluxes occurring simultaneously in the physical space and among different scales. The goal is to study whether and how turbulent drag-reduction strategies modify such fluxes, which represent statistical description of the energy cascade. A new tool that solves the GKE has been implemented and it turned out to be more than two order of magnitudes faster than the previous implementations. The analysis of the outcomes confirmed the TKE and MKE budgets' results and expanded them, proving differences in the energy paths' development between the canonical channel and the drag reduced channels.

Key words: Kolmogorov, drag reduction, energy paths, D.N.S., channel flow.

Sommario

Questo lavoro si propone di studiare come le proprietà energetiche di un flusso turbolento, confinato tra due pareti piane, siano modificate dalle tecniche di riduzione di resistenza.

È stato prodotto un nuovo database di simulazioni di canale piano ad un basso numero di Reynolds (il classico canale ed il canale con tecniche di drag reduction), tramite la tecnica di simulazione DNS. La particolarità di tale database sta nella strategia di simulazione adottata per muovere il flusso all'interno del canale. Tale approccio consiste nel mantenere la potenza utilizzata per il pompaggio costante ed è detto Costant Power Input (CPI). La tecnica CPI è lo strumento che permette un confronto corretto dal punto di vista energetico, tra il classico canale piano e il canale con l'impiego di tecniche di riduzione di resistenza.

Le equazioni di bilancio per l'energia cinetica del flusso turbolento (TKE) e l'energia cinetica del flusso medio (MKE) vengono analizzate per una descrizione dettagliata degli effetti del controllo sui trasferimenti di energia. Le equazioni integrali di bilancio per la TKE e la MKE, rappresentate in maniera compatta in termini di energy box, sono analizzate alla ricerca di un trend globale, ovvero comune a tutte le strategie di controllo. Tale analisi viene svolta in modo da capire gli effetti che le tecniche di riduzione di resistenza hanno sul modo in cui l'energia viene trasformata e dissipata all'interno del flusso turbolento. Più la tecnica di controllo è efficace (quindi la portata aumenta), maggiore è l'attenuazione del picco di produzione di energia cinetica turbolenta. I risultati derivanti dalla energy box dimostrano come sia ancora impossibile arrivare ad una conclusione per quanto riguarda il comportamento della dissipazione impiegando una strategia di controllo.

L'equazione di bilancio per la funzione di struttura di secondo ordine, meglio nota come Generalized Kolmogorov Equation, viene utilizzata per studiare i flussi di energia che si sviluppano simultaneamente nello spazio fisico e nello spazio delle scale. L'obiettivo è capire come le tecniche di controllo modifichino tali flussi, che rappresentano una descrizione statistica del processo di cascata di energia. Un nuovo programma che risolve la GKE è stato implementato e, si è dimostrato essere più veloce di due ordini di grandezza rispetto alle precedenti implementazioni. I risultati hanno confermato quanto era già stato dedotto dalle equazioni di bilancio di TKE ed MKE. Inoltre l'analisi dei termini nello spazio delle scale ha evidenziato delle differenze nello sviluppo dei percorsi di energia tra il classico canale piano e il canale piano con tecniche di riduzione di resistenza.

Parole chiave: Kolmogorov, riduzione di resistenza, percorsi di energia, D.N.S., canale piano.

List of Figures

List of Tables

Chapter 1

Introduction

In this statement Kolmogorov addresses respectively to *Alexander Obukhov* and *Andrei Monin*, referring to their fundamental works in these fields, based on discoveries made by the *Russian school* of turbulence before second World War and proves how *Turbulent flows* can be found in different forms in everyday life. The blood flow in the human body, the flow around an airplane, the flow of oil through a pipe in the deep ocean are some examples of situations in which turbulent flows can be found. This recurrence explains the interest of physicists and engineers for this kind of problems.

Due to the complexity of this kind of flows, a common definition for turbulence has not been reached yet. A first phenomenological definition was given by Reynolds in 1883 [7], analysing properties of vortex at high Reynolds number. Nowadays the most popular definition is based on repeatability of statistical properties. According to Pope [3], turbulence research is focused on three main fields:

- Theoretical comprehension of properties and dynamics of turbulent flows, which allows further developments in turbulence modelling and prediction;

- Experimental campaigns, both numerical and practical, which allows the discovery of qualitative and quantitative data on several turbulent flows;

- Flow control techniques, which allows the achievement of particular engineering goals through the change of particular flow characteristics.

This work focuses on developing the second point, in order to better understand energy transfer processes inside a turbulent flow (first point) and how control techniques change them (third point). In order to have an exhaustive comprehension of the main subject of the work, namely the development of the Generalized Kolmogorov Equation analysis tool, the energetic analysis of the flow should be introduced.

1.1   Drag reduction techniques: how do they work?

Reducing skin friction drag can bring to big advantages from an economic point of view. Fuel consumption of airplanes and power required to pump oil through a pipe are only two examples of the many fields in which this can be a money saving strategy. Up to now several drag reduction techniques have been tested. They can be grouped into two categories:

- passive drag reduction techniques: they don't require energy consumption to act;

- active drag reduction techniques: they require energy consumption.

Active drag reduction techniques can be further divided into open loop strategies, whose control law is pre-determined and do not require any measurement within the flow, and closed loop strategies, which have a feedback implementation. Among the open loop techniques, the most notable are the ones that impose a wall velocity function modulated in time and space, changing the boundary conditions of the problem. A huge number of studies have been made, trying to change both the way in which the wave was modulated and the direction of forcing. A good review about this kind of techniques can be found in [8].
Closed loop techniques are still in development from the theoretical point of view. The technological limit impedes the application of such strategies. It is in fact still difficult to put sensors, necessary for the feedback, inside the flow, without modifying the flow itself. One example of such kind of techniques is the damping of the near-wall spanwise fluctuations, first studied by Satake and Kasagi in [9] and later improved by Fronhapfel et al. in [10]. This technique consists in measuring spanwise velocity field inside a layer with a certain wall-normal thickness and in implementing a force that opposes it. It is simple to understand how it could be difficult to measure the velocity field in each point of the forcing layer and to act instantaneously an opposite force in the same point of measurement.

1.2   Energetic point of view

As it is said by Marati et al. in [11], wall-bounded turbulent flows are characterized by phenomena that may be thought to be distinguished in two different classes:

- phenomena which occur in *scale space*;

- phenomena which occur in *physical space.*

Important examples of the former are the energetic interactions that could be seen considering the flow field subdivided into a hierarchy of *scales*. This approach was first used by Richardson, when he introduced the concept of the cascade of energy. Richardson tried to show how energy is transferred from big scales to the smaller ones. Later *A.N. Kolmogorov* recalled the concepts introduced

by *Richardson* and extended them proving that, for sufficiently high Reynolds numbers, each wall-bounded flow approaches a universal statistical state. This study was presented in a first work in 1941 [12] and in a second work with Obukhov in 1962 [13]. The theory pursued by Kolmogorov was verified in a large data campaign carried out by Saddoughi and Veeravalli in [14], where a fit between experimental data and $-5/3$ trend of energy spectra was found in the log-layer region of the boundary layer of a turbulent flow. Considering the space of scales alone, it is impossible to have a complete description of energy phenomena in wall-bounded flows. A dual explanation in physical space suggests subdividing the non homogeneous direction of wall-bounded flows into regions in which different terms characterizing the Turbulent Kinetic Energy balance (namely *viscous*, *inertial*, *production*) have a different relevance. The peak of the Turbulent Kinetic Energy production, that balances the dissipation rate, is located in the buffer layer ($5 \leq y^+ \leq 20$) and it is irradiated partly to the wall, through the viscous sub-layer, and partly towards the bulk of the flow, to sustain turbulent motions. A first analysis was made experimentally (e.g analysis of the viscous sub-layer made by Eckelmann in [15]) and only after the introduction of DNS tool with [16], a first complete numerical analysis was made possible (a first discussion on data produced by Kim et al. can be found in [17]).

1.3 Generalized Kolmogorov Equation (GKE)

The presented views of wall-bounded flows seem to be mutually exclusive. They can be put together through a budget equation for the second-order moment of the velocity increments between two locations, tool introduced by *A.N. Kolmogorov* in [12] and called *second order structure function*. This equation was obtained as an extension of Kolmogorov's 5/3 law by Hill in [18]. Later, Hill's derivation was restricted to channel flows in studies made by Marati et al. in [11] and the equation was called *Generalized Kolmogorov Equation* (GKE). Two different kind of energy fluxes can be found in this equation:

- Energy flux through physical space;

- Energy fluxes through scale space.

The GKE mixes two different points of view and shows interactions between scale space and physical space phenomena. The first in-depth analysis of the terms of this equation was made by Cimarelli et al. in [19] on a simple channel flow. Due to the computational cost, the results have been analysed ignoring separations in wall-normal direction. This analysis outlined important things such as the dimension of structures at a certain wall-normal distance and the presence of a reverse energy cascade. The analysis was further improved in [20], focusing on the wall-normal separations. As it is said in the article, they tried to underline that real turbulent flows have a rich physics, involving, beside energy transfer, anisotropic production and inhomogeneous spatial fluxes. Such processes are strongly scale and position dependent and lead to a geometrically complex redistribution of energy.

1.4 Aim of the work

One question which is still open is how drag reduction techniques reach their goal of reducing drag. Some improvements have been made to better understand this topic (see for example the streamwise travelling waves of spanwise wall velocity strategy [21] or damping of the near-wall spanwise velocity fluctuations strategy [10]). The main questions can be rewritten as it follows: how do drag reduction techniques change the energy transfer processes and interactions of a simple not controlled wall-bounded flow? Is there a typical trend from which it is possible to understand how future implementations of drag reduction techniques can modify some characteristics of the flow, such as dissipation rate or production of Turbulent Kinetic Energy? Can we postulate that a drag reduction technique is a dissipative strategy? In order to find an answer to these questions, Direct Numerical Simulations (DNS) of a channel flow with a constant rate of energy input (CPI) are performed. The created database contains simulations with both open loop and closed loop drag reduction strategies. The Turbulent Kinetic Energy and the Mean Kinetic Energy budget equations' results have been analysed in their differential and integral form in order to find a global trend for different contributions to the equations.

The main achievement of this work is the implementation of a tool for the computation of each term of the Generalized Kolmogorov Equation in the four dimensional combined scale-physical space. The memory saving implementation, the use of convolution's theorem and the extended use of the statistical symmetries allow computing terms in the full 4D space (in the implementation used in [19] and [20] was not possible) in a relatively short time. This tool, used on the database, allows performing hypothesis on the change of the energy transfer process and physical-scale space interactions.

1.5 Structure of the work

The present work is structured in the following way:

- **Chapter 1: INTRODUCTION**

- **Chapter 2: TURBULENCE AND ENERGETIC OVERVIEW**
  Brief introduction to the energetic analysis of a turbulent flow, explaining theoretically environment for mixing the two different points of view.

- **Chapter 3: DIRECT NUMERICAL SIMULATION OF TURBU-LENT CHANNELS**:
  Description of the set of the equations that govern the flow in a channel and of the drag reduction techniques chosen to build the database for the energetic analysis.

- **Chapter 4: GENERALIZED KOLMOGOROV EQUATION**
  Theoretical description of the Generalized Kolmogorov Equation underlining the similarities and differences between the TKE budget equation. An in-depth analysis of the concepts used to build the code to compute different terms of the GKE is introduced, as well as a comparison with the previous implementation with the aim of emphasizing the advantages of the tool.

- **Chapter 5: TKE AND MKE ANALYSIS**
  Results concerning the TKE and MKE budget equations analysis, focusing on the change caused in a simple channel flow by the introduction of the control . A study on the integral budget and on the trend of the dissipation terms is done.

- **Chapter 6: ENERGY PATHS IN A CHANNEL FLOW**
  Results concerning GKE analysis are presented, focusing on additional information introduced by extended scale space. A new analysis on the changes brought by the control will be held.

- **Chapter 7: CONCLUSIONS AND FUTURE DEVELOPMENTS**

- **APPENDIX A: EXPANSION OF THE TERMS**
  Complete expansions of each term of the GKE used inside the implementation of the code.

- **APPENDIX B: TKE AND MKE: RESIDUALS AND FURTHER RESULTS**
  Results and residuals of the TKE and MKE budget equations applied to the database and not showed in the main text.

- **APPENDIX C: GKE: RESIDUALS AND FURTHER RESULTS**
  Residuals of the Generalized Kolmogorov Equation for each case analysed. Further results are showed for the simulated cases.

Chapter 2

Turbulence and energetic overview

Turbulence is thought to be one of the hardest problems within classical physics. Although the set of equations that describes the turbulent regime for a flow is well-known (Navier-Stokes equations), even the greatest mathematicians never managed to find a final solution for the definition. There are two main characteristics of the turbulent problem:

- the non-linear nature of equations describing the flow field;

- fluctuating statistics into the turbulent regime.

Before focusing on the core of this work, it is important to have a deep knowledge of the subject. The aim of this chapter is to give a background on turbulence, introducing the main concepts, which are useful to understand this work.

2.1 Early years

The turbulent phenomena were first studied and "visualized" only in 1883, when Osborne Reynolds conducted his seminal experiment [7]. Through the outcomes of this experiment, Reynolds showed the evidence that for different values of flow velocities, pipe diameters and viscosities, the transition between two regimes of the flow (nowadays better known as laminar and turbulent) would occur at roughly the same values of the well-known non dimensional number:

$$Re = \frac{UL}{\nu} \tag{2.1}$$

where U and L are characteristic velocity-scale and length-scale of the flow, whereas ν is the kinematic viscosity of the fluid. Signs of transition between the two regimes were to be seen in the form of change of some characteristics of the flow, such as the presence of eddies with different typical dimensions. In the most recent years many attempts have been conducted to reproduce Reynolds' experiment without being successful in mimicking the same transition Reynolds number.

Reynolds had already observed that background disturbances would affect the results of the experiment and nowadays the world is certainly different from 1883.

Figure 2.1: Osborne Reynolds' experiment asset used to observe the transition of the flow from the laminar to the turbulent regime [1].

2.2 Energy cascade

After the first World War, when works were mainly focused on stability studies (*Orr-Sommerfeld* and *Rayleigh*) and boundary layer theory (*Prandtl*), a more in-depth study about fully developed turbulent regime was needed. The aim of this section is to show the main ideas on how *energy* was thought to be transferred inside a turbulent flow are given.

2.2.1 Richardson

Between 1903 and 1929 Richardson formulated revolutionary ideas in the field of turbulence. Among the main achievements that is worth highlighting, there is the concept of the *energy cascade* in a turbulent flow field, introduced in the book *Numerical Weather Prediction by Numerical Process*. First of all, Richardson gives a definition of the characteristic velocity $u(l)$ and of the characteristic time scale $t(l) = l/u(l)$ called *eddy turnover time*. In Richardson's papers there is not a direct definition for the word *eddy*. The most commonly accepted definition is: a region of turbulent motion of size l. It is possible to define two characteristic scales:

- l_0: the dimension of the largest eddies. It is comparable to the scale of the flow $\mathscr{L}$, defined as the scale for which at sufficiently high Reynolds number, viscosity effects can be neglected;

- η: dissipation scale, where dissipation rate of kinetic energy ϵ is defined as:

$$\epsilon = 2\nu S_{ij} S_{ij} \tag{2.2}$$

and S_{ij} is *rate of strain* tensor, defined as:

$$S_{ij} = \frac{1}{2} \left(\frac{\partial u_i}{\partial x_j} + \frac{\partial u_j}{\partial x_i} \right) \tag{2.3}$$

The concept of energy cascade explains how the energy is transferred from larger scales to smaller ones.
Larger eddies are unstable and break up, transferring energy to smaller scales at a rate that is:

$$\Pi \sim \frac{u(l)^2}{t(l)} \sim \frac{u(l)^3}{l} \tag{2.4}$$

The numerator is proportional to Turbulent Kinetic Energy of an eddy, denominator is the typical breakdown time of this eddy.
In the inertial range no production and no energy dissipation is supposed to take place. Because of that, the flux of energy must be equal to the energy dissipation ϵ:

$$\Pi \sim \frac{u(l)^3}{l} \sim \epsilon \tag{2.5}$$

From this equation, it can be seen that that the scale velocity can be expressed as:

$$u(l) \sim \epsilon^{1/3} l^{1/3} \tag{2.6}$$

and turnover time can be expressed as:

$$t(l) = \epsilon^{-1/3} l^{2/3} \tag{2.7}$$

In the lowest part of the inertial zone, viscosity becomes important. The time that viscous diffusion takes to kill perturbation, for structures of size l, can be written as:

$$t(l)_{\text{kill}} \sim \frac{l^2}{\nu} \tag{2.8}$$

Equating the turnover time and $t(l)_{\text{kill}}$, it is possible to obtain an estimation for the size of eddies in the viscous range:

$$\eta \sim \left(\frac{\nu^3}{\epsilon} \right)^{1/4} \tag{2.9}$$

This image is of unique importance, because it introduces different concepts that can be useful for more specific studies:

- the concept of eddies, further discussed in the following years and nowadays still in definition;

- the subdivision of scales in different ranges.
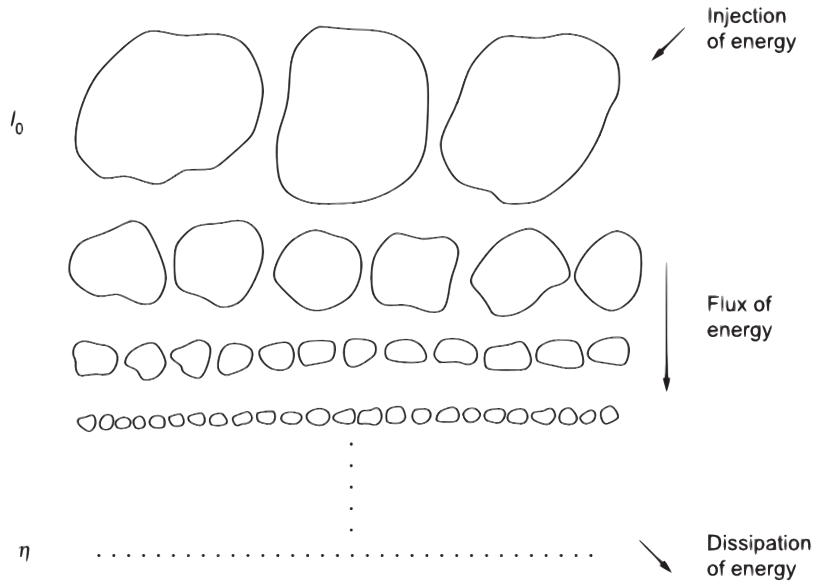
Figure 2.2: Richardson's cascade process [2].

2.2.2   Kolmogorov and K41

Richardson's cascade concept was the first attempt to find an answer to a closed theory for turbulence. The theory was further improved in 1941 by the mathematician Andrei Kolmogorov [12]. First of all, a strong hypothesis framework must be set up, namely the *Homogeneous Isotropic Turbulence* (HIT) hypothesis. From a statistical point of view the flow is:

- **homogeneous**: statistical properties of the flow are invariant under translations in space. The mechanism of turbulence production breaks statistical symmetries and the same can be said for the presence of a solid body. Root mean square of velocity on a body's boundary can't be the same of root mean square of velocity in body's wake, simply because fluctuations are cancelled out by the boundary conditions on the body's wall. Because of that the hypothesis is verified only at:

  - sufficiently high Reynolds number ($Re \gg 1$);
  - small scales ($l \ll l_0$), where l_0 is called *integral length scale* and is defined as:

$$l_0 = \int\limits_0^{+\infty} f(\boldsymbol{r},t)\mathrm{d}\boldsymbol{r} \qquad (2.10)$$

  where $f(r,t)$ is defined as a correlation in direction $\boldsymbol{r}$ of velocity component in the same direction;

  - away from the wall because of the strong mean shear generated by the presence of the wall.

- **locally isotropic** (definition took from [2]) : statistics are invariant under rotation of frame. At sufficiently high Reynolds numbers ($Re \gg 1$) and at small scales ($l \ll l_0$) directional informations are completely lost. This region is called *universal equilibrium region*.

Defining scales

Once the hypothesis are set up, it is important to understand the real dimension of the scale taken in exam. Recalling the concept of the energy cascade explained in section 2.2, the main processes are the energy transfer from bigger scales to smaller ones and dissipation. Two important quantities representing these processes are kinematic viscosity ν and dissipation rate of Turbulent Kinetic Energy (statistical equilibrium, as seen above with Richardson cascade, requires that the dissipation must be equal to rate of energy transfer) ϵ defined as in eq. (2.2).
Taken the scales in which the *universal equilibrium* hypothesis is defined ($l_{EI} \ll l_0$), it is possible to find, the typical length scale, velocity scale and time scale, called *Kolmogorov scales*, through dimensional analysis and considering the energy transfer and the dissipation, as:

$$\eta \equiv \left(\frac{\nu^3}{\epsilon}\right)^{\frac{1}{4}} \qquad\qquad u_\eta \equiv (\epsilon\nu)^{\frac{1}{4}} \qquad\qquad \tau_\eta \equiv \left(\frac{\nu}{\epsilon}\right)^{\frac{1}{2}} \qquad (2.11)$$

It is possible to see that the Reynolds number based on these scales is:

$$\frac{\eta u_\eta}{\nu} \sim 1 \qquad (2.12)$$

This means that Kolmogorov scales represent really small and dissipative scales. Furthermore, it is possible to express ratio between Kolmogorov scales and integral scales:

$$\frac{\eta}{l_0} \sim Re^{-\frac{3}{4}} \qquad\qquad \frac{u_\eta}{u_0} \sim Re^{-\frac{1}{4}} \qquad\qquad \frac{\tau_\eta}{\tau_0} \sim Re^{-\frac{1}{2}} \qquad (2.13)$$

Increasing the Reynolds number, the ratio becomes lower and lower. This means that for a sufficiently high Reynolds number there is a range of scales considered small with respect to integral scale (l_0) but bigger than Kolmogorov scale (η). In this region it is possible to assume that viscosity doesn't have a big relevance, so that in this region scales are completely determined by energy transfer from bigger scales to smaller scales.

It is possible to introduce four length scales (a schematic representation can be found in fig. 2.3):

- η: typical Kolmogorov length scale;

- l_{DI}: under this scale both viscous and inertial effects are important, over this, the only important process is the transport of energy from large scales to small scales;

- l_{EI}: scale separation between the universal equilibrium range and the energy containing range;

- l_0: integral length scale.
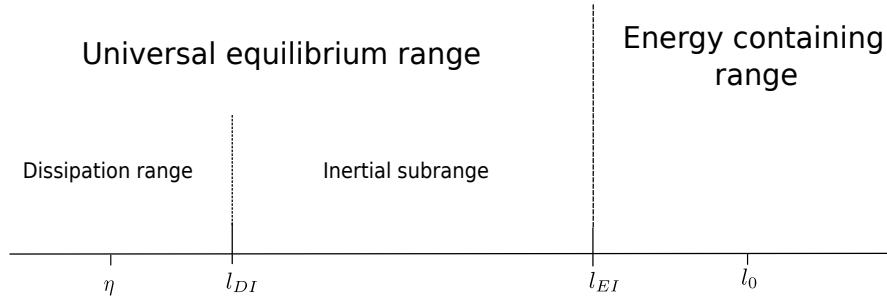
Figure 2.3: Eddy's sizes considering a logarithmic scale [3].

2.3 Channel flow and energy budget

Homogeneous Isotropic Turbulence (HIT) hypothesis is not realistic, but allows to clearly understand the behaviour of the small scales region and to access to the concept of energy cascade. From a practical point of view it is even more important to consider wall-bounded flows in which the flow is circumscribed by solid boundaries, so that there is at least one direction in which the flow is not homogeneous. In this work a *Channel flow* will be considered. The geometry is composed by two infinite flat plates separated by a distance of $2h$. It is possible to describe the flow through the channel with the set of incompressible Navier Stokes equations (eq. (2.14)).

$$\begin{cases} \dfrac{\partial \boldsymbol{u}}{\partial t} + (\boldsymbol{u} \cdot \nabla)\,\boldsymbol{u} + \nabla P - \nu \nabla^2 \boldsymbol{u} = 0 \\ \nabla \cdot \boldsymbol{u} = 0 \end{cases} \tag{2.14}$$

Experimentally the fluid runs through a duct, moved by external actions, otherwise it would be stopped by viscous drag (In the case of the channel, only friction is responsible for the drag). A term that mimics this external action is needed in eq. (2.14). In order to implement this action, three main approaches are used:

- **C**onstant **P**ressure **G**radient (**CPG**): pressure gradient is kept constant, whereas flow rate fluctuates in time;

- **C**onstant **F**low **R**ate (**CFR**): flow rate is kept constant, whereas pressure gradient fluctuates in time;

- **C**onstant **P**ower **I**nput (**CPI**): the rate of energy that goes into the system is kept constant. As said in [22], pumping power can be written as:

$$P_p = -\frac{\partial p}{\partial x} h U_b \tag{2.15}$$

where $-\frac{\partial p}{\partial x}$ is the pressure gradient, whereas U_b is the bulk velocity and it is defined as in eq. (2.16).

$$U_b = \frac{1}{2h} \int_0^{2h} \langle u \rangle \mathrm{d}y \tag{2.16}$$

where brackets represent time average operator defined as:

$$\langle ... \rangle = \frac{1}{T} \int_0^T ...\mathrm{d}t \tag{2.17}$$

where T represents the time units used for the average.

Shear stress can be defined as:

$$\tau_w = \mu \frac{\partial \langle U \rangle}{\partial y} - \rho \langle uv \rangle \tag{2.18}$$

and friction coefficient as:

$$c_f = \frac{\tau_w}{1/2 \rho U_b^2} \tag{2.19}$$

where $\langle uv \rangle$ are called *Reynolds stresses*. Near the wall the viscosity (ν) and the viscous stress (τ_w) have a high value, thus appropriate scales to describe near wall behaviour for the flow are the *viscous scales*. Through dimensional analysis considerations, it is possible to build a viscous length-scale (δ_ν) and a viscous velocity-scale (u_τ). They can be written as:

$$u_\tau = \sqrt{\frac{\tau_w}{\rho}} \qquad \delta_\nu = \frac{\nu}{u_\tau} \tag{2.20}$$

It is common to scale near wall variables with quantities given in eq. (2.20). These non dimensional values are represented with + superscript and are called *viscous units*.

$$u^+ = \frac{u}{u_\tau} \qquad y^+ = \frac{y}{\delta_\nu} \tag{2.21}$$

Classical analysis of the channel flow splits it into different regions where viscous and inertial effects have different relevance. The first who considered this subdivision was Theodore Von Kàrmàn in [23]. The region below $y^+ = 5$ is called *viscous sublayer*. Here the inertial effects are negligible with respect to the viscous ones. For $30 \leq y^+ \leq 50$ the *logarithmic region* is present, where the velocity profile follows a logarithmic law, and the viscous effects become less important compared to inertial ones. The *buffer layer* ($5 \leq y^+ \leq 30$) links the logarithmic region to the viscous sublayer.

2.3.1 Turbulent Kinetic Energy budget equation

Once the process of transferring energy is known, and once it is clear to access this quantity in a HIT flow, it is also worth to understand this behaviour without this set of hypothesis (e.g in a channel flow). Defined a completely developed turbulent velocity field as $\boldsymbol{U}(\boldsymbol{x},t)$, it is possible to decompose it into two components (The first person who performed this decomposition was Reynolds in 1894):

$$\boldsymbol{U}\left(\boldsymbol{x},t\right) = \langle \boldsymbol{U}\left(\boldsymbol{x},t\right)\rangle + \boldsymbol{u}\left(\boldsymbol{x},t\right) \tag{2.22}$$

where the symbol $\langle...\rangle$ represents the time average. $\langle \boldsymbol{U}\left(\boldsymbol{x},t\right)\rangle$ is called mean velocity field, and it is independent from time. $\boldsymbol{u}\left(\boldsymbol{x},t\right)$ is the fluctuation velocity field. It is possible to use this decomposition inside incompressible Navier-Stokes equations (eq. (2.14)). Applying eq. (2.22) to the eq. (2.14) and using the Reynolds decomposition, it is possible to obtain:

$$\frac{\partial \boldsymbol{U}}{\partial t} + \nabla \cdot (\langle \boldsymbol{U}\rangle \langle \boldsymbol{U}\rangle) + \nabla \cdot \langle \boldsymbol{u}\cdot\boldsymbol{u}\rangle = -\frac{1}{\rho}\nabla\langle p\rangle + \nu\nabla^2\langle \boldsymbol{U}\rangle \tag{2.23}$$

Eq. (2.23) is called URANS (**U**nsteady **R**eynolds **A**veraged **N**avier **S**tokes) equation.

The term $\langle \boldsymbol{uu}\rangle$ plays an important role in this equation and it is called *Reynolds stress tensor*. According to [3], eq. (2.23) can be rewritten grouping together similar terms.

$$\frac{\partial\langle U_j\rangle}{\partial t} + \langle U_j\rangle\left(\frac{\partial\langle U_i\rangle}{\partial x_j}\right) = \frac{\partial}{\partial x_i}\left[\mu\left(\frac{\partial\langle U_i\rangle}{\partial x_j} + \frac{\partial\langle U_j\rangle}{\partial x_i}\right) - \langle p\rangle\,\delta_{ij} - \rho\langle u_iu_j\rangle\right] \tag{2.24}$$

Eq. (2.24) explains why the term $\langle \boldsymbol{u}\cdot\boldsymbol{u}\rangle$ is called Reynolds stress tensor. Analyzing eq. (2.24) it is possible to identify three kind of stresses:

- viscous stress;

- isotropic stress;

- apparent stress of Reynolds' stress tensor.

Turbulent kinetic energy is defined as the half of the trace of the Reynolds stress tensor:

$$k = \frac{1}{2}\langle \boldsymbol{u}\cdot\boldsymbol{u}\rangle = \frac{1}{2}\langle u_iu_i\rangle \tag{2.25}$$

By subtracting URANS equation to Navier Stokes equation, it is possible to obtain the Turbulent Kinetic Energy (TKE) budget equation.

$$\underbrace{\left(\frac{\partial}{\partial t} + \langle U_i\rangle\frac{\partial}{\partial x_i}\right)k}_{1} - \underbrace{\frac{\partial}{\partial x_i}\left(\frac{1}{2}\langle u_iu_ju_j\rangle + \frac{\langle u_ip\rangle}{\rho} - 2\nu\langle u_jS_{ij}\rangle\right)}_{2} =$$

$$\underbrace{\langle u_iu_j\rangle\frac{d\langle U_i\rangle}{dx_j}}_{3} - \underbrace{2\nu\left\langle\frac{\partial u_i}{\partial x_j}\frac{\partial u_i}{\partial x_j}\right\rangle}_{4} \tag{2.26}$$

It is possible to identify four terms. The first is the unsteady and transport term of the Turbulent Kinetic Energy (1). The transport is made by inhomogeneity in the mean velocity profile. The second term is the convection term (2), composed by a turbulent part, a pressure part and a viscous part. The third term (3) is the production term, and it is possible to see how turbulence is produced by inhomogeneity in the mean flow. No production of the Turbulent Kinetic Energy is possible. Eventually it is possible to identify the sink of the Turbulent Kinetic Energy in the equation: pseudo dissipation term (4).

2.3.2 Mean Kinetic Energy budget equation

Considering $\langle \boldsymbol{U}(\boldsymbol{x}, t)\rangle$, it is possible to determine the kinetic energy related to the mean flow:

$$E = \frac{1}{2}\langle \boldsymbol{U}\rangle \cdot \langle \boldsymbol{U}\rangle \tag{2.27}$$

It is possible to write an evolutive budget equation for the Mean Kinetic Energy. Pre multiplying by $\langle \boldsymbol{U}\rangle$ equation 2.23, it is possible to obtain:

$$\left(\frac{\partial}{\partial t} + \langle U_i\rangle \frac{\partial}{\partial x_i}\right) E + \frac{\partial}{\partial x_i}\left(\langle U_j\rangle \langle u_i u_j\rangle + \frac{1}{\rho}\langle U_i\rangle \langle p\rangle - 2\nu \langle U_j\rangle \bar{S}_{ij}\right) =$$

$$\tag{2.28}$$

$$- \langle u_i u_j\rangle \frac{d\langle U_i\rangle}{dx_j} - 2\nu \left(\frac{\partial \langle U_i\rangle}{\partial x_j} \frac{\partial \langle U_i\rangle}{\partial x_j}\right) + \langle U_i\rangle \frac{dp}{dx_i}$$

It is easy to see that the equation looks similar to the one showed for the TKE budget in eq. (2.26). The term $\langle U_i\rangle \frac{dp}{dx_i}$ is the *pumping term*. It is important to highlight how the turbulent production term $\langle u_i u_j\rangle \frac{d\langle U_i\rangle}{dx_j}$ is available in both the equations for the mean and the turbulent kinetic energy budget. This term is the true responsible of interaction between the mean flow and the fluctuations, furthermore it is generally positive and supplies energy from mean flow to turbulent flow.

2.3.3 Integral budgets

Energetic analysis aims to understand how power input in the system is divided between mean flow and fluctuations, through the pumping term in eq. (2.28). This analysis can explain what happens from a physical point of view inside the channel, and how Reynolds number or changes in boundary conditions would affect different terms' weight. It is useful to integrate eq. (2.28) and eq. (2.26) along the channel's height. Integrating the Mean Kinetic Energy equation, is possible to obtain:

$$\underbrace{\Pi_p}_{\text{pumping power}} = \underbrace{P_{uv}}_{\text{turbulent production}} + \underbrace{D_{\overline{U}}}_{\text{mean flow dissipation}} \tag{2.29}$$

Meanwhile integrating the Turbulent Kinetic Energy budget equation:

$$\underbrace{P_{uv}}_{\text{turbulent production}} = \underbrace{\epsilon}_{\text{turbulent flow dissipation}} \tag{2.30}$$

It is possible to observe that, integrating the budget equations, the contribution of the fluxes disappears completely. This is due to the fact that the mechanism of energy transfer inside the fluid flow find a balance in a global budget equation. The *energy box* (fig. 2.4) is a compact way to observe the results of the global budget equation. First introduced by Ricco et al. in [24], this representation gives
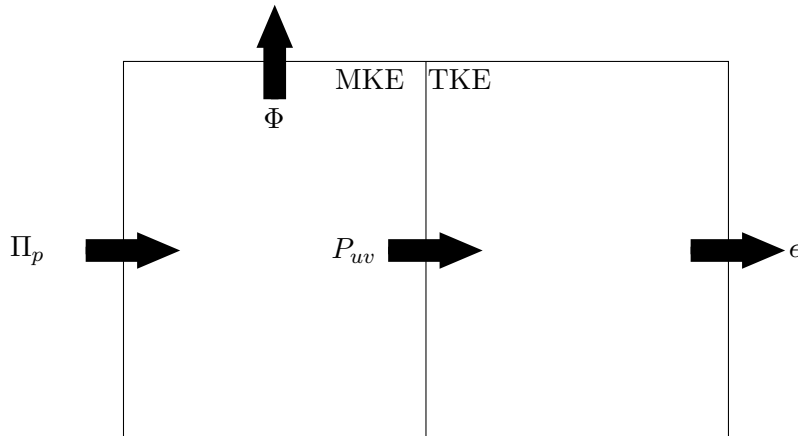
Figure 2.4: Energy box representation of a channel flow.

a good and compact overview on how mean flow and fluctuations interact, how the power supplied by the pumping term is used in the flow, how much it is dissipated by the mean flow and how much it is dissipated by the fluctuations. A global balance for the energy box can be written as:

$$\Pi_p = D_{\overline{U}} + \epsilon. \tag{2.31}$$

Hence pumping power must balance the total dissipation.

2.4 A unifying view

In the last sections two important approaches for assessing to the energetic behaviour of the flow have been outlined:

- description of the energy transfer through scales, with the concept of the energy cascade first described by Richardson and later refined by Kolmogorov;

- description of the energy transfer in the physical space, with analysis tools such as the TKE budget equation, the MKE budget equation, the integration of the former and the latter.

These two approaches turned out to be mutually exclusive. It is interesting to try to put these two points of view together to explain the scale-dependent fluxes of energy in the presence of the spatial fluxes induced by the inhomogeneity. An important step had already been made by Andrei Kolmogorov in [12]. He introduced the function that groups the two approaches together. The *second order structure*

function is function of the wall-normal direction and of the separations between scales. It is defined as the second order moment statistic of difference velocity between two locations:

$$\langle \delta u^2 \rangle (\boldsymbol{X_c}, \boldsymbol{r}) = \left\langle \left[\boldsymbol{u} \left(\boldsymbol{X_c} + \frac{\boldsymbol{r}}{2} \right) - \boldsymbol{u} \left(\boldsymbol{X_c} - \frac{\boldsymbol{r}}{2} \right) \right]^2 \right\rangle \tag{2.32}$$

where brackets represent the time average. Second-order structure function can
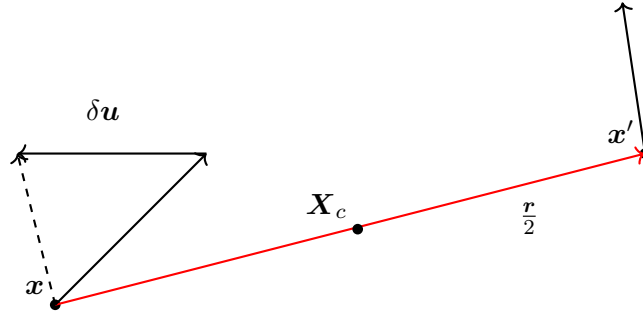
Figure 2.5: Graphical representation of the framework to build the second order structure function. Velocity in $\boldsymbol{x}$ and $\boldsymbol{x}'$ are used to build velocity increment $\delta \boldsymbol{u}$. Distance between two points is $\boldsymbol{r}$, while $\boldsymbol{X}_C$ is the middle point between $\boldsymbol{x}$ and $\boldsymbol{x}'$.

be interpreted as the amount of energy for a structure of a given separation $\boldsymbol{r}$ at a certain position in the flow field $\boldsymbol{X}_C$, because of that fluid dynamicists usually refer to it as *scale energy*. It is possible to write a budget equation for the second order structure function. This budget equation was first written by Kolmogorov in a second article published in 1941 [25]. As the whole K41 theory, this equation is made on HIT hypothesis. As a consequence, the *scale energy* does not depend on $\boldsymbol{X}_C$. The budget equation for the scale energy can be obtained through a rearrangement of *Karman-Howarth equation* [26], which is an evolutive equation for two points correlation tensor in homogeneous isotropic turbulence.

In more recent years, Hill tried to find a more constrained form for this equation, removing the hypothesis of homogeneity. In his first work in 2001 [27] he described a procedure to write equations for structure function of a random order, later in 2002 he published a work [18] in which he explained how it is possible to obtain a general budget equation for the second order structure function. This equation is called *Generalized Kolmogorov Equation* and allows to group the two views previously seen in the physical space and in the scale space.

2.5 Coherent Structures

To better understand better what happens in the near wall region and the nature of self sustaining turbulence, fluid dynamicists focused their studies on trying to find structures with a certain coherence: the *coherent structures*. Despite the great number of studies, a common definition of coherent structure is not yet reached. A well accepted definition can be found in an excellent review made by Robinson [28] *"a coherent motion is a three dimensional region of the flow over*

which at least one fundamental flow variable exhibits significant correlation with itself or with another variable over a range of space and/or time that is significantly larger than the smallest local scales of the flow".

In recent years important studies have been published, among them the most relevant is the one made by Schoppa and Hussain [29]. They identify the self sustaining mechanism of turbulence, studying in deep the well-known *wall cycle.* This phenomenon is characterized by violent events of burst of low speed fluid towards the centerline, and sweep of high speed fluid towards the wall. Recalling the classical subdivision of the channel flow introduced in section 2.3, in the viscous sublayer typical spanwise vortexes are generated by instabilities. The mean flow stretch vortex and typical structures called quasi streamwise vortex are generated. It has been discovered that, at typical position of log-layer the turbulent fluctuations create well-defined coherent motions consisting of quasi-streamwise vortices. This vortices are the tails of typical hairpin structures. A trace of the tail vortexes can be seen also in the viscous sublayer. These structures are named LSS (Low Speed Streaks). It is possible to find a wide and deep experimental description of wall cycle as described here in [4].
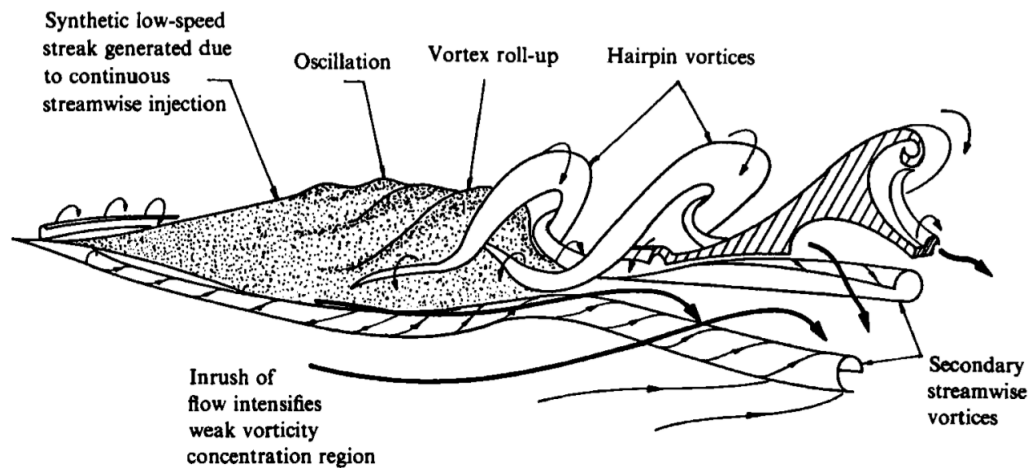
Figure 2.6: Evolution of coherent structures for a wall-bounded flow ([4]).

Chapter 3

Direct Numerical Simulation of turbulent channels

The DNS method has the purpose to solve all scales of turbulence up to the Kolmogorov universal scale, without using any model. The geometry used in this work is the channel flow. It is a simple shape that in the last years has been used as an important tool to better investigate boundary layer's behaviour. The DNS method had not been largely used to access turbulent channel flow characteristics before 1987 and before Kim Moin Moser article [16], because of problems related to the computational power and the difficulties in shaping the numerical problem. In the first part of the chapter a theoretical overview of the channel flow problem will be given. In the second part of the chapter, after a brief introduction to the drag reduction techniques under study, an in-depth analysis of the parameters used to build the database will be discussed.

3.1   Geometry description

Cartesian axes are used to describe the problem of the channel flow. x direction is the streamwise direction, z is the spanwise direction and y is the wall-normal direction. Velocity components are respectively u, v and w. x and z are directions in which walls are considered to be of infinite extent. Since a finite domain is needed, it is possible to identify two statistically homogeneous directions namely x and z, so that the Reynolds averaged streamwise velocity $\langle \boldsymbol{u} \rangle$ depends only on the wall-normal coordinate. Considering a finite box of dimensions L_x, L_z it is eventually possible to end up imposing periodic boundary conditions at each end:

$$u_j \left(L_x, y, z \right) = u_j \left(0, y, z \right) \qquad u_j \left(L_z, y, z \right) = u_j \left(x, y, 0 \right) \qquad j = x, y, z \qquad (3.1)$$
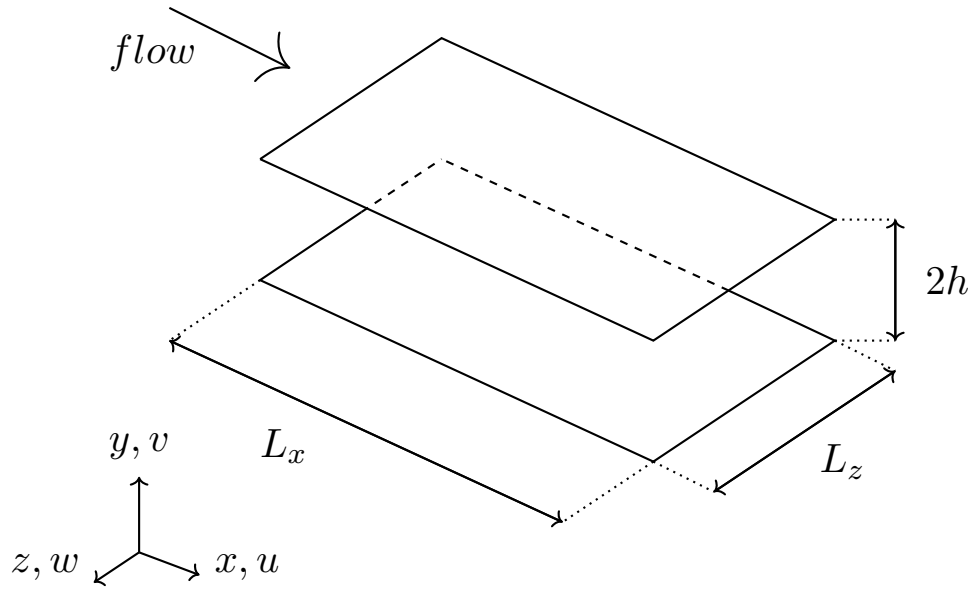
Figure 3.1: Graphical representation of the channel flow in a Cartesian reference system.

3.2   Formulation of the problem

3.2.1   Incompressible Navier Stokes equations

The Flow inside a channel is well described by the system of *unsteady incompressible Navier-Stokes equations*. The system is composed by two partial differential equations: one stating the conservation of momentum, the other the conservation of mass.

$$
\begin{cases}
\dfrac{\partial \boldsymbol{u}}{\partial t} + (\boldsymbol{u} \cdot \nabla)\,\boldsymbol{u} + \dfrac{\nabla P}{\rho} = \nu \nabla^2 \boldsymbol{u} \\
\nabla \cdot \boldsymbol{u} = 0
\end{cases}
\tag{3.2}
$$

Based on different length-scale and velocity-scale, it is possible to define several Reynolds numbers in an incompressible flow.
One of the most classical Reynolds number defined for the channel flow is the one based on velocity-scale U_b:

$$
Re_b = \frac{U_b h}{\nu}
\tag{3.3}
$$

It is also possible to set the half width of the channel as length-scale, and the maximum velocity (U_p) as velocity-scale inside the channel, defining:

$$
Re_p = \frac{U_p h}{\nu}
\tag{3.4}
$$

Considering the laminar velocity profile for a Poiseuille flow in a laminar flow, it is possible to find a relation between U_p and U_b.

$$U_b = \frac{2}{3}U_p \tag{3.5}$$

One of the most used Reynolds numbers in DNS simulations of channel flows is based on the velocity-scale u_τ with the definition given in eq. (2.20).

$$Re_\tau = \frac{u_\tau h}{\nu} \tag{3.6}$$

As it is described in [22], in the case of CPI pumping technique , if the dissipation rate is equated with the pumping power, it is possible to obtain the velocity-scale U_Π, which represents the flow rate (per unit width) that can be reached with a given constant pumping power in the laminar regime.

$$U_\Pi = \sqrt{\frac{P_p h}{3\mu}} \tag{3.7}$$

The Reynolds number that it is possible to build using the velocity-scale described in eq. (3.7) (Re_Π) is defined as it follows:

$$Re_\Pi = \frac{U_\Pi h}{\nu} \tag{3.8}$$

Incompressible Navier-Stokes equations are usually implemented in their non-dimensional form. Choosing a proper scaling velocity and length, so that it is possible to build the most suitable Reynolds number for the considered problem, the system eq. (3.2) becomes:

$$\begin{cases} \dfrac{\partial u}{\partial t} + u\dfrac{\partial u}{\partial x} + v\dfrac{\partial u}{\partial y} + w\dfrac{\partial u}{\partial z} + \dfrac{\partial P}{\partial x} = \dfrac{1}{Re}\nabla^2 u \\[2mm] \dfrac{\partial v}{\partial t} + u\dfrac{\partial v}{\partial x} + v\dfrac{\partial v}{\partial y} + w\dfrac{\partial v}{\partial z} + \dfrac{\partial P}{\partial y} = \dfrac{1}{Re}\nabla^2 v \\[2mm] \dfrac{\partial w}{\partial t} + u\dfrac{\partial w}{\partial x} + v\dfrac{\partial w}{\partial y} + w\dfrac{\partial w}{\partial z} + \dfrac{\partial P}{\partial z} = \dfrac{1}{Re}\nabla^2 w \\[2mm] \dfrac{\partial u}{\partial x} + \dfrac{\partial v}{\partial y} + \dfrac{\partial w}{\partial z} = 0 \end{cases} \tag{3.9}$$

The three former equations are the momentum conservation equations, the last one is the mass conservation equation and it is decoupled from the first three equations. Pressure in this case does not have a thermodynamic meaning, but only the meaning of Lagrangian multiplier. Mass conservation equation simply represents a kinematic constraint that needs to be satisfied in every point of the flow field, at any time.

The problem of eq. (3.9) can be solved providing a set of initial and boundary conditions:

$$\begin{cases} \mathbf{u}(x, y, z, 0) = \mathbf{u_0}(x, y, z) \\ \mathbf{u}(x, 0, z, t) = 0 \\ \mathbf{u}(x, 2h, z, t) = 0 \\ \mathbf{u}(L_x, y, z) = \mathbf{u}(0, y, z) \\ \mathbf{u}(x, y, L_z) = \mathbf{u}(x, y, 0) \end{cases} \qquad (3.10)$$

Initial and boundary conditions must respect the following compatibility conditions:

$$\begin{cases} \nabla \cdot u_0 = 0 \\ \oint \hat{\mathbf{n}} \cdot \boldsymbol{u} dS \\ \hat{\mathbf{n}} \cdot \boldsymbol{u}_0(x)|_S = \hat{\mathbf{n}} \cdot \mathbf{u}(\mathbf{x}_0, 0)|_S \end{cases} \qquad (3.11)$$

3.3   Simulation tools

The simulation tool which is used is a program written in CPL language explained in [30] by Quadrio and Luchini. Navier-Stokes equations are projected in a divergence free space through $v - \eta$ projection method as it is reported in [16] by Kim et al. In the homogeneous directions it is possible to discretize equations with a discrete Fourier series expansion. Defined two characteristic wave numbers in direction x and z as:

$$\alpha_0 = \frac{2\pi}{L_x} \qquad \beta_0 = \frac{2\pi}{L_z} \qquad (3.12)$$

it is possible do rewrite solution as the following expansions:

$$v(x, y, z, t) = \sum_{h=-N_x/2}^{N_x/2} \sum_{l=-N_z/2}^{N_z/2} \hat{v}(\alpha, y, \beta, t) e^{i\alpha_0 ht} e^{i\beta_0 lt} \qquad (3.13)$$

$$\eta(x, y, z, t) = \sum_{h=-N_x/2}^{N_x/2} \sum_{l=-N_z/2}^{N_z/2} \hat{\eta}(\alpha, y, \beta, t) e^{i\alpha_0 ht} e^{i\beta_0 lt} \qquad (3.14)$$

h and l are indexes that span domain respectively in the directions x and z. N_x and N_z are respectively the maximum number of Fourier modes in which each direction is divided. Wall-normal direction derivatives are computed using a compact finite difference scheme with a molecule of five nodes, while the simulation is advanced in time by a combination of Crank-Nicholson scheme and Runge-Kutta scheme. Once the flow field is obtained, pressure can be recovered by the use of Poisson equation:

$$\nabla^2 P = -\nabla \cdot (\boldsymbol{u} \cdot \nabla \boldsymbol{u}) \qquad (3.15)$$

CPI approach is the adopted pumping technique (implementation is described in [22]) and hence Re_Π is the Reynolds number chosen for the non-dimensional

set of equations in eq. (3.9). The velocity field resulting from the computation will be given in Π *units* (addressed in the following also as power units). The non-dimensional velocity and length are defined as:

$$u^* = \frac{u}{U_\Pi} \qquad\qquad y^* = \frac{y}{h} \qquad\qquad (3.16)$$

Since they are the natural outcome of the DNS computations, hereafter this non dimensional quantities will be simply addressed without asterisk.

3.4 Database building

The DNS tool is used to run simulations of the channel flow considering representative active drag reduction strategies with the aim of an energetic comparison. Pursuing this goal, parameters of the simulations are carefully chosen so that robust statistics can be computed.

3.4.1 Choice of discretization parameters

As it is said in [16] the computational domain size is chosen to assure that the turbulent fluctuations are uncorrelated at a separation of one half-period in the homogeneous directions. Given the streamwise length of $L_x = 4\pi$ and spanwise length of $L_z = 2\pi$, it is necessary to choose the number of Fourier modes at which the series should be truncated . The number of Fourier modes is $N_x = 256$ in the streamwise direction and $N_z = 256$ in the spanwise direction. The spatial resolution in viscous units is always better than $\Delta x^+ = 9.79$ and $\Delta z^+ = 4.89$. This resolution is computed with a number of modes before the introduction of the dealiasig with the 3/2 rule. After the application of the rule, resolution becomes $\Delta x^+ = 6.53$ and $\Delta z^+ = 3.26$. In wall-normal direction the grid must be refined near the lower and upper boundaries and be courser near the centreline. An hyperbolic tangent distribution for the points is chosen, so that the minimum wall-normal resolution is of $\Delta y^+ = 0.7$, with a total node number of $N_y = 256$ points. For every simulation a Constant Power Input approach is used and because of that the reference Reynolds number is Re_Π, set to a constant value of $Re_\Pi = 6500$.

3.4.2 Reference channel flow

Simulation plan

The calculations start from an initial condition where the flow has already reached statistical equilibrium and are advanced for further 4000 time units. During this time 200 flow fields are written on the disk. This time resolution allows to get uncorrelated fields with the aim of obtaining more robust statistics.

Case	Re_Π	Re_τ	L_x/h	L_z/h	$n_x \times n_y \times n_z$	Δx^+	Δz^+
REF	6500	199.7	12.56	6.28	$256 \times 256 \times 256$	9.79	4.89

Table 3.1: Parameters of the simulation for the reference channel flow.

3.4.3 Damping of the near-wall spanwise velocity fluctuations

Theory
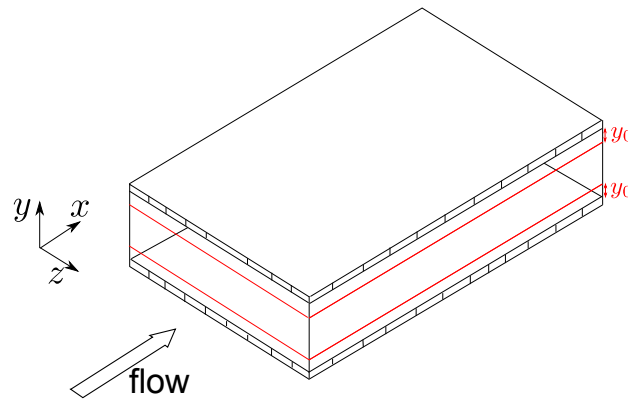
Figure 3.2: Graphical representation of the damping of the near-wall spanwise velocity fluctuations drag reduction technique.

Fluid dynamicists have noticed that a possible physical mechanism for drag reduction is to impede spanwise motion of fluid, killing or attenuating quasi-streamwise vortex in log-layer region [31]. As a consequence Satake and Kasagi in [9] and later Fronhapfel et al. in [32] implemented an active closed loop drag reduction technique in which a thin layer adjacent to the wall is assumed to exist, where a body force act to impede spanwise velocity fluctuations. In this sense the virtual force is introduced in the w-momentum balance equation:

$$\frac{\partial w}{\partial t} + u\frac{\partial w}{\partial x} + v\frac{\partial w}{\partial y} + w\frac{\partial w}{\partial z} = -\frac{\partial p}{\partial z} + \frac{1}{Re_\Pi}\left(\frac{\partial^2 w}{\partial x^2} + \frac{\partial^2 w}{\partial y^2} + \frac{\partial^2 w}{\partial z^2}\right) - \alpha w \quad (3.17)$$

Implementation

During the implementation, the first problem that should be considered is the force inside the channel. It must be implemented like a term $\alpha(y)$ that is active in the layer near the two walls of the channel and zero in the rest of it. Due to the fact that derivatives in the wall-normal direction are computed by compact finite difference scheme, with a computational molecule composed of five points, it has been tested that a derivable shape for the shift from the end of the layer through the null force zone is better than a step, implemented by a common conditional

structure. After an optimization procedure made by trial and error technique, the final shape chosen has been set to:

$$\alpha(y) = -\tanh\left[m(y - y_0)\right] + \tanh\left\{m\left[y(h - y_0)\right]\right\} \tag{3.18}$$
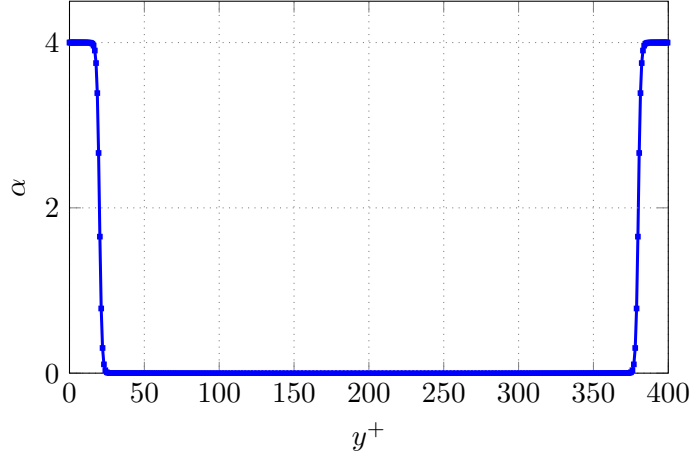
Figure 3.3: Graphical representation, in viscous units, of the shape used for the implementation of the force in eq. (3.17). In this plot parameters used are $y_0 = 0.10$ and $m = 120$. This trend is took from one of the simulation performed (BF10).

The second problem that should be addressed is the constraint of a divergence free force field:

$$\nabla \cdot \boldsymbol{f} = 0 \tag{3.19}$$

A force $f_z = -\alpha w$ is imposed in the w-momentum, the divergence free constraint imposes that other components in other directions will be created. An attempt to remove this constraint turned into a complete failure of the drag reduction technique. Some tests have been made on a domain with less discretization points, considering a case with the divergence free constraint and a case without this constraint. In fig. 3.4 it is possible to see the difference of the wall-normal derivative at lower boundary with respect to time. In the case of simulation with no divergence free constraint the force seems not to act because it is filtered by $v - \eta$ projection of the algorithm.

The computation of control's power is the last thing to consider during the implementation of the damping of the near-wall spanwise velocity fluctuations strategy. This can be computed by averaging the product of force applied and spanwise fluctuations on a plane and summing up all planes in wall-normal direction.

$$P = \sum_{iy=0}^{ny} \langle f_z(iy)w(iy) \rangle \tag{3.20}$$
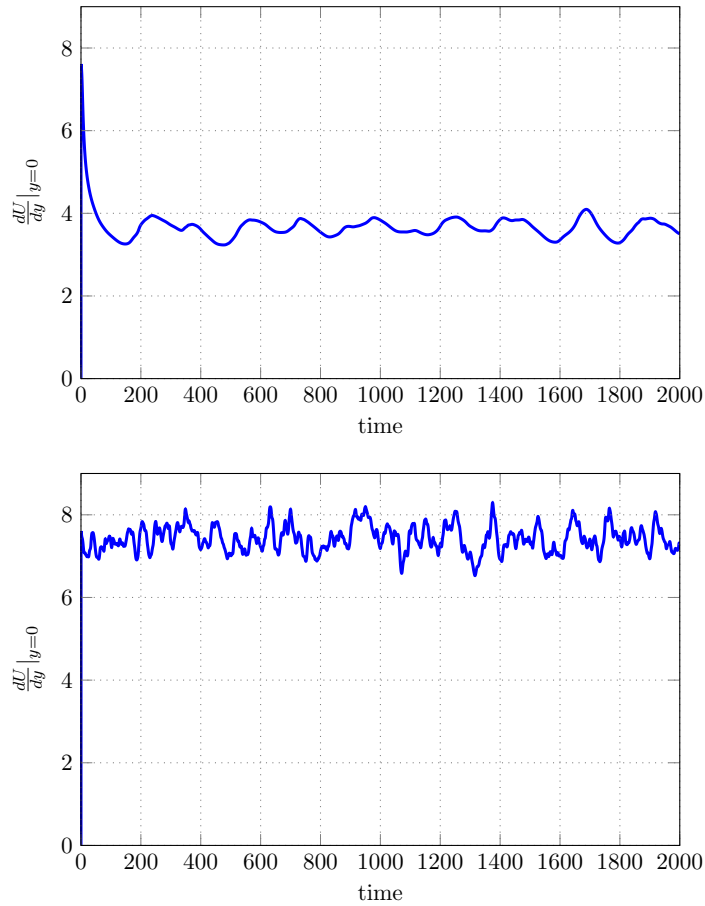
Figure 3.4: Wall-normal derivative of the velocity measured at the wall of the two simulations of the channel flow with damping of the near-wall spanwise velocity fluctuations with a resolution of $n_y, n_x, n_z = 100, 72, 72$. Upper: the case with divergence free constraint. At the bottom: the case without the constraint.

Simulations plan

Two different damping of the near-wall spanwise velocity fluctuations simulations have been performed. One considering damping layer until $y^+ = 10$, the other considering it until $y^+ = 20$. The force magnitude α is set in both cases to $\alpha = 4$, matching experiments of Satake et al. in [9]. The simulation is performed starting from a statistically full developed channel flow field. The sudden introduction of a force into the equations could cause the explosion of the simulation. In order to avoid that, the force is activated gradually following a ramp that lasts ten time units. Time development of the simulation and number of the field saved are the same of the reference channel flow case. Database characteristics are resumed in table 3.2.

Case	Re_Π	Re_τ	y_d^+	L_x/h	L_z/h	$n_x \times n_y \times n_z$	Δx^+	Δz^+
BF20	6500	166.73	20	12.56	6.28	$256 \times 256 \times 256$	8.18	4.09
BF10	6500	178.34	10	12.56	6.28	$256 \times 256 \times 256$	8.74	4.37

Table 3.2: Parameters for the simulations of the channel flow with damping of the near-wall spanwise velocity fluctuations.

3.4.4 Streamwise travelling waves of spanwise wall velocity

Theory
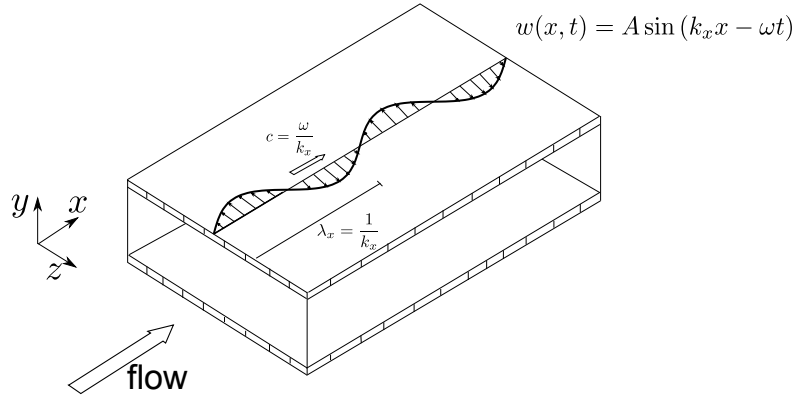
Figure 3.5: Graphical representation of the streamwise travelling wave of spanwise wall velocity drag reduction technique.

The technique was first introduced by Quadrio et al. in [33] grouping together not so effective techniques of [34] and [35]. This technique consists in imposing at the wall the following law of velocity:

$$W_w(x,t) = A\sin(k_x x - \omega t) \tag{3.21}$$

W_w is the spanwise velocity enforced at the wall, A is the amplitude of the forcing, k_x is the streamwise wavenumber, ω is the angular frequency, and x and t are respectively the streamwise coordinate and time. A graphical representation can be seen in fig. 3.5. The way in which this technique reduces viscous drag is still under study. A first step has been made by Quadrio and Ricco [21], when they saw that the spanwise flow, induced by the wave, is a thin modulated streamwise boundary layer called Generalized Stokes Layer (GSL). Considering the phase of the wave which is sufficiently different from the turbulent convection velocity and considering the time scale of the forcing which is sufficiently different from the life time of the near-wall turbulent structures, drag reduction is found to scale with the Stokes layer thickness.

Performance parameters

In order to evaluate if a drag reduction technique is successful, there are different performance parameters, which are more or less suitable with respect to the technique adopted.

The first analysed paramenter is the raw drag reduction parameter $\mathscr{R}$, defined as:

$$\mathscr{R} = 1 - \frac{c_{f,0}}{c_f} \tag{3.22}$$

where $c_{f,0}$ is the friction coefficient of the reference flow without drag reduction technique, while c_f is the friction coefficient with drag reduction technique. This is the worst conceivable parameter for active drag reduction techniques. It does not take into account the power used to run the drag reduction strategy. A more suitable parameter is the net energy savings $\mathscr{S}$ defined as:

$$\mathscr{S} = \mathscr{R} - \frac{P_{\text{in}}}{P_0} \tag{3.23}$$

where P_0 is the power (per unit area) required to drive the uncontrolled channel flow, while P_{in} is the control input. In this work P_0 is constant because of CPI pumping technique.

Simulations plan

The simulations parameters have been chosen taking into account an in-depth research of optimum parameters made in [5].
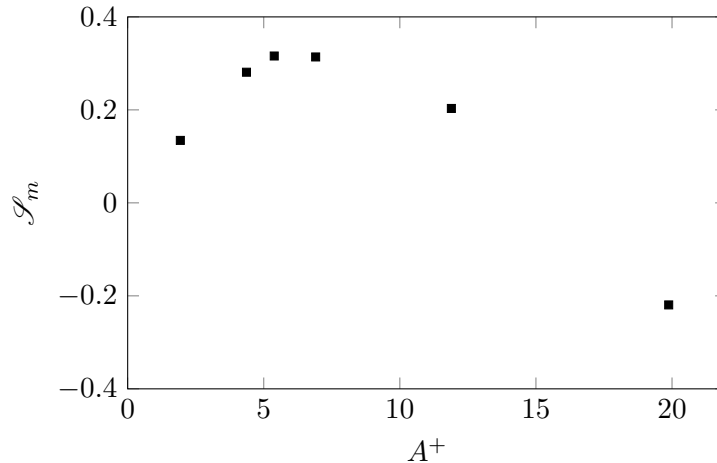
Figure 3.6: Peak of the net power savings $\mathscr{S}$ for different amplitude in viscous units ([5])

For each simulation it is necessary to set amplitude, phase and wave number (A, ω, k_x). The amplitude is chosen, considering the plateau in the neighbourhood of maximum energy savings (fig. 3.6). An amplitude $A^+ = 5.5$ is chosen for two different simulations, considering two slightly different set of (ω, k_x), as it can be seen in table 3.3. The number of nodes in wall-normal direction has been decreased

with respect to the other simulations of the database. This choice is justified by the fact that a courser grid gives good results for energetic analysis and speed up the computation at the same time. Time development of the simulation and the number of the saved fields are the same of the reference channel flow case.

Case	Re_Π	Re_τ	A^+	ω^+	k_x^+	L_x/h	L_z/h	$n_x \times n_y \times n_z$	Δx^+	Δz^+
TW1	6500	186.48	5.5	0.0408	0.0125	12.56	6.28	$256 \times 128 \times 256$	9.15	4.57
TW2	6500	187.96	5.5	0.027	0.01	12.56	6.28	$256 \times 128 \times 256$	9.22	4.61

Table 3.3: Parameters for the simulations of the channel flow with streamwise travelling waves of spanwise wall velocity.

Chapter 4

Generalized Kolmogorov Equation

In this chapter, the Generalized Kolmogorov Equation (GKE), a budget equation for the second order structure function, is exploited to study the energetics of the turbulent channel flow with and without drag reduction strategies. As a result of the computation of each term of the GKE, it is possible to perform an in-depth analysis of the energy paths in the physical space and in the space of scales. The first part of the chapter deals with the theoretical background and with the similarities and the differences between this approach and the classical energy analysis performed in the physical space. In the second part of the chapter technical details about the implementation of the terms of the GKE will be given.

4.1 Definition

Defined u_i the components of the velocity field in a Cartesian reference frame and $x_i = X_{Ci} - \frac{r_i}{2}$, $x'_i = X_{Ci} + \frac{r_i}{2}$ two points inside the fluid domain, the second order structure function $\langle \delta u^2 \rangle$ can be written as $\langle \delta u^2 \rangle = \langle \delta u_i \delta u_i \rangle$. The brackets represent ensemble average in time. In the classical turbulent channel flow defined in a Cartesian geometry, the second order structure function is a function of the separation between two points ($r_i = x'_i - x_i$) and of the wall-normal direction (Y_c). Hence is defined in a four dimensional space (r_x, r_y, r_z, Y_c). Examining the TKE definition and comparing it with the second order structure function, it is easy to see that the latter makes the former expand in the space of scales. Restricting the derivation made by Hill in [18] to a channel flow like geometry, the second order structure function budget equation, hereafter called the *Generalized Kolmogorov Equation*, can be written as:

$$\frac{\langle\delta u^2 \delta u_i\rangle}{\partial r_i} + \frac{\langle\delta u^2 \delta U_i\rangle}{\partial r_i} - 2\nu\frac{\partial^2\langle\delta u^2\rangle}{\partial r_i\partial r_i} + \frac{\partial\langle v^*\delta u^2\rangle}{\partial Y_c} + \frac{2}{\rho}\frac{\partial\langle\delta p\delta v\rangle}{\partial Y_c} - \frac{\nu}{2}\frac{\partial^2\langle\delta u^2\rangle}{\partial Y_c^2} =$$
$$= -2\langle\delta u\delta v\rangle\left(\frac{dU}{dy}\right)^* - 2\langle\delta uv^*\rangle\,\delta\left(\frac{dU}{dy}\right) - 4\langle\epsilon^*\rangle$$

$$(4.1)$$

where v is the wall-normal fluctuating velocity field component, asterisk represents the average of quantities evaluated at points $(X_{c,i}\pm r_i)/2$, *pseudo-dissipation* (ϵ) is defined as :

$$\epsilon = \nu\left(\frac{\partial u_i}{\partial x_j}\frac{\partial u_i}{\partial x_j}\right) \tag{4.2}$$

and hereafter the mean flow $\langle U\rangle$ will be addressed as U.

Marati et al. in [11] and later Cimarelli et al. in [19] stated that it is useful to group together terms, in order to better understand the nature of this budget equation and to make a comparison with the TKE budget equation. It is possible to define the *source term* ξ as:

$$\xi = \underbrace{-2\langle\delta u\delta v\rangle\left(\frac{dU}{dy}\right)^* - 2\langle\delta uv^*\rangle\,\delta\left(\frac{dU}{dy}\right)}_{\text{production}}\underbrace{-4\langle\epsilon^*\rangle}_{\text{dissipation}} \tag{4.3}$$

Taking into account the *source term* of the TKE budget equation, it is defined as:

$$\xi_{TKE} = \underbrace{\langle uv\rangle\frac{\partial U}{\partial y}}_{\text{production}}\underbrace{-\langle\epsilon\rangle}_{\text{dissipation}} \tag{4.4}$$

The type of terms of ξ is very similar to the one of ξ_{TKE}. The main difference is that the GKE makes available information also in the space of scales. Through the analysis of the GKE, three dimensions are gained with respect to the TKE budget equation.
Terms that in eq. (4.1) are differentiated by the wall-normal coordinate can be grouped together in the *physical flux* (Φ_c), defined as:

$$\Phi_c = \underbrace{\langle v^*\delta u^2\rangle}_{\text{turbulent}} + \underbrace{\frac{2}{\rho}\langle\delta p\delta v\rangle}_{\text{pressure}} - \underbrace{\frac{\nu}{2}\frac{\partial\langle\delta u^2\rangle}{\partial Y_c}}_{\text{viscous}} \tag{4.5}$$

In the TKE budget equation a global energy flux can be defined in the same way as:

$$\Phi_{TKE} = \underbrace{\frac{1}{2}\langle u^2 v\rangle}_{\text{turbulent}} + \underbrace{\frac{1}{\rho}\langle pv\rangle}_{\text{pressure}} - \underbrace{\frac{\nu}{2}\frac{d\langle u^2\rangle}{dy}}_{\text{viscous}} \tag{4.6}$$

As for the source term, the type of terms for the fluxes in the physical space are almost the same both in the GKE and in the TKE budget equation. The physical flux of the GKE adds the analysis in the space of scales to the TKE budget equation.

The *scale flux* vector of components $\left(\phi_{r_x}, \phi_{r_y}, \phi_{r_z}\right)$ can be defined as:

$$\boldsymbol{\Phi_r} = \left(\Phi_{r_x}, \Phi_{r_y}, \Phi_{r_z}\right) = \underbrace{\left\langle \delta u^2 \delta \mathbf{u} \right\rangle}_{\text{turbulent}} - \underbrace{2\nu \nabla_r \left\langle \delta u^2 \right\rangle}_{\text{viscous}} + \underbrace{\left\langle \delta u^2 \delta \boldsymbol{U} \right\rangle}_{\text{viscous}} \tag{4.7}$$

This flux is a completely new term that was absent in the TKE budget equation. It embodies the analysis of the flux throughout scales. In order to better understand the nature of this term it is possible to think of it as the flux that in *Richardson* theory represents the transfer of energy through the cascade mechanism. The definitions given in eq. (4.3),eq. (4.5) and eq. (4.7), can be grouped together and the Generalized Kolmogorov Equation can be rewritten as:

$$\nabla_r \boldsymbol{\Phi_r}\left(Y_c, \boldsymbol{r}\right) + \frac{\partial \Phi_c\left(Y_c, \boldsymbol{r}\right)}{\partial Y_c} = \xi\left(Y_c, \boldsymbol{r}\right) \tag{4.8}$$

where $\nabla_r = (\partial/\partial r_x, \partial/\partial r_y, \partial/\partial r_z)$.

4.2 Implementation of the solving tool

The various terms appearing in equations 4.3,4.5 and 4.7, are computed numerically through a code which has been developed for the present work. This new tool is designed to be fast, very simple, parallel. The strengths of the code can be resumed in four bullet points:

- memory-saving implementation;

- decomposition of every term of eq. (4.3),eq. (4.5) and eq. (4.7) into simpler correlation terms, easy to compute with a relatively small computational effort;

- extensive use of the *Parseval theorem*, in homogeneous directions, to compute convolutions;

- use of a parallelized environment with a *shared memory* approach.

4.2.1 Reference system

It is necessary to introduce the reference frame where each term of the code is developed. A different reference system with respect to the one used to define the GKE in section 4.1 $(\boldsymbol{r}, Y_c)$ is proposed. Consider a Cartesian reference frame. Two wall-normal direction coordinates will be used: y_1 and y_2 (fig. 4.1). The generic form of a velocity difference δu_i can be written as:

$$\delta u_i = u_{i,iy2}\left(\boldsymbol{x} + \boldsymbol{\Delta x}\right) - u_{i,iy1}\left(\boldsymbol{x}\right) \tag{4.9}$$

Since the input of the program are the resulting fields of the DNS computations, the spatial discretization can be considered the same, and hence in x and z directions, $2n_x + 1$ and $2n_z + 1$ Fourier modes will be used. Because of the memory saving needs, the results are computed and saved averaging the upper half and the lower half of the channel in the wall-normal direction. Results for each of the 200 fields are computed and eventually an ensemble average is performed.
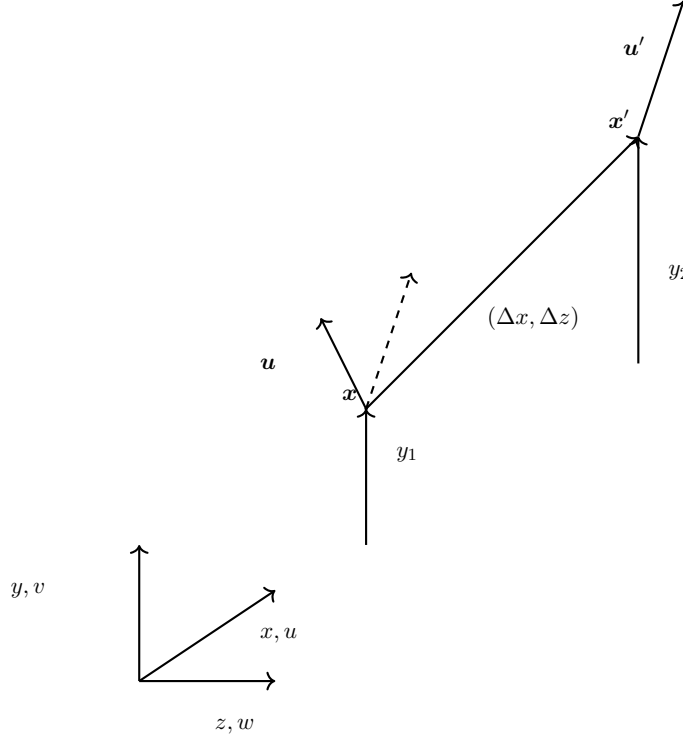
Figure 4.1: Reference system used for the implementation.

4.2.2 Expansion of the terms

Each term of the Generalized Kolmogorov Equation is rewritten so that simple correlations can be obtained. Consider, for example, the source term of eq. (4.3) for a given y_1, y_2 at a fixed separation $\boldsymbol{\Delta x}$. The production term contains correlation $\langle \delta u \delta v \rangle$. Considering eq. (4.9), the product can be further expanded as:

$$\langle \delta u \delta v \rangle = \langle [u_{iy2}(\boldsymbol{x} + \boldsymbol{\Delta x}) - u_{iy1}(\boldsymbol{x})] [v_{iy2}(\boldsymbol{x} + \boldsymbol{\Delta x}) - v_{iy1}(\boldsymbol{x})] \rangle \qquad (4.10)$$

multiplying different terms, it is possible to obtain:

$$\langle \delta u \delta v \rangle = \langle u_{iy1}(\boldsymbol{x}) v_{iy1}(\boldsymbol{x}) \rangle - \langle u_{iy2}(\boldsymbol{x} + \boldsymbol{\Delta x}) v_{iy1}(\boldsymbol{x}) \rangle +$$
$$- \langle u_{iy1}(\boldsymbol{x}) v_{iy2}(\boldsymbol{x} + \boldsymbol{\Delta x}) \rangle + \langle u_{iy2}(\boldsymbol{x} + \boldsymbol{\Delta x}) v_{iy2}(\boldsymbol{x} + \boldsymbol{\Delta x}) \rangle \qquad (4.11)$$

Eventually the product between the velocity differences is split in simple correlations. This step allows fastening up computation of the scale/space fluxes and of the source term. Double and triple correlations repeat in expansions for each term of eq. (4.7), eq. (4.5) and eq. (4.3). Correlations are computed one time and later assembled to form each piece of the equation. All the expansions are reported in appendix A.

4.2.3 Correlation computation

Expansion of terms of the GKE leads to different types of correlations:

- *double cross correlations*: this kind of terms have the following analytical form:

$$\langle uv \rangle (\Delta x, y_1, y_2, \Delta z) =$$
$$\frac{1}{T} \int_{t=0}^{T} \int_{-\infty}^{+\infty} \int_{-\infty}^{+\infty} u(x, y_1, z, t) \, v(x + \Delta x, y_2, z + \Delta z, t) \, \mathrm{d}x \mathrm{d}z \mathrm{d}t \quad (4.12)$$

It is possible to reckon these terms in the Fourier space, considering the Fourier expansions in the homogeneous directions. In the Fourier space is possible to use the Parseval's theorem to compute cross correlations. Considering a Cartesian reference system, two different functions $f(\boldsymbol{x}, t)$ and $g(\boldsymbol{x}, t)$ and their Fourier transform in space $F(\boldsymbol{k}, t)$, $G(\boldsymbol{k}, t)$ is possible to write the identity:

$$\int_{-\infty}^{+\infty} \int_{-\infty}^{+\infty} f(\boldsymbol{x}, t) \, g(\boldsymbol{x} + \boldsymbol{\Delta x}, t) \, d\boldsymbol{x} = F(\boldsymbol{k}, t) \cdot G(\boldsymbol{k}, t)^* \quad (4.13)$$

where the * is complex conjugate operator and $\boldsymbol{k}$ is the vector of wave numbers.

In the discrete framework presented in this work, is possible to apply convolution's theorem for given $(iy1, iy2, ix, iz)$ to correlation in eq. (4.12):

$$\langle u_{iy1} v_{iy2} \rangle (ix, iz) =$$
$$\frac{1}{n_f} \sum_{t=0}^{n_f} \sum_{h=-N_x/2}^{N_x/2} \sum_{l=-N_z/2}^{N_z/2} \hat{u}(\alpha, iy1, \beta, t) \, e^{i\alpha_0 ht} e^{i\beta_0 lt} \cdot \hat{v}(\alpha, iy2, \beta, t) \, e^{-i\alpha_0 ht} e^{-i\beta_0 lt}$$
$$(4.14)$$

where t is an index that ranges on each of 200 velocity fields saved through DNS computation;

- *triple cross correlations*: this kind of terms have the shape for example of:

$$\langle uuv \rangle (y_1, y_2, \Delta x, \Delta z) =$$
$$\int_{t=0}^{T} \int_{-\infty}^{+\infty} \int_{-\infty}^{+\infty} u(x, y_1, z, t) \, u(x, y_1, z, t) \, v(x + \Delta x, y_2, z + \Delta z, t) \, \mathrm{d}x \mathrm{d}z \mathrm{d}t$$
$$(4.15)$$

Correlation's theorem in discrete Fourier space can be applied to the equation above. In that case computation is performed in two steps. First of all convolutions in plane y_1 are computed and saved. Later convolutions between saved values and velocity at plane y_2 are computed.

4.2.4   Memory-saving implementation and symmetries

The algorithm aims at containing the memory requirements to a minimum. The GKE is composed by terms developed in a four dimensional space, thus saving every variable for the whole channel with DNS de aliased resolution would be impossible. Several symmetries are available for terms of the GKE and hence for each plane considered at a wall-normal distance of y_1 only GKE terms for y_2 planes that ranges from y_1 to $n_y - y_1$ are computed and saved. An example of the saving strategy is reported in fig. 4.2.
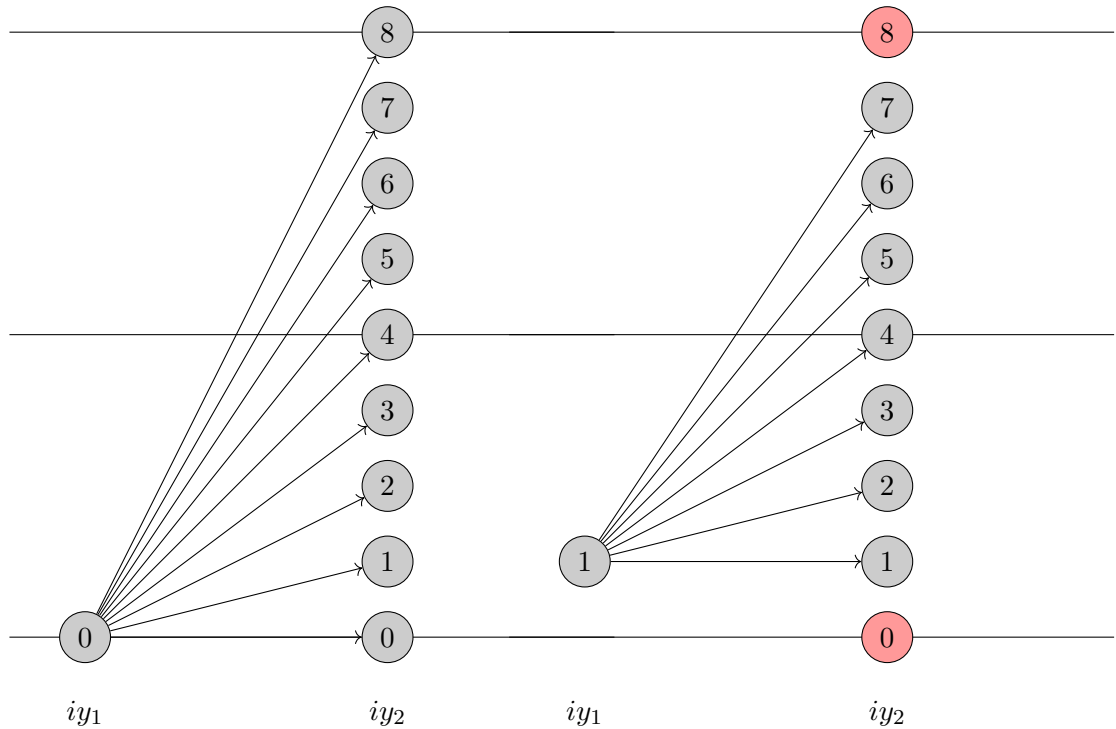
Figure 4.2: Graphical representation of the saving strategy for a simple case with $ny = 10$. On the left side $iy1 = 0$, on the right $iy1 = 1$. As it is possible to see from the figure, terms which involves nodes $iy2$ that ranges between $iy1$ and $ny - iy1$, are computed and saved. External nodes to this region (marked in red in the figure on the right side) are excluded from the computation.

Symmetries

As stated by Cimarelli in [19], both scale and space fluxes, exhibit particular statistical symmetries, which can be exploited to reduce the storage requirements of the various GKE terms. Returning to reference system in $(Y_c, \boldsymbol{r})$, suppose to

change the sign of the separation vector $\boldsymbol{r}$, and to remain at the same Y_c. $\boldsymbol{\Phi}_r$ computed through algorithm changes the sign changing the direction of the separation vector, while Φ_c doesn't switch its sign. Changing the sign of the separation vector would cause a change in points involved in the correlation. This transformation leaves quantities like second order structure function and v^* statistically invariant while changes the sign of vectors like δu_i and hence the sign of $\langle \delta u^2 \delta u_i \rangle$ is changed, while sign of $\langle \delta u^2 v^* \rangle$ does not change. Another important transformation is the one that changes the sign of the wall-normal coordinate Y_c ($Y_c \to -Y_c$) and separation in the wall-normal direction ($r_y \to -r_y$), while r_x and r_z remain invariant. The sign of ϕ_{rx} and ϕ_{rz} does not vary, while the sign of ϕ_c and ϕ_{ry} varies.

Implementation of symmetries

In the implementation of this work, symmetries are useful to recover terms of the GKE in not saved part of the channel, so for $iy2 < iy1$ and $iy2 > ny - iy1$ with $-1 \leq iy1 \leq ny/2 + 1$. Therefore there are two possible scenarios:

1. $iy2 < iy1$: to recover terms for which $iy1$ is above $iy2$, it is possible to change the order between $iy2$ and $iy1$, paying attention to the fact that for antisymmetric terms (e.g $\langle \delta u^2 \delta v \rangle$), also sign of convolution must be changed due to the fact that the separation vector $\boldsymbol{r}$ is inverted.
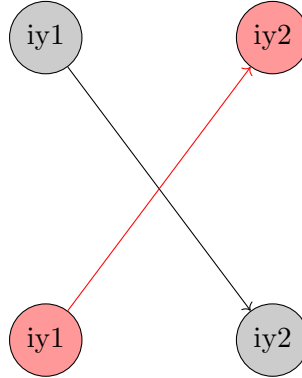
Figure 4.3: Graphical representation of the implementation of the first symmetry. While terms considering planes marked in grey are not saved, because $iy2 < iy1$, terms marked in red are saved.

2. $iy2 > ny - iy1$: to recover terms for which $iy2$ is above $ny - iy1$ it is possible to consider terms that involves nodes $ny - iy2$ and $ny - iy1$, paying attention as for the previous case, that sign of the separation vector $\boldsymbol{r}$ is changed.
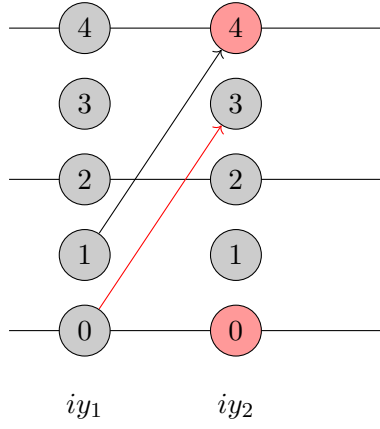
Figure 4.4: Graphical representation of the implementation of the second symmetry. red circled terms are not saved and hence correlation represented with black arrow is the same (taking care of the matter if the term considered is symmetric or antisymmetric) of the one with red arrow, where $iy1 = ny - iy2$ and $iy2 = ny - iy1$.

4.2.5   Derivatives

In the fluxes there are two kind of derivatives. In the case of scale fluxes there is the term $-2\nu\nabla_r \langle \delta u^2 \rangle$. Derivatives in the space of separations r_x and r_z can be computed easily in the Fourier space, by transforming in homogeneous direction r_x, r_z term $\langle \delta u^2 \rangle$. This is really useful, because the differential becomes a simple arithmetic operator in Fourier space. Calling the streamwise separation vector r_x as Δx, it is possible to compute derivatives in r_x direction as:

$$\frac{\partial \langle \delta u^2 \rangle}{\partial r_x} (\Delta x, \Delta z, y_1, y_2) =$$
$$\frac{1}{n_f} \sum_{t=0}^{n_f} \sum_{h=-N_x/2}^{N_x/2} \sum_{l=-N_z/2}^{N_z/2} -i\alpha_0 \langle \hat{\delta u^2} \rangle (\alpha, iy1, iy2, \beta, t) \, e^{i\alpha_0 ht} e^{i\beta_0 lt} \tag{4.16}$$

While derivative in r_z as:

$$\frac{\partial \langle \delta u^2 \rangle}{\partial r_z} (\Delta x, \Delta z, y_1, y_2) =$$
$$\frac{1}{n_f} \sum_{t=0}^{n_f} \sum_{h=-N_x/2}^{N_x/2} \sum_{l=-N_z/2}^{N_z/2} -i\beta_0 \langle \hat{\delta u^2} \rangle (\alpha, iy1, iy2, \beta, t) \, e^{i\alpha_0 ht} e^{i\beta_0 lt} \tag{4.17}$$

Derivatives in the wall-normal direction separation r_y as well as the wall-normal direction derivative in Y_c $\left(\frac{\partial \langle u^2 \rangle}{\partial Y_c} \right)$, can't be computed in Fourier space, because wall-normal direction is a not homogeneous direction for the channel. First of all is necessary to apply transformation $(r_y, Y_c) \rightarrow (y_1, y_2)$. Derivatives can be computed as:

$$\frac{\partial}{\partial r_y} = \frac{1}{2}\left(\frac{\partial}{\partial y_2} - \frac{\partial}{\partial y_1}\right) \qquad\qquad \frac{\partial}{\partial Y_c} = \frac{1}{2}\left(\frac{\partial}{\partial y_2} + \frac{\partial}{\partial y_1}\right) \qquad (4.18)$$

Derivatives in y_1 direction and y_2 direction are computed using symmetries showed in section 4.2.4, through a finite difference scheme with a five point computational molecule. Considering a grid on $n_y + 1$ nodes y_j, with $0 \leq j \leq ny$, is possible to approximate the derivative with molecule centred in y_j as:

$$\mathcal{D}_n \left(f(y)\right)|_{y=y_j} = \sum_{i=-2}^{2} d_n^j(i) f\left(y_{j+i}\right) \qquad (4.19)$$

where $d_n^j(i)$ are the coefficients for the n-th derivative centred in y_j. To obtain an accuracy of 4-th order is necessary to derive the coefficients thinking about the error of discrete operator $d_4 d_0^{-1}$ decreases with step size according with power law with exponent -4. Is possible to derive coefficients in a proper way, following Pade' theory [36]. Choosing a set t_m of polynomials of y of increasing degree

$$t_m(y) = 1, y, y^2, ..., y^m \qquad (4.20)$$

Analytical derivatives are computed and a system of the following shape is derived:

$$d_j\left(t_m\right) - d_0\left(\mathcal{D}_j\left(t_m\right)\right) = 0 \qquad m = 0, ..., 8 \qquad (4.21)$$

where j is the derivative order. It is possible to obtain the coefficient d_0 by the normalization condition:

$$\sum_{i=-2}^{2} d_0(i) = 1 \qquad (4.22)$$

thus other coefficients are derived by applying eq. (4.21).

4.2.6 Algorithm

Algorithm is built so that three main loops can be recognized. The first loop is made on 200 fields saved through the DNS algorithm. Data from three different kinds of files are given as inputs into the algorithm:

1. Field files: velocity field file produced through DNS algorithm;

2. Pressure files: pressure field files computed through Poisson equation (eq. (3.15));

3. Mean velocity profile field components.

While values are read, there is the shift to Fourier space, through the FFT algorithm. Fluctuation field is computed by applying classical Reynolds decomposition of velocity field. The second loop is opened (*outer loop*) with $iy1$ going from -1 to $ny+1$. It is necessary to add a node to the boundaries of the domain, because a five point computational molecule is employed for the computation of derivatives in the wall-normal direction. The computation of the in-plane convolutions is made.

The third loop is opened (*inner* loop), ranging $iy2$ from $iy1$ to $ny - iy1$. For a given $iy1$, for every $iy2$, double and triple correlations are computed in Fourier's space, using Parseval's theorem. Returning to the physical space through the IFT algorithm, correlation computed are grouped together to form turbulent contribution of the fluxes terms and of the source term. At this point the derivative in homogeneous directions are computed to build up the viscous part of the scale fluxes Φ_{rx} and Φ_{rz}. When the inner loop is closed, the data are saved in a specific structure averaging the upper and the lower part of the channel and averaging in time. The outer loop is closed and a new field is loaded to recompute the GKE terms. The last part of the algorithm performs derivatives $\frac{\partial}{\partial r_y}$ and $\frac{\partial}{\partial Y_c}$, to build the viscous part of Φ_{ry} and Φ_c.

4.2.7 Parallelization

One of the most relevant feature of the code is that it is possible to use a *parallelization strategy*. The plan of action used inside this program is to perform a *shared memory* parallelization strategy in x and z directions. For this kind of implementation, all the *threads* "see" at the beginning of the process the same memory. This kind of parallelization strategy is the most used when a Fourier discretization is deployed. In order to perform such a discretization a thread must see all the variables of the field. Despite the misleading name *shared memory*, the memory is not shared while all the threads are running, but only when a barrier is made by the programmer that *syncs* all processes at one point of the program and forces computed variables on the cache memory to return on the RAM.

4.3 Comparison with the previous implementations

During the most recent years other implementations of the GKE were written to perform the energetic analysis of the simple channel flow. The most advanced was the one used by Cimarelli in articles [19],[37],[38] and [20]. Data was made available by the author, thus it is possible to make a comparison of computational costs, to highlight how fast the tool, which is implemented in the present workm is. Cimarelli's implementation did not have the feature of this code (use of symmetries, expansion of each term of the equation in much simpler convolutions) and computed only the $3D$ spaces, hence (r_x, r_z, Y_c) space, or (r_x, r_y, Y_c) space. Considered the former space, with separations of $r_x = 250$ and $r_z = 125$, the time for computing correlations in one plane was of 2.7 seconds, considering that averages in x and z directions were made through undersampling of 4 nodes. Analysing 64 planes in the wall-normal direction and averaging 100 fields in time, for the computation of every term of the GKE in extended space (r_x, r_z, Y_c), Cimarelli's implementation would require 286 minutes, an equivalent of almost 5 hours, without using a parallelization strategy. The tool presented in this work computes the whole $4D$ space (r_x, r_y, r_z, Y_c) with a number of points considered of $384 \times 256 \times 384 \times 128$ averaging 200 time samples in 24 hours on 64 cores in shared memory. Id we want to normalize this data in order to compare them with Cimarelli's implementation, consider that for each $r_x - r_z$ plane in full resolution this implementation

would require 1.63 seconds with a linear scaling on all the number of cores, while in Cimarelli's implementation (with a lower number of separations considered) would require 43 seconds, in full resolution. Considering the same resolution used in the database simulated in this work, time for computation of each plane would rise to 198 seconds.

Chapter 5

TKE and MKE analysis

The TKE and MKE budget equations offer us deep insight regarding the behaviour of turbulent flows. This great volume of information, calls for a detailed analysis in order to try at clarify how energy is transferred through the flow. In this chapter data from DNS database will be used to try to understand how fluctuations and mean flow interact among themselves and how a successful active drag reduction technique can affect this mechanism. To develop this analysis, only one case for each drag reduction technique will be taken into account. For streamwise travelling waves of spanwise wall velocity we will consider the case TW1, while for damping of the near-wall spanwise fluctuations the case BF20 would be considered. Both simulations were performed at $Re_\Pi = 6500$ and details about the parameters chosen can be found in table 3.3 and table 3.2. Further results for the other simulated cases can be found in appendix B.

5.1 TKE and MKE budgets

Recalling eq. (2.26) and eq. (2.28), each term is computed taking into account the average of 200 velocity fields obtained through the DNS tool thus all parameters of space discretization are the same ones for DNS computation. Being in statistically stationary case, unsteady terms cancel out. The tool used is a simple parallelized script, written in CPL language, that makes wide use of Parseval's theorem. Considering the channel flow, eq. (2.26) for the TKE budget can be rewritten in the following way:

$$
\underbrace{\xi}_{\text{source}} = \underbrace{\langle uv \rangle \frac{\partial U}{\partial y}}_{\text{turbulent production } (P_{uv})} - \underbrace{\nu \left\langle \frac{\partial u_i}{\partial x_j} \frac{\partial u_i}{\partial x_j} \right\rangle}_{\text{pseudo dissipation } (\epsilon)}
$$

$$
\underbrace{\Phi}_{\text{flux}} = - \underbrace{\frac{1}{2} \langle v u_i^2 \rangle}_{\text{turb. transport } (\phi_t)} + \underbrace{\frac{\nu}{2} \frac{\partial \langle u_i^2 \rangle}{\partial y}}_{\text{viscous diffusion } (\phi_\nu)} - \underbrace{\langle vp \rangle}_{\text{pressure transp } (\phi_p)}
$$

$$
\left. \right\} \quad \frac{d\Phi}{dy} = \xi \quad (5.1)
$$

while eq. (2.28) for MKE budget can be rewritten as:

$$
-\underbrace{u\frac{dp}{px}}_{\text{Pumping}(\Pi_p)} =
$$

$$
-\underbrace{\langle uv\rangle \frac{\partial U}{\partial y}}_{\text{turbulent production } (P_{uv})} -\frac{\partial}{\partial y}\underbrace{(\langle uv\rangle U)}_{\text{turbulent transport}(\phi_t)} +\frac{\partial}{\partial y}\underbrace{\nu\left(U\frac{\partial U}{\partial y}\right)}_{\text{mean flow transport}(\phi_\nu)} -\underbrace{\nu\left(\frac{dU}{dy}\right)^2}_{\text{MKE dissipation rate}(\Phi_{\overline{U}})}
$$

$$(5.2)$$

From a theoretical point of view spanwise velocity must be zero, because z is a homogeneous direction. Looking at DNS computation some numerical noise can be seen, but since it is several orders of magnitude weaker than other terms, every term containing W (the spanwise mean velocity component) can be neglected. During the computations, the average of each term of the budget equations is calculated in homogeneous directions, such that the only dependency is the one in the wall-normal direction.

5.1.1   Reference channel flow

Considering the reference channel flow case, analysis of each term of the TKE budget equation can be seen in fig. 5.1. The peak of production is located at $y^+ = 11.59$, precisely in the region addressed in the classical subdivision of the channel as the *buffer layer*. This is the zone in which most of the *ejection* and *sweep* events would happen, giving a positive contribution (through the term $\langle uv\rangle$) to production (for experimental evidence see [39] and [40]). Dissipation is evidently very high near the wall, where viscosity plays an important role. On the other hand there seems to be a plateau corresponding to the beginning of the *buffer layer* (the derivative of pseudo dissipation term is almost zero for $y^+ \approx 7$). Here production mechanisms start to overwhelm the dissipative one, resulting in a surplus of turbulent kinetic energy that must be redistributed throughout the channel. Moving along the bulk of the flow, production and dissipation are almost balanced, and fluxes are constant, as is evident from the zero-derivative of the flux terms. A better overview of how TKE is redistributed in the flow is given by fig. 5.2.
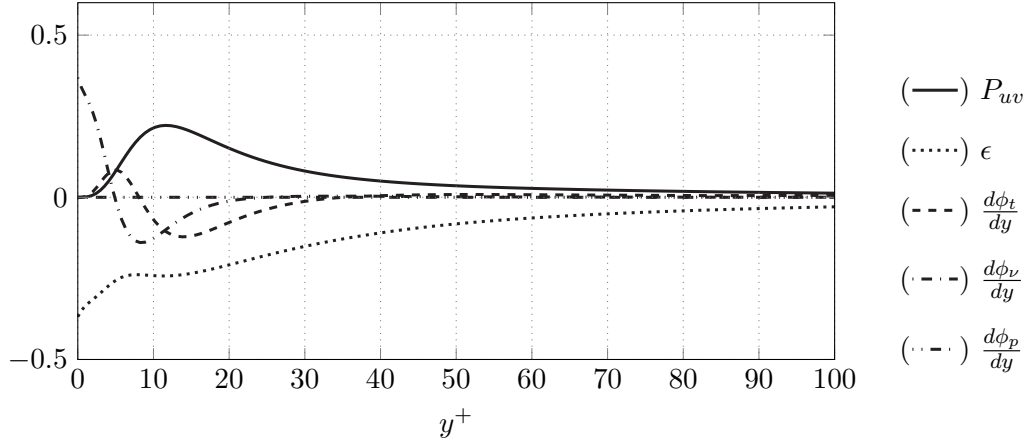
Figure 5.1: Terms of the TKE budget equation for the reference channel flow (REF with $Re_\Pi = 6500$ and $Re_\tau = 199.7$) with respect to the wall-normal direction. Both the magnitude of the terms and the wall-normal direction are in viscous units. In the plot: production term (P_{uv}), pseudo-dissipation (ϵ), derivative of the turbulent transport ($\frac{d\phi_t}{dy}$), of the viscous diffusion ($\frac{d\phi_\nu}{dy}$) and of the pressure transport ($\frac{d\phi_p}{dy}$) terms.
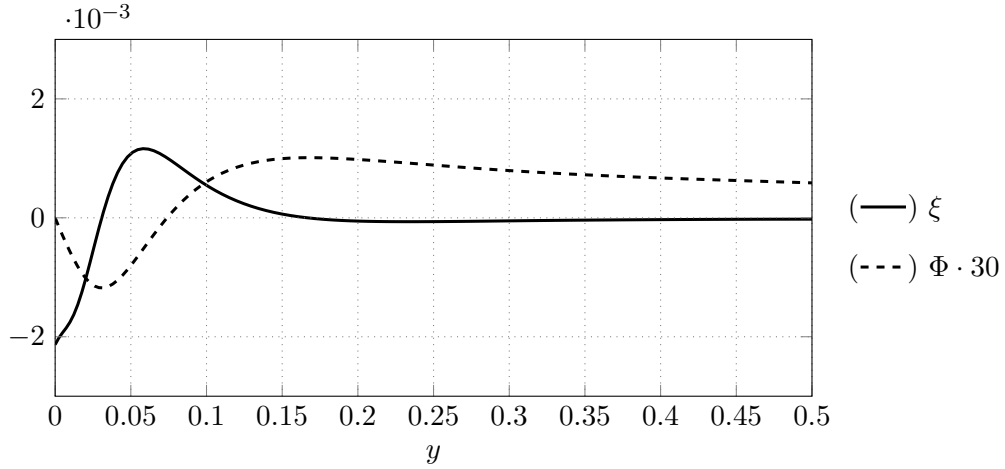
Figure 5.2: Source and global flux terms for the TKE budget equation of the reference channel flow (REF with $Re_\Pi = 6500$ and $Re_\tau = 199.7$) with respect to the wall-normal direction. Both the magnitude of the terms and the wall-normal direction are in power units, therefore in Π units.

Around the peak, the production term (P_{uv}) is substantially larger than pseudo dissipation (ϵ) and, the TKE global flux (Φ) , contributes to the energy supply of regions below and above. Negative values of flux below the source peak mean that it is directed towards the wall. In the regions above the peak, the flux is positive, so it is directed towards the bulk of the flow. In the logarithmic region, instead, the production– dissipation ratio is nearly one and the flux is almost constant. The energy carried through this region is used for sustaining the fluctuations in the bulk region of the flow.

The Mean Kinetic Energy budget gives almost the same information as the Turbulent Kinetic Energy budget. Mean flow and fluctuations interact through the production term which is the same in fig. 5.1 and fig. 5.3. Part of the Mean Kinetic Energy pumped through the pumping term goes into fluctuations production and another part dissipates through mean flow dissipation towards the wall.
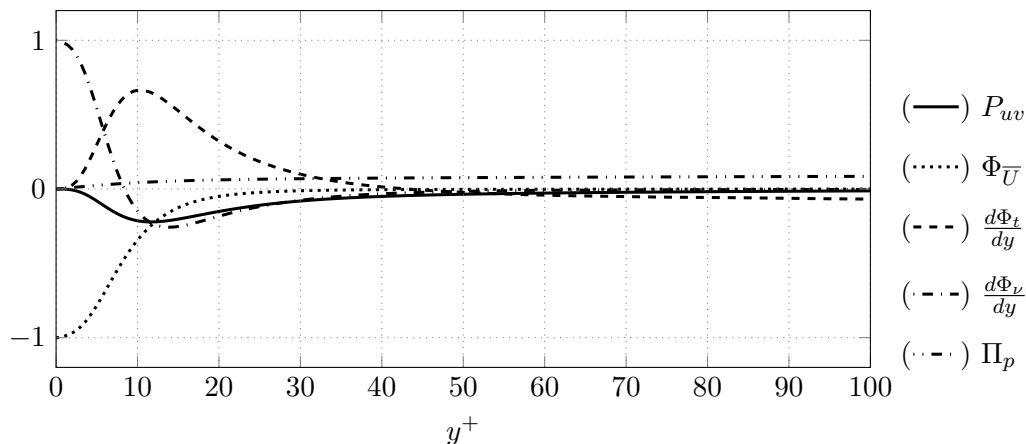
Figure 5.3: Terms of the MKE budget equation for the reference channel flow (REF with $Re_\Pi = 6500$ and $Re_\tau = 199.7$) with respect to the wall-normal direction. Both the magnitude of the terms and the wall-normal direction are in viscous units. In the plot: production term (P_{uv}), mean flow dissipation ($\Phi_{\overline{U}}$), derivative of the turbulent transport term ($\frac{d\Phi_t}{dy}$), derivative of the viscous diffusion term ($\frac{d\Phi_\nu}{dy}$) and the pumping term (Π_p).

5.1.2 Damping of the near-wall spanwise fluctuations

Employing the damping of the near-wall spanwise fluctuations drag reduction strategy, the production peak is shifted away from the buffer layer, towards the bulk of the flow, and its magnitude is weakened (fig. 5.4 and fig. 5.5). The TKE terms analysis shows that the peak of production is at $y/h = 0.177$ (in viscous units $y^+ = 29.555$). In the reference channel flow case (REF) the peak is located at $y/h = 0.058$ (in viscous units $y^+ = 11.58$). The magnitude of the peak is lowered i.e. the ratio between the peak of the damping strategy flow and the one of the reference channel flow in viscous units is $P^+_{20,max}/P^+_{REF,max} = 0.76$. An explanation for the shift of the production peak is that the layer, where the spanwise fluctuations are cancelling out, could be seen as a displacement of the wall equal to the thickness of the forcing region. Shifting the production trend towards the wall (fig. 5.5), the production peaks of the reference channel flow and of the damping strategy nearly are located at the same wall-normal coordinate in viscous units (the difference between them is of $\Delta y^+ = 2.034$ with an error margin of almost 20%). This analysis method can be further improved. It is possible to observe that the production term is zero at the wall due to the no-penetration condition (term $\langle uv \rangle$ must be zero). From fig. 5.5 it is possible to see that this doesn't happen in the case of shifting, but one can also observe that in

the case of not shifted profile, a plateau is present at $y^+ \approx 18$. This plateau does not correspond to zero because of fluctuations generated by the divergence free constraint applied to the force. The attempt to make two peaks of the controlled and uncontrolled cases coincide, brings back the no penetration condition at the wall also for the uncontrolled case (fig. 5.6). It is possible to rewrite the translation in a way that takes into account this constraint. The pseudo dissipation term and its derivative are not zero at the wall and in all of the forcing region because the divergence free constraint is imposed to the force, causing the components of the fluctuation in x and z directions, which contribute to the pseudo dissipation term. Therefore, the production term and fluxes terms are not zero in the damping zone, instead fluctuating around zero. Starting from $y^+ = 20$, the reference channel flow fluxes trend is recovered. Surplus of Turbulent Kinetic Energy is redistributed throughout the channel, partly being carried by fluxes towards the wall, and partly being carried towards the bulk region of the flow, to sustain fluctuations.
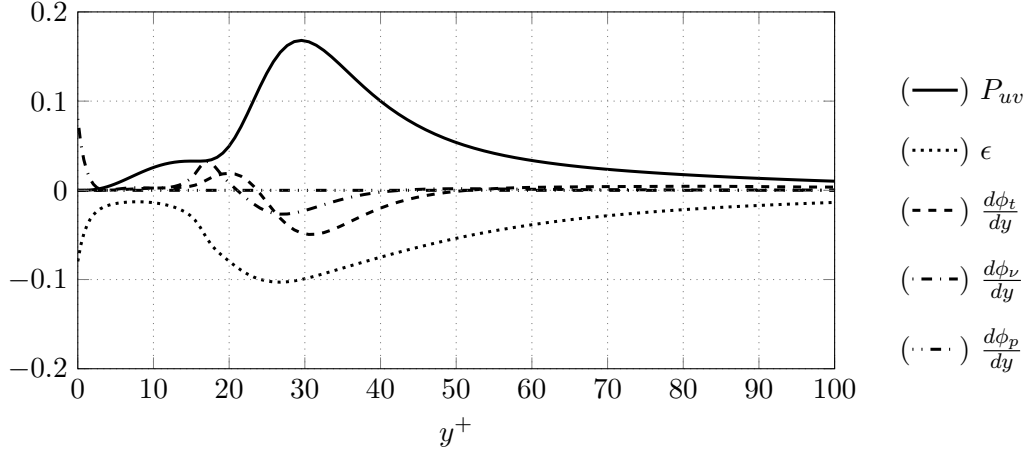
Figure 5.4: Terms of the TKE budget equation for the channel flow with damping of the near-wall spanwise fluctuations drag reduction strategy (BF20 of table 3.2 with $Re_\Pi = 6500$ and $Re_\tau = 166.73$) with respect to the wall-normal direction. Both the magnitude of the terms and the wall-normal direction are in viscous units. In the plot: production term (P_{uv}), pseudo-dissipation (ϵ), derivative of the turbulent transport ($\frac{d\phi_t}{dy}$), of the viscous diffusion ($\frac{d\phi_\nu}{dy}$) and of the pressure transport ($\frac{d\phi_p}{dy}$) terms.
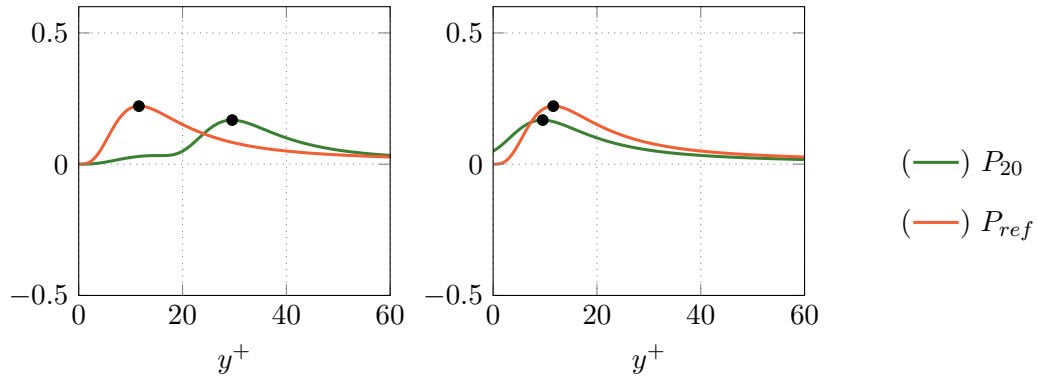
Figure 5.5: Production term of the TKE budget equation for the reference channel flow (REF of of table 3.1) and for the channel flow with damping of the near-wall spanwise fluctuations drag reduction strategy (BF20 of table 3.2) in viscous units. On the right production profile of drag reduction case is shifted of $\Delta y^+ = 20$ away from the wall. The peak of the production term is stressed with a black mark.
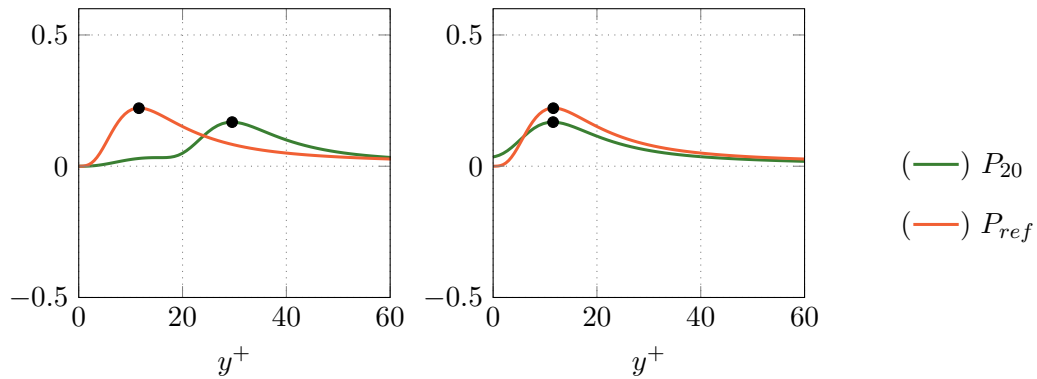
Figure 5.6: Production term of the TKE budget equation for the reference channel flow (REF of of table 3.1) and for the channel flow with damping of the near-wall spanwise fluctuations drag reduction strategy (BF20 of table 3.2) in viscous units. On the right production profile of drag reduction case is shifted of $\Delta y^+ = 18$ away from the wall. The peak of the production term is stressed with a black mark.
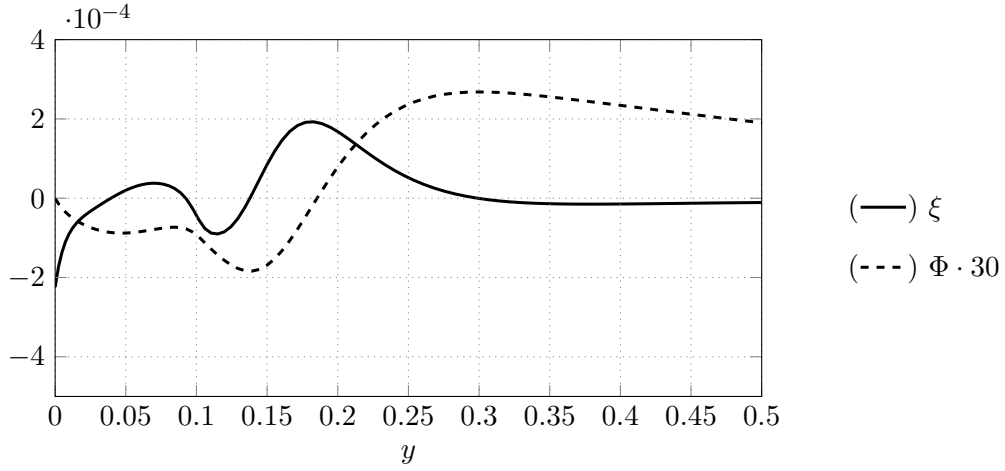
Figure 5.7: Source and global flux terms of the TKE budget equation for the channel flow with damping of the near-wall spanwise fluctuations drag reduction strategy (BF20 of table 3.2 with $Re_\Pi = 6500$ and $Re_\tau = 166.73$) with respect to the wall-normal direction. Both the magnitude of the terms and the wall-normal direction are in power units, therefore in Π units.

Figure 5.8: Terms of the MKE budget equation for the channel flow with damping of the near-wall spanwise fluctuations drag reduction strategy (BF20 of table 3.2 with $Re_\Pi = 6500$ and $Re_\tau = 166.73$) with respect to the wall-normal direction. Both the magnitude of terms and the wall-normal direction are in viscous units. In the plot: production term (P_{uv}), mean flow dissipation ($\Phi_{\overline{U}}$), derivative of the turbulent transport term ($\frac{d\Phi_t}{dy}$), derivative of the viscous diffusion term ($\frac{d\Phi_\nu}{dy}$) and pumping term (Π_p).

5.1.3 Streamwise travelling waves of spanwise wall velocity

From the analysis of the terms of the TKE budget equation for the channel flow with streamwise travelling waves of spanwise wall velocity strategy, it appears that the control strategy decreases the production peak (for the case TW1 the ratio in viscous units it is $P^+_{TW1,max}/P^+_{REF,max} = 0.93$), shifting it slightly away from the wall (the peak position for TW1 in viscous units is $y^+ = 16.59$, shifted by $\Delta y^+ = 5$ with respect to the reference channel flow case). The results seem to be exactly the same as in the damping layer method application, the production term is shifted and lowered. Differently from the damping layer method and the reference case, the sum of fluxes is not zero at the wall. This is due to the fact that the boundary condition is different. At the wall, a streamwise wave of spanwise velocity is imposed. This can be written:

$$w = A \cdot Re\left[e^{ik_x(x-ct)}\right] \tag{5.3}$$

This wave produces a thin, unsteady and spanwise-modulated boundary layer called Generalized Stokes Layer (GSL). This spanwise turbulent stokes layer which is generated is relatively similar to the laminar one. Energy which is invested in the flow through the boundary condition, must be transferred towards the bulk of the flow. Therefore positive fluxes are generated at the wall. This positive flux mainly result from the viscous transport term.
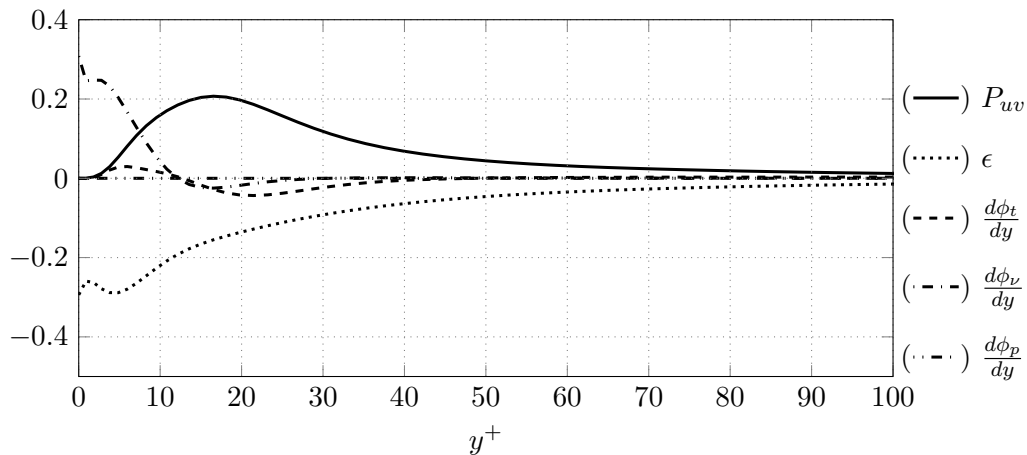
Figure 5.9: Terms of the TKE budget equation for the channel flow with streamwise travelling waves of spanwise wall velocity (TW1 of table 3.3 with $Re_\Pi = 6500$, $Re_\tau = 186.48$) with respect to the wall-normal direction. Both the magnitude of the terms and the wall-normal direction are in viscous units. In the plot: production term (P_{uv}), pseudo-dissipation (ϵ), derivative of the turbulent transport ($\frac{d\phi_t}{dy}$), of the viscous diffusion ($\frac{d\phi_\nu}{dy}$) and of the pressure transport ($\frac{d\phi_p}{dy}$) terms.
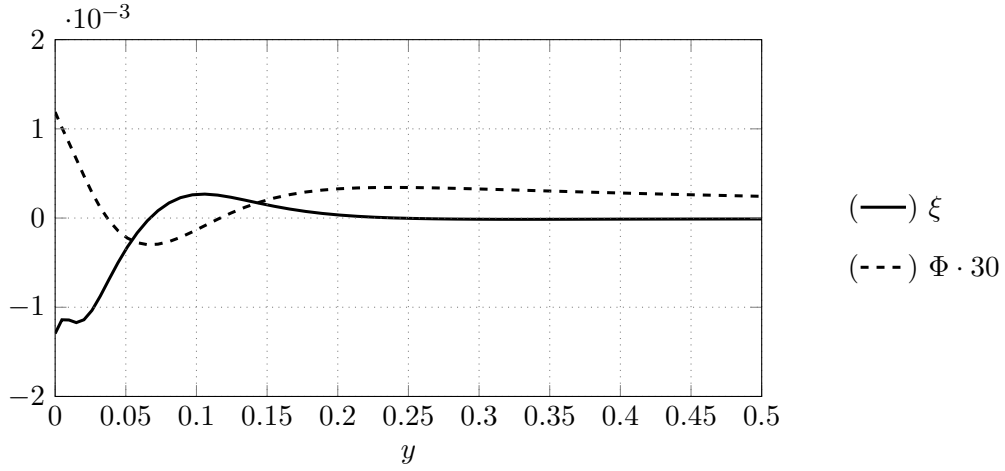
Figure 5.10: Source and global flux terms of the TKE budget equation for the channel flow with streamwise travelling waves of spanwise wall velocity (TW1 of table 3.3 with $Re_\Pi = 6500$, $Re_\tau = 186.48$) with respect to the wall-normal direction. Both the magnitude of the terms and the wall-normal direction are in power units, therefore in Π units.
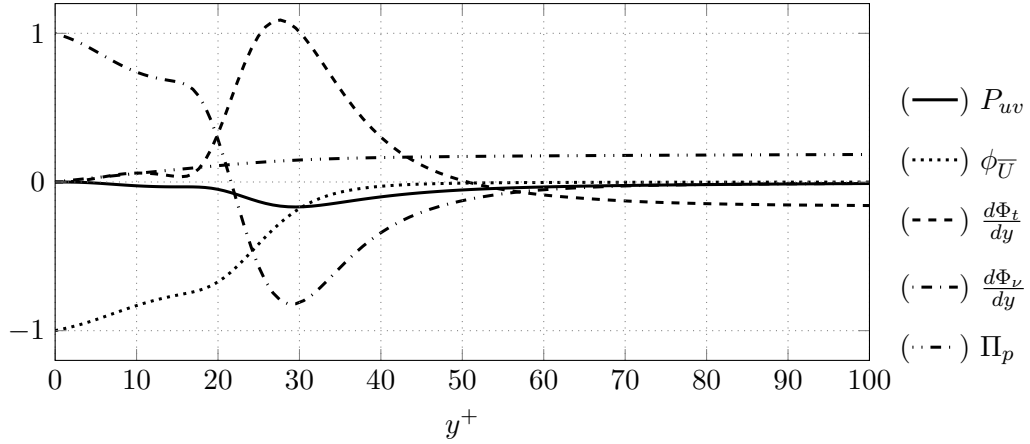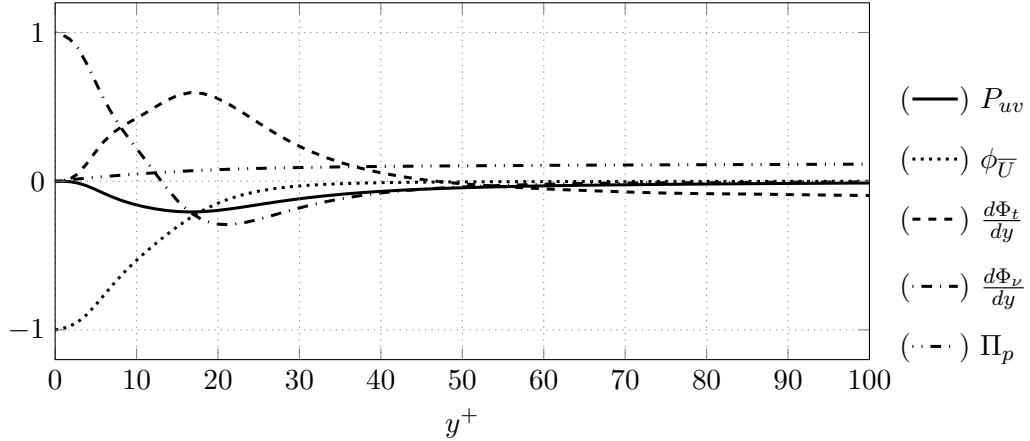

Figure 5.11: Terms of the MKE budget equation for the channel flow with streamwise travelling waves of spanwise wall velocity (TW1 of table 3.3 with $Re_\Pi = 6500$, $Re_\tau = 186.48$) with respect to the wall-normal direction. Both magnitude of the terms and the wall-normal direction are in viscous units. In the plot: the production term (P_{uv}), the mean flow dissipation ($\Phi_{\overline{U}}$), the derivative of the turbulent transport term ($\frac{d\Phi_t}{dy}$), the derivative of the viscous diffusion term ($\frac{d\Phi_\nu}{dy}$) and the pumping term (Π_p).

5.1.4   Lessons learned from TKE and MKE analysis

From the analysis of TKE and MKE budget equations, a common pattern in all the channel flows can be seen. With or without drag reduction, energy fluxes work as a vector which supplies energy to the fluctuations to the bulk of the flow and towards the wall, starting from the peak of production of TKE. Table 5.1 and fig. 5.12 prove that control is effective at reducing production peaks and moving them away from the wall. Furthermore it seems this characteristic to be related to the reduction of Re_τ. The way in which the production peak is shifted away

from the wall depends on the *physics* behind the drag reduction strategy. In the case of damping layer of the near-wall spanwise fluctuations, it was proved that applying force is similar to adding a displacement to the wall equal to the forcing layer's thickness. The peak will then be shifted approximately by this length. The streamwise travelling waves of spanwise wall velocity strategy acts in such a way which causes a Generalized Stokes Layer to be created, such that the peak is thought (but it is not still proved) to be shifted away from the wall approximately by the thickness of the Generalized Stokes Layer.

An increase of U_b implies a successful drag reduction technique, because it means that the flow rate is increased. From table 5.1 one can see that the more drag reduction strategy increases U_b, the more the production peak is reduced.

Looking at the TKE budget in simple channel flow and in the case of damping layer of the near-wall spanwise fluctuations, it appears that single contributions to the flux, follow the trend of the global flux, being approximately zero at the wall, negative before the production peak and positive afterwards. In the travelling waves cases, the global flux is positive at the wall, due to the viscous contribution applied by the presence of the Generalized Stokes Layer.
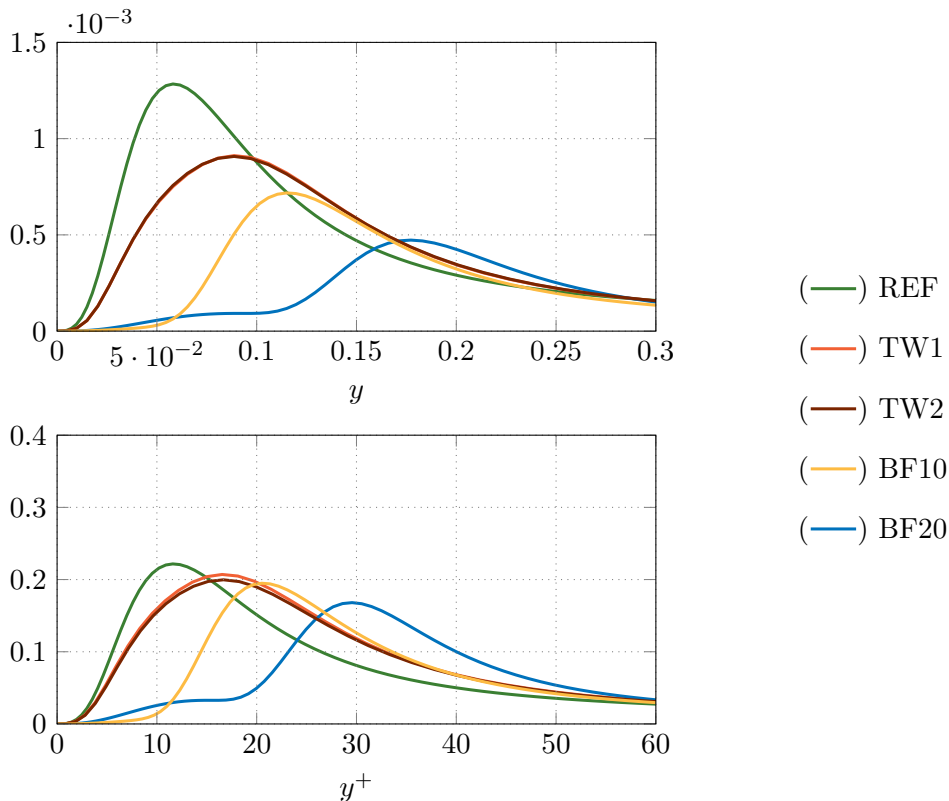
Figure 5.12: Comparison of the production terms for the cases of the present database.

Case	Re_Π	Re_τ	P_{max}^+	$P_{max}^+/P_{max,ref}^+$	P_{max}	y^+	y/h	U_b
REF	6500	199.7	0.221	1	0.00128	11.58	0.058	0.488
BF20	6500	166.73	0.168	0.76	0.00047	29.55	0.177	0.700
BF10	6500	178.34	0.195	0.88	0.00072	20.510	0.115	0.612
TW1	6500	186.48	0.207	0.93	0.00091	16.59	0.089	0.559
TW2	6500	187.96	0.202	0.78	0.00091	16.72	0.089	0.560

Table 5.1: Resume of the maxima of production for the simulations in present work's database.

5.2 Integral budget

5.2.1 Energy box

It is useful to inspect more in depth how energy supplied to the system through the pumping term, is utilized by the flow. In the case of statistical equilibrium, a balance between the energy pumped into the system and the energy dissipated must be reached. The dissipation can be split into two contributions. One is due to the mean flow and one is due to the fluctuations:

$$D = D_{\overline{U}} + \epsilon \tag{5.4}$$

The aim of the present study is to understand how control affects energy transfer and dissipation (referring to the sum of fluctuation term and mean flow term). In order to obtain these information, it is necessary to integrate the TKE and MKE budget equations along the channel height (eq. (5.1),eq. (5.2)). Therefore it is necessary to apply the operator defined in [24]:

$$[f]_g = \int_0^{2h} f \, dy. \tag{5.5}$$

Considering first the MKE budget equation, it is possible to obtain:

$$\underbrace{\left[u\frac{dp}{dx}\right]_g}_{P_p} = \underbrace{\left[\langle uv\rangle\frac{dU}{dy}\right]_g}_{P_{uv}} + \underbrace{\left[\nu\left(\frac{dU}{dy}\right)^2\right]_g}_{D_{\overline{U}}} \tag{5.6}$$

$$P_p = P_{uv} + D_{\overline{U}}. \tag{5.7}$$

It turns out that the power input into the system must be balanced by the dissipation of the mean flow and production of fluctuating field.
In the case of TKE budget equation, integral budget turns out to be:

$$\underbrace{\left[\nu\left\langle\frac{\partial u_i}{\partial x_j}\frac{\partial u_i}{\partial x_j}\right\rangle\right]_g}_{\epsilon} = \underbrace{\left[\langle uv\rangle\frac{dU}{dy}\right]_g}_{P_{uv}} \tag{5.8}$$

$$\epsilon = P_{uv} \pm P_c. \tag{5.9}$$

Therefore dissipation must balance the production term and the control power. The contribution of the control power can be positive or negative, depending on the control technique used. Furthermore it can be implicitly or explicitly contained into the TKE budget equation or rise from boundary conditions.

It is possible to make a comparison between reference channel flow and two control strategies, through *energy box* representation, as shown in fig. 5.13, fig. 5.14 and fig. 5.15. Three simulations were performed with a CPI strategy and for this reason the pumping power has been chosen as the normalization parameter.

In the case of the reference channel flow (fig. 5.13), 58.9% of the pumping power $P_p = 0.000922$ ($P_p^+ = 31.8$) is dissipated through the mean flow, while the other 41% goes into production term. Considering the latter, all the energy input is dissipated by the fluctuations.
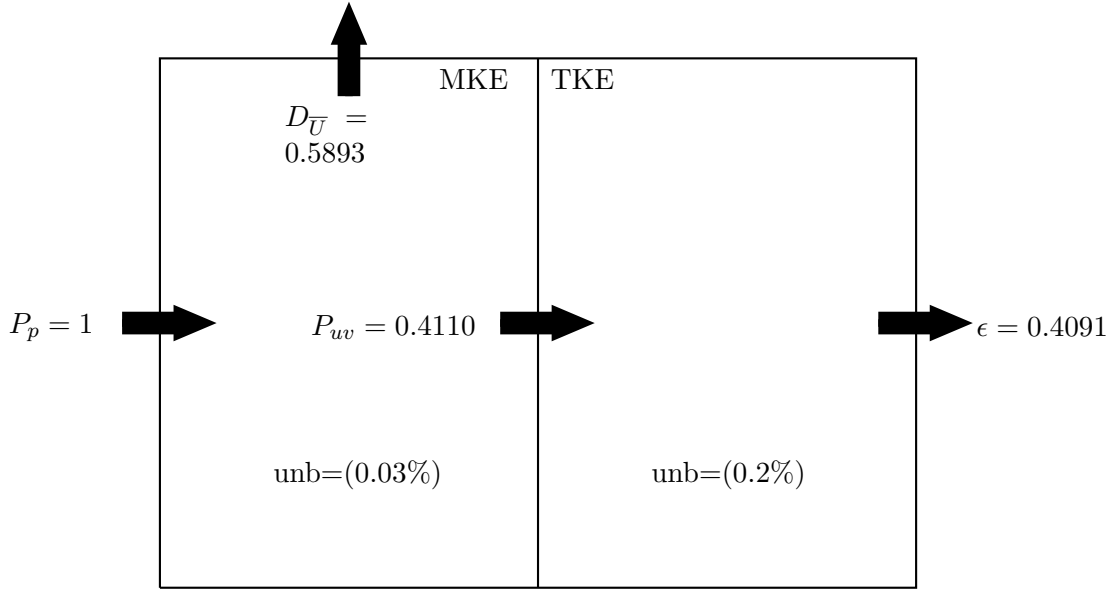
Figure 5.13: Energy box representation for the reference channel flow (REF, $Re_\Pi = 6500$, $Re_\tau = 199.7$). Unbalance is due to the terms neglected from the budgets. All values are normalized with respect to the pumping power, since all the simulations of the database are run with a CPI strategy.

The damping layer of the spanwise wall velocity has the characteristic that no power is necessary to apply the control. Instead the power is subtracted from the system, as is possible to see in the energy box in fig. 5.14. Power subtracted by the control is gained by the integration of an additional term that can be added to the rhs of the TKE budget equation. This term can be written as:

$$P_c = \left[-\alpha \left\langle w^2 \right\rangle \right]_g \tag{5.10}$$

The control changes substantially the energy box. 81.05% of the pumping power $P_p = 0.000920$ ($P_p^+ = 54.5$) is dissipated through the mean flow, indicating an increase of 37.6% with respect to the reference channel flow case. An additional 18.9% of the pumping power goes into the production of the fluctuating field, showing a decrease of 53.9% with respect to the reference case. This is a consequence of the subtraction of 0.4% of the pumping power from the fluctuating field, due to the damping layer that cancels fluctuations. This affects also the dissipation of the fluctuating field that changes from 40.9% of the reference channel flow case to 18.2%, demonstrating a decrease of 55.4%.
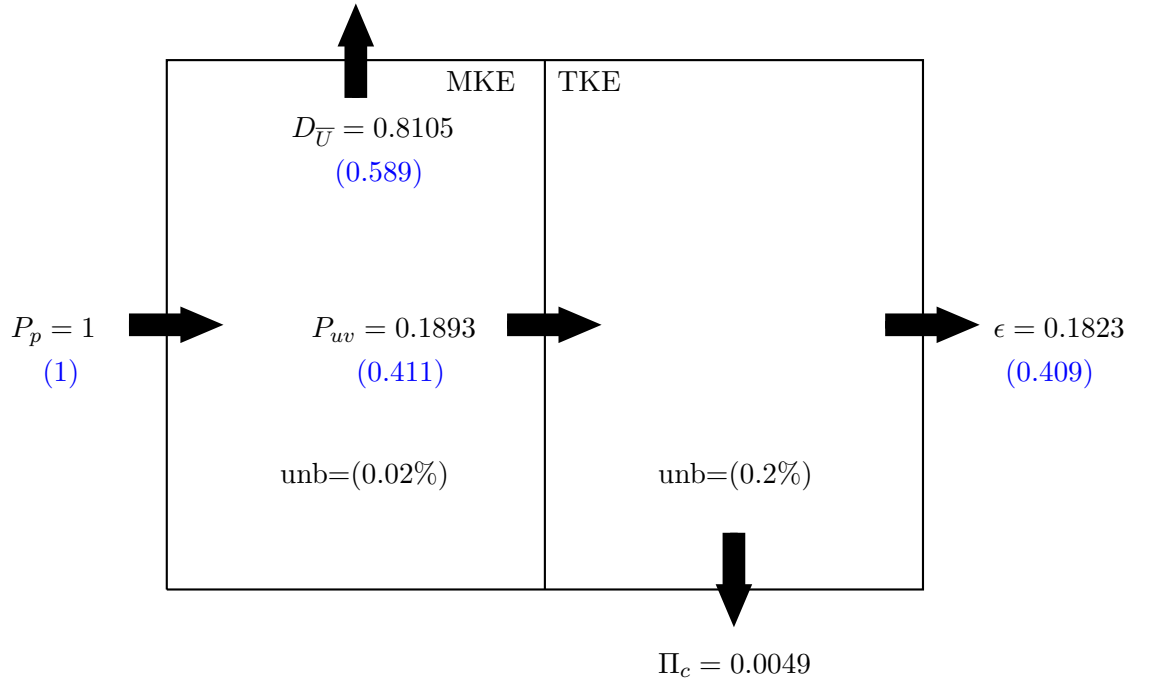
Figure 5.14: Energy box representation for the channel flow with damping of the near-wall spanwise fluctuations strategy (BF20,$Re_\Pi = 6500$, $Re_\tau = 166.73$). The Unbalance is due to the terms neglected from the budgets. All values are normalized with respect to the pumping power, since all the simulations of the database are run with a CPI strategy. The blue numbers indicate values for the reference channel flow.

Looking at the streamwise travelling wave of spanwise wall velocity strategy, we can see that 63.4% of the pumping power $P_p = 0.000922$ ($P_p^+ = 39$) is actually dissipated through the mean flow, indicating an increase of 7.7% with respect to the reference case. An additional 18.9% of the pumping power goes into production of the fluctuating field, demonstrating a decrease of 10.8% (fig. 5.15). Differently from the damping layer technique, this control strategy needs power supply to work properly. The power invested in control participates in the TKE budget equation through the integral of the viscous diffusion. This term is no negligible anymore due to the GSL generated by the spanwise wall velocity. This causes a rise of the dissipation resulting from the fluctuations which increase from 40.9% of

pumping power to 44.9%, demonstrating an increase of 9.9% with respect to the reference channel flow.
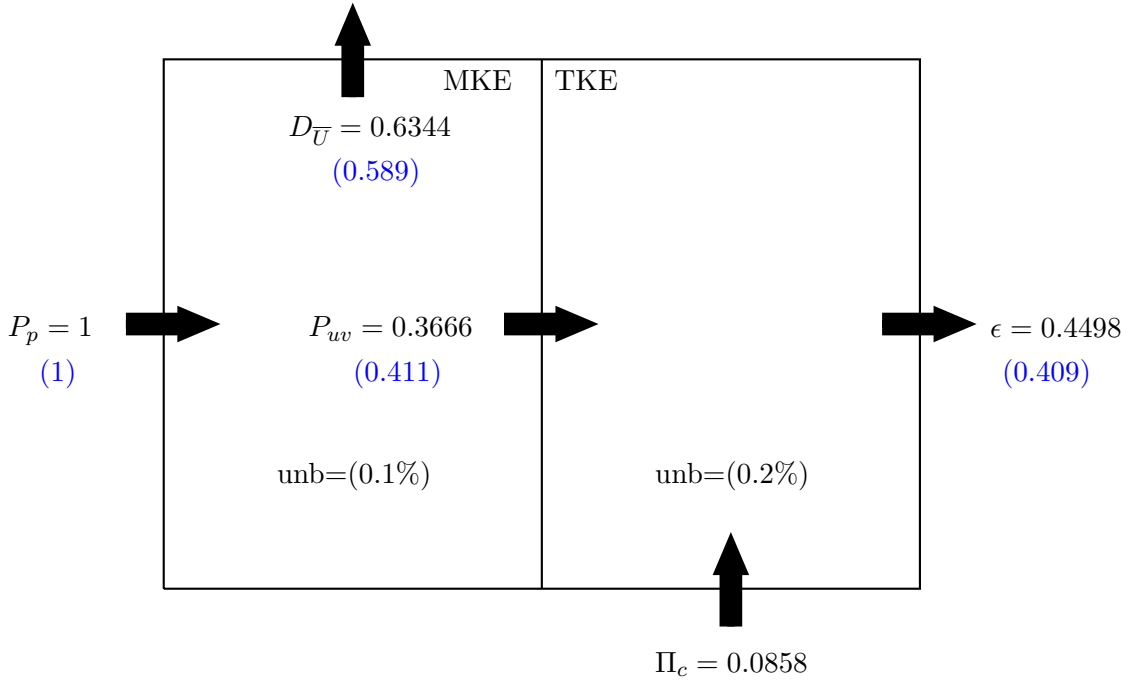
Figure 5.15: Energy box representation for the channel flow with streamwise travelling waves of spanwise wall velocity drag reduction technique (TW1,$Re_\Pi = 6500$, $Re_\tau = 186.48$). Unbalance is due to terms neglected from the budgets. All the values are normalized with respect to pumping power, since all the simulation of the database are run with a CPI strategy. The blue numbers indicate values for the reference channel flow.

A common feature of both drag reduction techniques is that they reduce the production of TKE and raise the dissipation which is connected to the mean flow. The dissipation due to the fluctuating field changes in a different way between the two drag reduction techniques. This last term deeply depends on the physics behind the drag reduction strategy. In the case of the streamwise travelling waves of spanwise wall velocity, the energy is input into the system and further dissipation is thus required to reach balance. In the case of damping of the near-wall spanwise fluctuations, the energy is subtracted by the control strategy. This reduces the dissipation term.

It can be useful to analyse different drag reduction techniques with different effectiveness (e.g: an increase in Re_b indicates that the flow rate is increased within the channel). Employing this analysis it might be possible to extrapolate a global trend which is independent from the physics behind drag reduction strategy and to try and understand if a certain drag reduction technique is successful in increasing dissipation.

5.2.2   Global trends

Analysis performed on components of the dissipation which are associated with the fluctuating field (ϵ) (fig. 5.17,fig. 5.16), do not lead to a clear conclusion regarding the dissipative behaviour of drag reduction techniques which aim to increase the effectiveness of the drag reduction by increasing Re_b. The fact that the dissipation component associated with the mean flow tends to increase while increasing Re_b (fig. 5.18), indicates that by knowing ϵ, the only component for which we can not extrapolate a global trend, the global dissipative behaviour of drag reduction techniques can be understood completely.
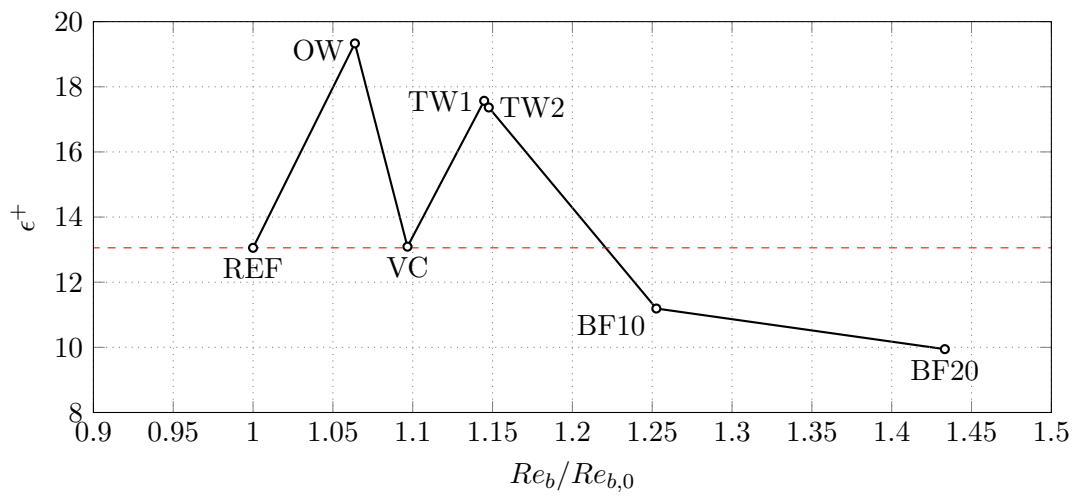
Figure 5.16: The component of the dissipation related to the fluctuating flow, in viscous units, for different drag reduction cases with respect to the ratio $Re_b/Re_{b,0}$. Details in table 5.2.
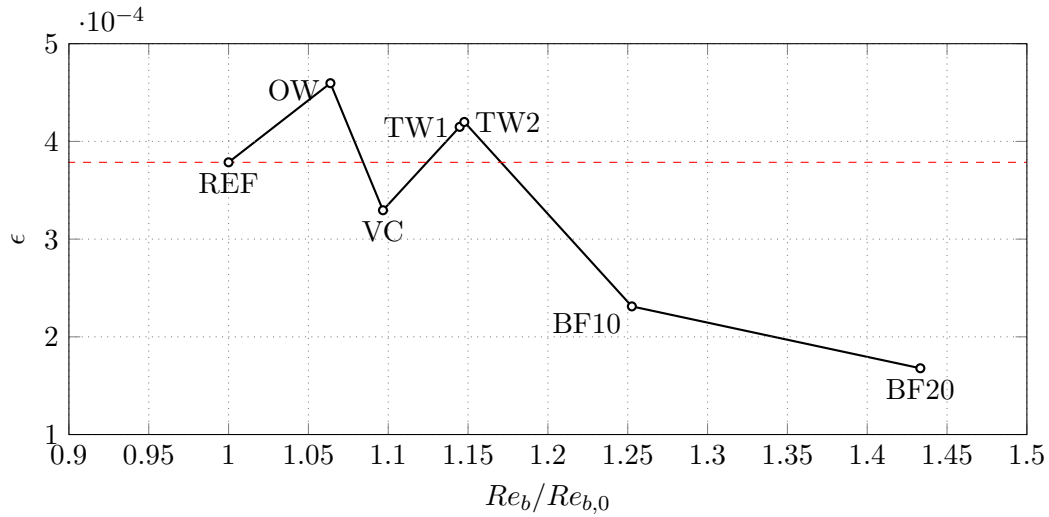
Figure 5.17: The component of dissipation related to fluctuating flow, in power units, for different drag reduction cases with respect to the ratio $Re_b/Re_{b,0}$. Details in table 5.2.
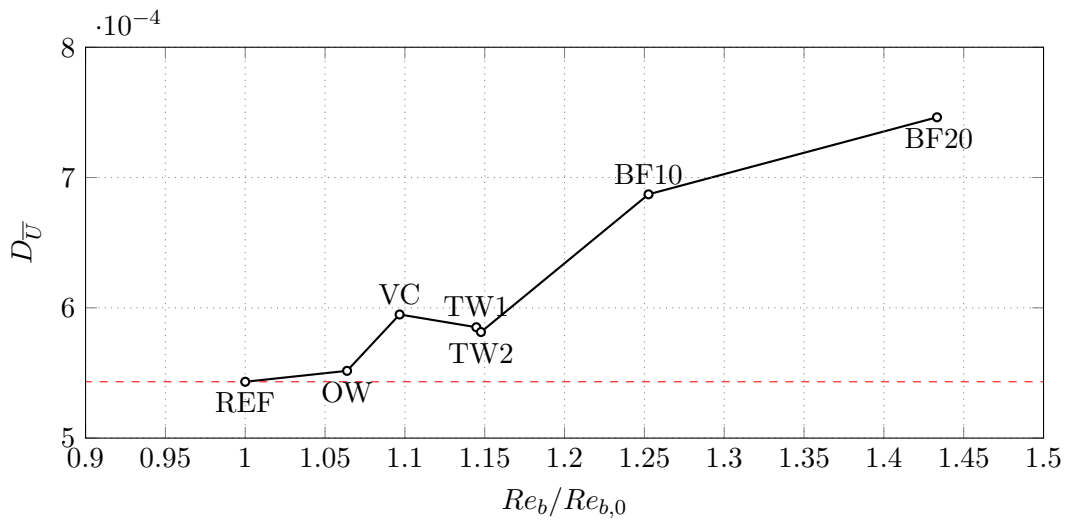
Figure 5.18: The component of dissipation related to the mean flow, in power units, for different drag reduction cases with respect to ratio $Re_b/Re_{b,0}$. Details in table 5.2.
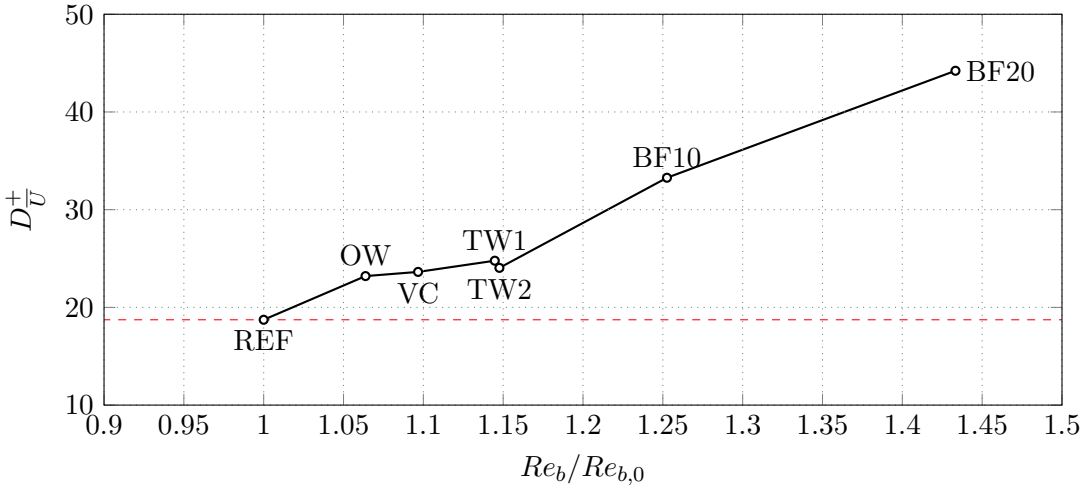
Figure 5.19: The component of the dissipation related to the mean flow, in viscous units, for different drag reduction cases with respect to the ratio $Re_b/Re_{b,0}$. Details in table 5.2.

Case		Re_Π	Re_b	Re_τ	$Re_b/Re_{b,0}$	U_b	P_p	P_p^+	$\Phi_{\overline{U}}$	$\Phi_{\overline{U}}^+$	P_{uv}	P_{uv}^+	ϵ	ϵ^+	Π_c
ref	CpPI	6500	3176.8	199.7	1	0.488	0.000923	31.82	0.00054	18.73	0.00038	13.08	0.00037	13.05	0
OW	CpPI	6500	3379.4	186.9	1.064	0.520	0.000923	38.83	0.00055	23.20	0.00037	15.63	0.00046	19.33	$8.99 \cdot 10^{-5}$
VC	CpPI	6500	3484	190.5	1.097	0.536	0.000922	36.63	0.00059	23.63	0.00033	13.02	0.00033	13.09	$3.19 \cdot 10^{-6}$
BF10	CpPI	6500	3979.22	178.34	1.25	0.612	0.000922	44.65	0.00068	33.26	0.00023	11.40	0.00023	11.19	$-2.57 \cdot 10^{-6}$
BF20	CpPI	6500	4553.23	166.73	1.43	0.700	0.000920	54.55	0.00074	44.21	0.00017	10.32	0.00017	9.94	$-4.52 \cdot 10^{-6}$
TW1	CpPI	6500	3636.62	186.48	1.144	0.559	0.000922	39.05	0.00058	24.77	0.00034	14.31	0.00041	17.56	$8.01 \cdot 10^{-5}$
TW2	CpPI	6500	3645.81	187.96	1.147	0.560	0.000923	38.15	0.00058	24.04	0.00034	14.11	0.00042	17.36	$9.62 \cdot 10^{-5}$

Table 5.2: Energy analysis for the data from the database computed in this work and the database used during ITI Bertinoro conference [6].

Chapter 6

Energy paths in a channel flow

The algorithm developed and exploited in chapter 4 has been used on fields generated from the DNS tool. In the following chapter the analysis made through the TKE and MKE budgets in chapter 5 is further expanded into an analysis which contains the different terms that compose the GKE in the space (r_x, r_y, r_z, Y_c). Fields resulting from the simulations REF, BF20 and TW1 are examined, in order to inspect in greater details which attributes of energy behaviour are affected by the control. Starting from the statements proposed by Cimarelli in [19] and [20] a detailed analysis of all the data from the simulations in spaces (r_x, r_z, Y_c) and (r_z, r_y, Y_c) is conducted.

6.1 The space (r_x, r_z, Y_c)

Equation 4.1 can be analysed in the plane $r_y = 0$ of the extended space. A new conservative form of the GKE can be written:

$$\frac{\partial \Phi_{r_x}(r_x, r_z, Y_c)}{\partial r_x} + \frac{\partial \Phi_{r_z}(r_x, r_z, Y_c)}{\partial r_z} + \frac{\partial \Phi_c(r_x, r_z, Y_c)}{\partial Y_c} = \psi(r_x, r_z, Y_c) \qquad (6.1)$$

Introducing the new *reduced-source* ψ:

$$\psi = \xi - \frac{\partial \Phi_{r_y}}{\partial r_y} \qquad (6.2)$$

In this section, the genuine source term (ξ) will be showed. The term $\frac{\partial \Phi_{r_y}}{\partial r_y}$ is related to the fluxes, which will be analysed in the space (r_z, r_y, Y_c) in the following sections. Inspecting the results for the reference channel flow (REF), it is possible to witness in fig. 6.1 to the complexity of the energetic paths into the three dimensional space. This information was completely absent while observing the terms of the one point TKE and MKE budget equations. The peak of the source term is located in the buffer region at the zero separation in the streamwise direction, $r_z = 0.196$ ($r_z^+ = 39.21$) in spanwise direction and at a wall-normal distance of $Y_c = 0.0580$ ($Y_c^+ = 11.59$). While the peak of the source of fluctuating field has already being identified using TKE budget equation (in section 5.1.1 the

peak of source term was measured at $y^+ = 11.58$), the separation at which it is located is a new information given by the GKE. For a comparison of the two results see fig. 6.3. The zone, for which an iso-surface at $\xi = 0.004$ is drawn and where is placed the peak of the source term of the GKE, is referred to by Cimarelli in [19] as the *Driving Scale Range* (DSR). Fluxes have only one singular point along their paths located at a wall-normal distance of $Y_c \approx 0.077$ ($Y_c^+ \approx 15.37$), zero streamwise separation and a spanwise separation of $r_z^+ \approx 55.916$. The fluxes originate from this point, transferring energy through extended physical-scale space. It is possible to see that the energy transferred towards the bulk of the flow follows a spiral path, originating from small structures before shifting towards the larger ones in the streamwise separations. This particular trend for the fluxes highlights the presence of a reversal cascade. This is a new and important result, which was impossible to reach using only the analysis of the one point TKE budget equation. At a certain point the energy paths bend towards the $r_x, r_z = 0$ axis, moving along the wall-normal direction. This behaviour constitutes a proof of the famous energy cascade introduced by Richardson, with the additional information regarding the process of how the scale energy is transferred throughout the wall-normal direction. In order to better understand how fluxes' paths are developed, it is possible to look at fig. 6.4. The fluxes' paths emerging from the DSR are directed towards two different sinks: one located at the wall ($Y_c = 0$) and the other located on the zero separation axis ($r_x = 0$, $r_z = 0$). The fluxes' field gradually aligns with the normal to the two sinks, where the scale energy is conveyed and dissipated through the viscosity. Between the two sinks, the nature of the dissipation is profoundly different. Dissipation at the wall is related to the wall-normal gradients of velocity:

$$\langle \epsilon^* \rangle = \nu \left\langle \frac{\partial u_j}{\partial y} \frac{\partial u_j}{\partial y} \right\rangle \tag{6.3}$$

while the dissipation at the zero separation sink ($r_x, r_z = 0$) is given by the classical dissipation subtracting the wall-normal gradients of velocity:

$$\left\langle \epsilon - \frac{\partial u_j}{\partial y} \frac{\partial u_j}{\partial y} \right\rangle \tag{6.4}$$

The analytical results are obtained by balancing fluxes and source on a disc on the extended physical-scale space from [19].

This analysis can be also considered from the point of view of the *coherent motions*. The turbulent fluctuations in the buffer layer were found to organize in well-defined coherent structures consisting of quasi-streamwise vortices, which are the main contributors to the production term through events such as *burst* and *sweep*. Experimental verification made by Smith & Metzler in [41] proved that the typical spanwise separation for this kind of structure is $r_z^+ \approx 50$, which is very close to the peak of the source of the scale energy found in the present analysis.
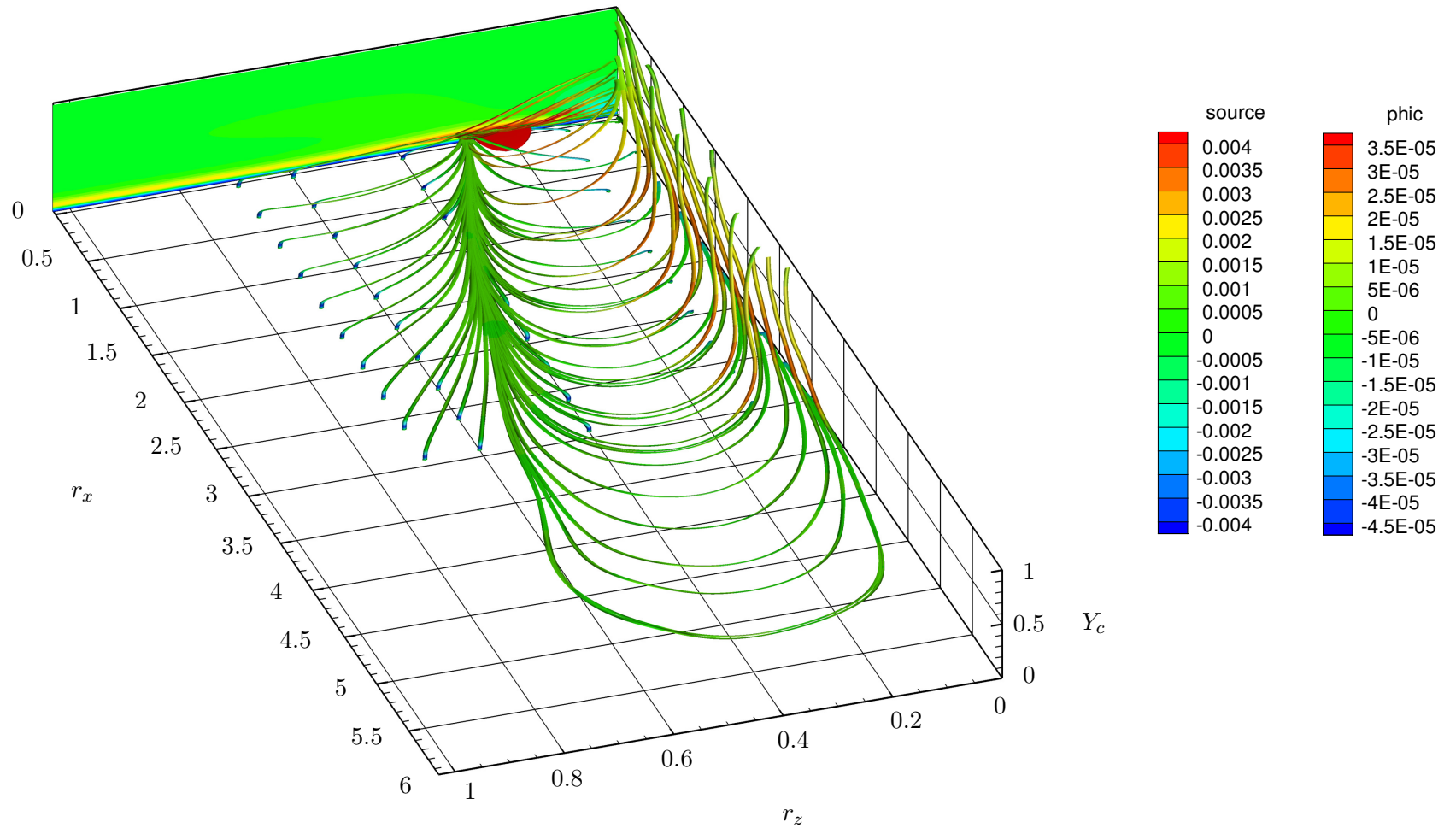
Figure 6.1: The results for the GKE analysis of a turbulent channel flow (REF) at $Re_\Pi = 6500$, in the space (r_x, r_z, Y_c) and at $r_y = 0$. The volume streamlines represent the reduced flux vector field $(\phi_{r_x}, \phi_{r_z}, \phi_c)$ and the colour code indicates the magnitude of physical flux ϕ_c. Contours at separation $r_x = 0$ represent the source term of the GKE in the same plane. The peak of the source term is highlighted with an iso surface ($\xi = 0.004$).
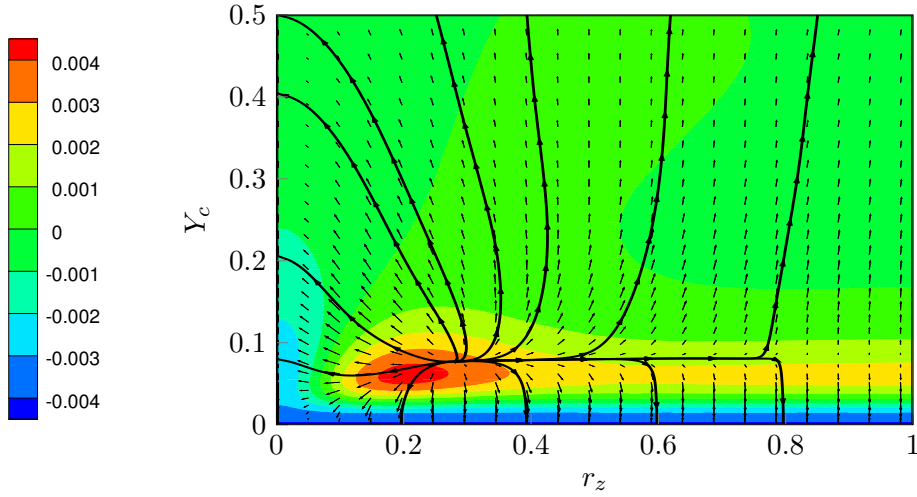
Figure 6.2: Contours of the source term of the GKE for the reference channel flow (REF) driven at constant pumping power input with $Re_\Pi = 6500$ and $Re_\tau = 199.7$ in the plane $r_x = 0$, $r_y = 0$. The vector field has components (ϕ_{r_z}, ϕ_c). The axes and the contours are in power units.

;
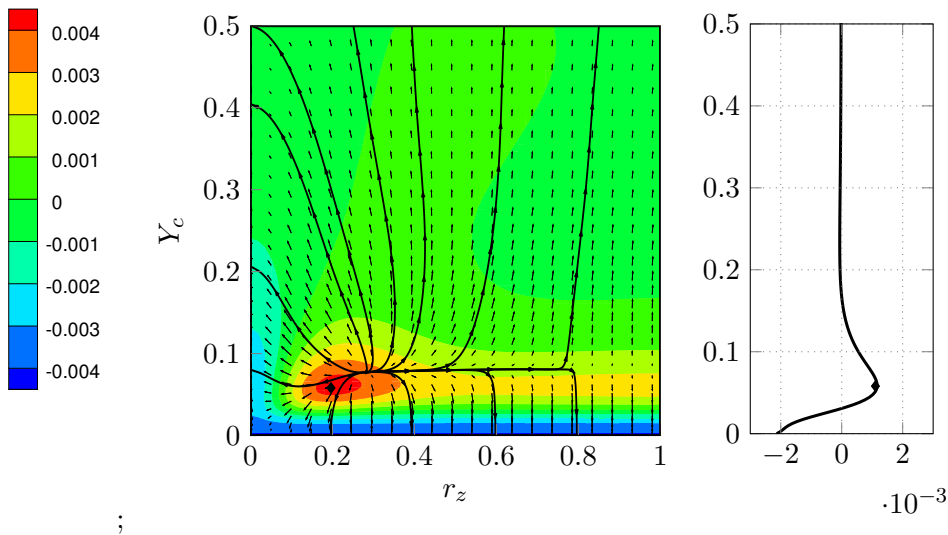
Figure 6.3: On the left: contours of the source term of the GKE for the reference channel flow (REF) driven at constant pumping power input with $Re_\Pi = 6500$ and $Re_\tau = 199.7$ in the plane $r_x = 0$, $r_y = 0$. Vector field has components (ϕ_{r_z}, ϕ_c). The axes and the contours are in power units. On the right: source term of the TKE budget equation for the reference channel flow (REF). The peaks are marked with diamonds and as can be seen from the two plots, are placed at the same wall-normal distance.
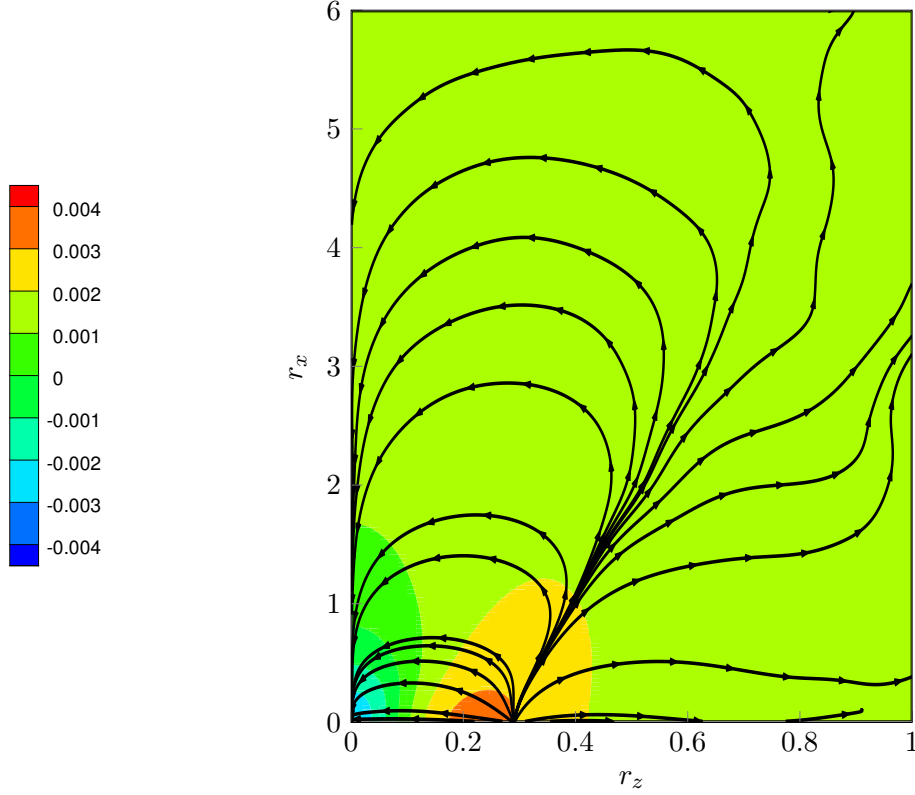
Figure 6.4: Contours of the source term of the GKE for the reference channel flow (REF) driven at constant pumping power input with $Re_\Pi = 6500$ and $Re_\tau = 199.7$ in the plane (r_x, r_z) with $r_y = 0$, slice placed at $Y_c = 0.0882$ ($Y_c^+ = 17.13$). The streamlines are the integration of the vector field with components (ϕ_{r_z}, ϕ_{r_x}).The axes and the contours are in power units.

6.1.1 Application of drag reduction techniques

The terms of the GKE are computed using the fields generated through the DNS tool for two drag reduction techniques (BF20,TW1). The goal is to compare them with the ones which were calculated for the reference channel flow (REF). The GKE analysis can be used in order to better understand the influence of the control on the paths of fluxes and the shift of the peak of the source of the scale energy. This constitute an expansion of the analysis already done in the previous chapter.

Damping of the near-wall spanwise velocity fluctuations

Using the damping of the near-wall spanwise velocity fluctuations strategy one can see the shift of the peak away from the wall (fig. 6.5). It is therefore possible to confirm the deduction that the damping layer can be interpreted as a displacement of the wall which equals the thickness of the region in which feedback force is applied. The peak of the source term of the GKE is placed at a wall-normal distance of $Y_c = 0.177$ ($Y_c^+ = 29.55$). This represents a shift towards the bulk of the flow by $\Delta Y_c = 0.119$ ($\Delta Y_c^+ = 17.96$) with respect to the reference channel

flow case. It initially appears that the spanwise scale separation of the peak of the source term is affected by the control. The peak is located at $r_z = 0.245$. This attribute appears to scale with Re_τ. A close observation indicates that while in power units, the peak appears to be located at larger spanwise separations, in viscous units its position remains approximately unchanged (BF20: $r_z^+ = 40.92$, REF: $r_z^+ = 39.21$). The magnitude of the peak is also reduced (REF magnitude: $\xi^{max} = 0.0044$, BF20 magnitude: $\xi^{max} = 0.00165$, decrease: $\Delta\xi^{max} \approx 62.5\%$), matching the data obtained from the TKE budget analysis.

Based on the similarity hypothesis regarding the relation between this drag reduction technique and the wall shift distance, it is sufficient to compare slices of the surface (r_x, r_z) located at different wall-normal coordinates (REF: $Y_c^+ = 17.13$, BF20: $Y_c^+ = 37.13$, displacement: $\Delta Y_c^+ = 20$). The energy paths remain almost unchanged as can be seen in fig. 6.6. The only noticeable difference is in the way in which the fluxes bend back towards the direct energy cascade. The slope of the streamlines going into the inverse energy cascade in slightly larger in the BF20 case with respect to the reference case (REF). This indicates that the scale energy fluxes depart from a singular point and are heading towards larger structures in the streamwise direction. It appears that this property seems not to scale with Re_τ. Another interesting difference that can be observed is the way in which fluxes keep moving after the end of the inverse energy cascade. They form a plateau and move along it at a constant r_x, before falling into the direct energy cascade.
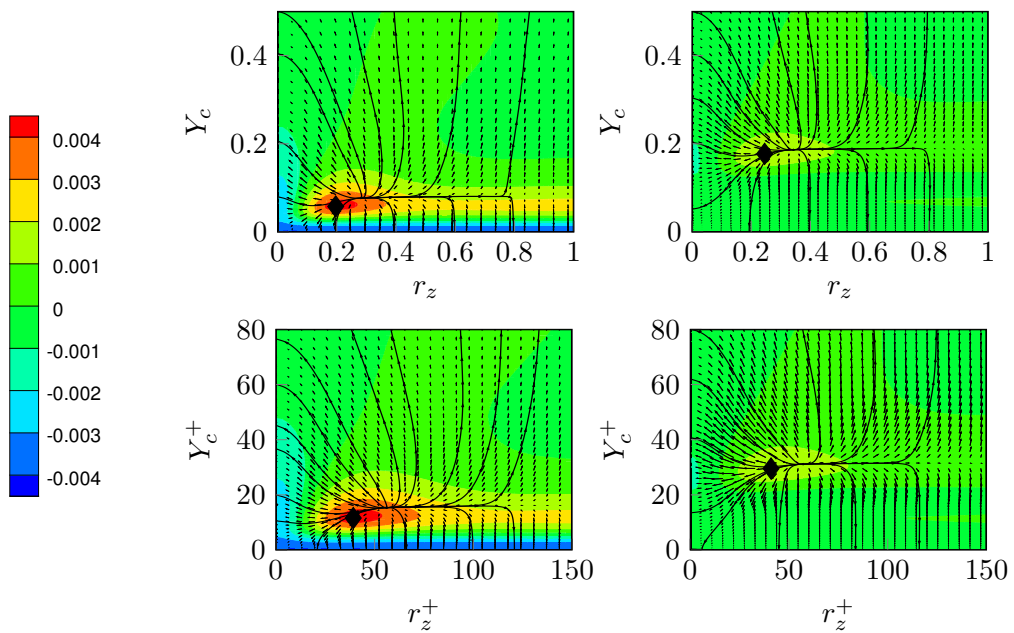
Figure 6.5: On the left: contours of the source term of the GKE for the reference channel flow (REF) driven at constant pumping power input with $Re_\Pi = 6500$ and $Re_\tau = 199.7$ in the plane (r_z, Y_c) at $r_y = 0$, $r_x = 0$. On the right: contours of the source term for the BF20 case driven at constant pumping power input with $Re_\Pi = 6500$ and $Re_\tau = 166.73$ in the plane (r_z, Y_c) with $r_y = 0$, $r_x = 0$. The streamlines are the integration of the vector field with components (ϕ_{r_z}, ϕ_c). On the upper part axes are in power units, on the lower part axes are in viscous units.
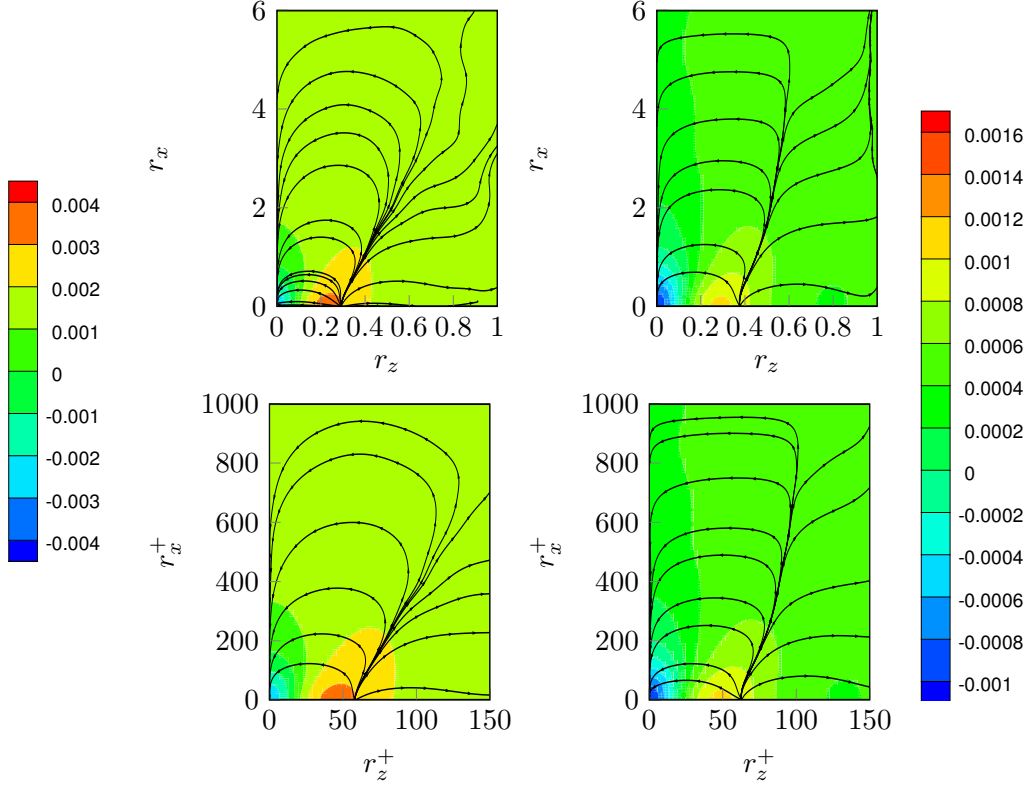
Figure 6.6: On the left: contours of the source term of the GKE for the reference channel flow (REF) driven at constant pumping power input with $Re_\Pi = 6500$ and $Re_\tau = 199.7$ in the plane (r_x, r_z) at $r_y = 0$, $Y_c = 0.0882$ ($Y_c^+ = 17.13$). On the right: contours of the source term for the BF20 case driven at constant pumping power input with $Re_\Pi = 6500$ and $Re_\tau = 166.73$ in the plane (r_x, r_z) at $r_y = 0$, $Y_c = 0.222$ ($Y_c^+ = 37.13$). The streamlines are the integration of the vector field with components (ϕ_{r_z}, ϕ_{r_x}). On the upper part axes are in power units, on the lower part axes are in viscous units.

Streamwise travelling waves of spanwise wall velocity

Using the streamwise travelling waves of spanwise wall velocity strategy the peak of the source term of the GKE is shifted away from the wall (fig. 6.7). It is located at a wall-normal distance of $Y_c = 0.097$ ($Y_c^+ = 18.11$), shifted by $\Delta Y_c = 0.039$ ($\Delta Y_c^+ = 6.52$) away from the wall. The spanwise scale of the peak is also affected by the control strategy. The peak is located at $r_z = 0.213$. This attribute appears to scale with Re_τ. A close observation indicates that while in power units, the peak appears to be located at larger spanwise separations, in viscous units its position remains approximately unchanged (TW1: $r_z^+ = 39.66$, REF: $r_z^+ = 39.21$). The magnitude of the peak is also reduced (REF: $\xi^{max} = 0.0044$, TW1: $\xi^{max} = 0.0024$, decrease : $\Delta \xi^{max} \approx 45\%$), matching the data obtained from the TKE budget analysis

Unlike in the TKE analysis here positive fluxes at the wall can not be found. This occurs due to the viscous contribution to the fluxes of the GKE involving scale energy which result in velocity differences. In order to properly analyse the

behaviour of the fluxes of the GKE in (r_x, r_z) plane, we're looking at slices located at the respective source term's peak wall-normal distance in the REF and TW1 cases (fig. 6.8). In the TW1 case the divergence line's slope remains unchanged with respect to the REF case. The behaviour of the streamlines which result from integrating the vector field across the slice, does change with respect to the REF case (the change occurs in the inverse and direct energy cascade). First the streamlines move outwards, towards larger structures in the spanwise direction. Along their path they bend back and keep following a wider path, finally ending at a sink located at $r_z = 0$. In fig. 6.9 one can see that next to the sink at $r_z = 0$, in TW1 case, the magnitude of the fluxes seems to be greater than in REF case.
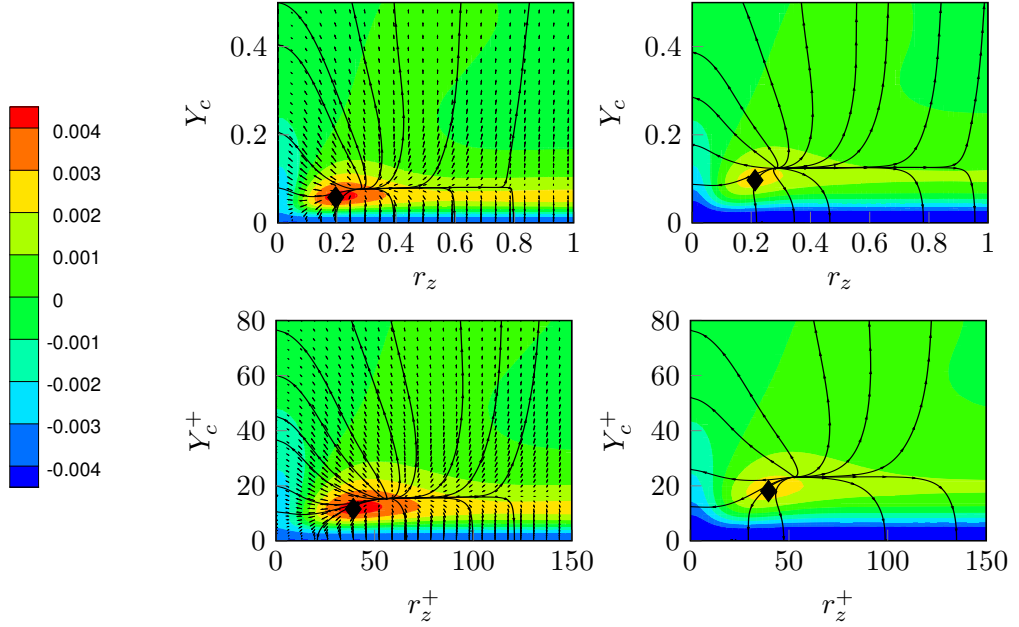
Figure 6.7: On the left: contours of the source term of the GKE for the reference channel flow (REF) driven at constant pumping power input with $Re_\Pi = 6500$ and $Re_\tau = 199.7$ in the plane (r_z, Y_c) with $r_y = 0$, $r_x = 0$. On the right: contours of the source term for the TW1 case driven at constant pumping power input with $Re_\Pi = 6500$ and $Re_\tau = 186.48$ in the plane (r_z, Y_c) with $r_y = 0$, $r_x = 0$.. The streamlines are the integration of the vector field with components (ϕ_{r_z}, ϕ_c). On the upper part axes are in power units, on the lower part axes are in viscous units.
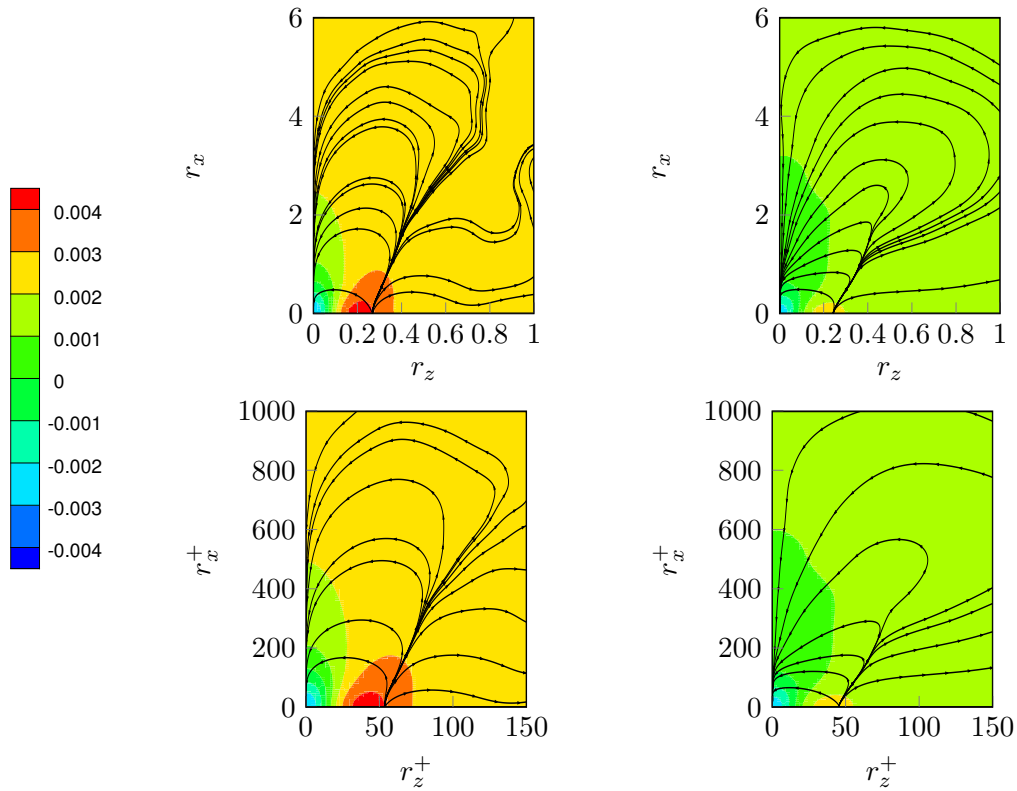
Figure 6.8: On the left: contours of the source term of the GKE for the reference channel flow (REF) driven at constant pumping power input with $Re_\Pi = 6500$ and $Re_\tau = 199.7$ in the plane (r_x, r_z) with $r_y = 0$, slice at $Y_c = 0.0580$ ($Y_c^+ = 11.59$). On the right: contours of the source term for the TW1 case driven at constant pumping power input with $Re_\Pi = 6500$ and $Re_\tau = 186.48$ in the plane (r_x, r_z) with $r_y = 0$, slice at $Y_c = 0.0971$ ($Y_c^+ = 18.11$). The streamlines are the integration of the vector field with components (ϕ_{r_z}, ϕ_{r_x}). On the upper part axes are in power units, on the lower part axes are in viscous units.
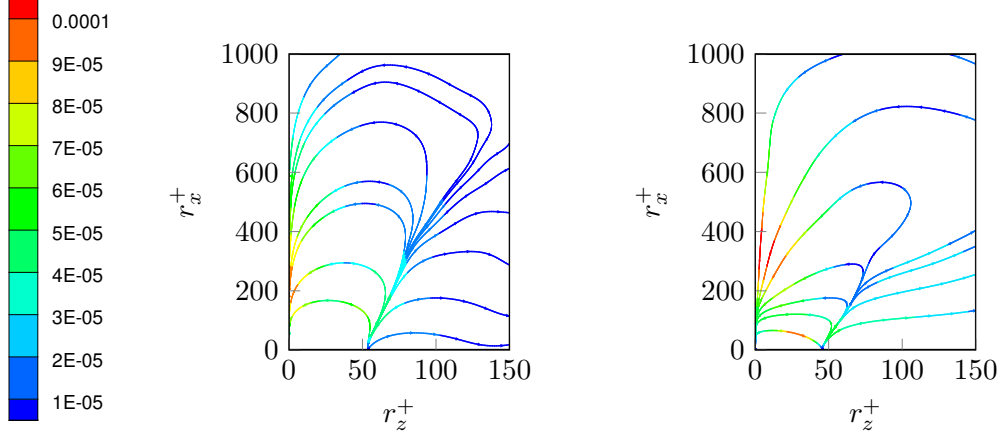
Figure 6.9: Streamlines integrated over the vector field with components (ϕ_{r_z}, ϕ_{r_x}). The axis and the contours are in power units. Taking a look at the plot is easy to see two sinks for the scale energy. On the left the slice of the REF case at a wall-normal distance of $Y_c = 0.058$ ($Y_c^+ = 11.59$). On the right the slice of the TW1 case at a wall-normal distance of $Y_c = 0.097$ ($Y_c^+ = 18.11$). Colour code indicates the magnitude of the vector field, hence $m = \sqrt{\phi_{r_x}^2 + \phi_{r_z}^2}$.

6.1.2 Conclusions

table 6.1 shows some similarities and some differences between the different analysed cases. The attributes of the source peak of the GKE are affected by applying a drag reduction technique. In the wall-normal direction it is shifted away from the boundary and its value is lowered. This information that was already known by the analysing of the one point budget equations for the TKE and the MKE. GKE gives the results also in the scale space. The position of the peak remains unchanged in the spanwise separation measured in viscous units ($r_z^+ \approx 40$). Further information is given by streamlines with the components (ϕ_{r_x}, ϕ_{r_z}). The path they follow is altered by the control technique. In the BF20 case they bend towards small spanwise scales and they form a plateau between the inverse and the direct energy cascades. In the TW1 case they bend slightly outwards. A sink for the fluxes with a strong divergence is located at the zero separation in the spanwise direction.

Case	Re_Π	Re_τ	Y_c	Y_c^+	r_x	r_z	r_z^+	ξ	ξ^+
REF	6500	199.70	0.0580	11.59	0	0.196	39.21	0.0044	0.881
BF20	6500	166.73	0.177	29.55	0	0.245	40.92	0.00165	0.276
TW1	6500	186.48	0.097	18.11	0	0.213	39.66	0.0024	0.45

Table 6.1: Data for the peaks of the source term of the GKE for different cases analysed.

6.2   The space (r_z, r_y, Y_c)

In order to verify the mechanism of direct-inverse energy cascade offered by Cimarelli in [37] and presented above, consider the space (r_z, r_y, Y_c). Here r_y is limited by the presence of the wall, and hence r_y can only vary in the range $r_y \in [0, 2Y_c]$. The results for velocity differences with negative separations are neglected. They can be easily recovered from the positive separation velocity differences, using the symmetries.

In fig. 6.10 it is possible to observe that there are streamlines of the vector field with components $\left(\phi_{r_z}, \phi_{r_y}, \phi_c\right)$ leaving the peak of the GKE's source, which carry scale energy from the small scales into the near-wall region. From there they continue towards the bulk of the flow, feeding larger and taller structures before ultimately converging to small dissipative scales. This is further proof of the inverse-direct energy cascade behaviour analysed above. The fluxes depart from the peak of the source initially moving along a divergence line. From there they align with the plane $r_y = 2Y_c$, moving towards larger spanwise separations. While ascending the fluxes bend gradually towards a distributed dissipation region located at the zero separation ($r_z = 0$, $r_y = 0$).

6.2.1   Application of drag reduction techniques

The drag reduction techniques TW1 and BF20 are analysed in the following section, in an attempt to validate the conjectures made for the space in which $r_y = 0$. Previous analysis in the (r_z, Y_c) plane had indicated that the peak of the scale energy source is invariant with respect to r_z^+. Therefore we will consider a slice of the plane (r_y, Y_c) at $r_z^+ = 40$. In fig. 6.11 one can notice that the energy paths between three cases remain almost entirely unchanged. The dissipative region near the wall (here represented by the line $r_y = 2Y_c$) in the TW1 case is slightly larger. Here lies the final proof for the shifting of the peak of the source term for the GKE. The plot matches the data appearing in table 6.1. A last and important observation is that in each of the three cases, the source peak is located at $r_y = 0$.
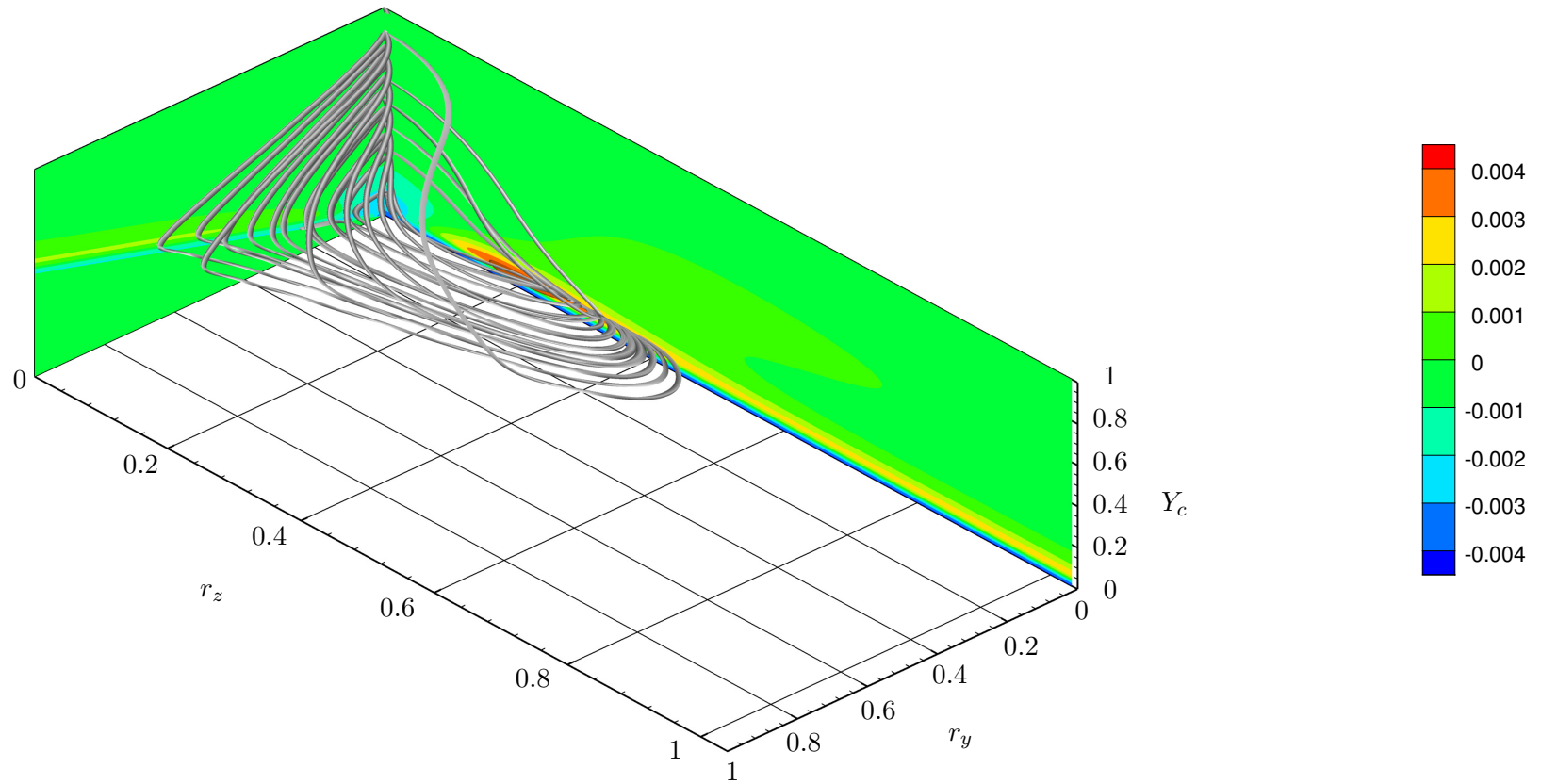
Figure 6.10: Results for the GKE analysis of the reference channel flow (REF) at $Re_\Pi = 6500$, in the space (r_z, r_y, Y_c) and $r_x = 0$. The volume streamlines represent the reduced flux vector field $(\phi_{r_z}, \phi_{r_y}, \phi_c)$. The contours at separation $r_z = 0$ and $r_y = 0$ represent the source term of the GKE in the same plane. The peak of the source term is highlighted with an iso surface ($\xi = 0.004$).
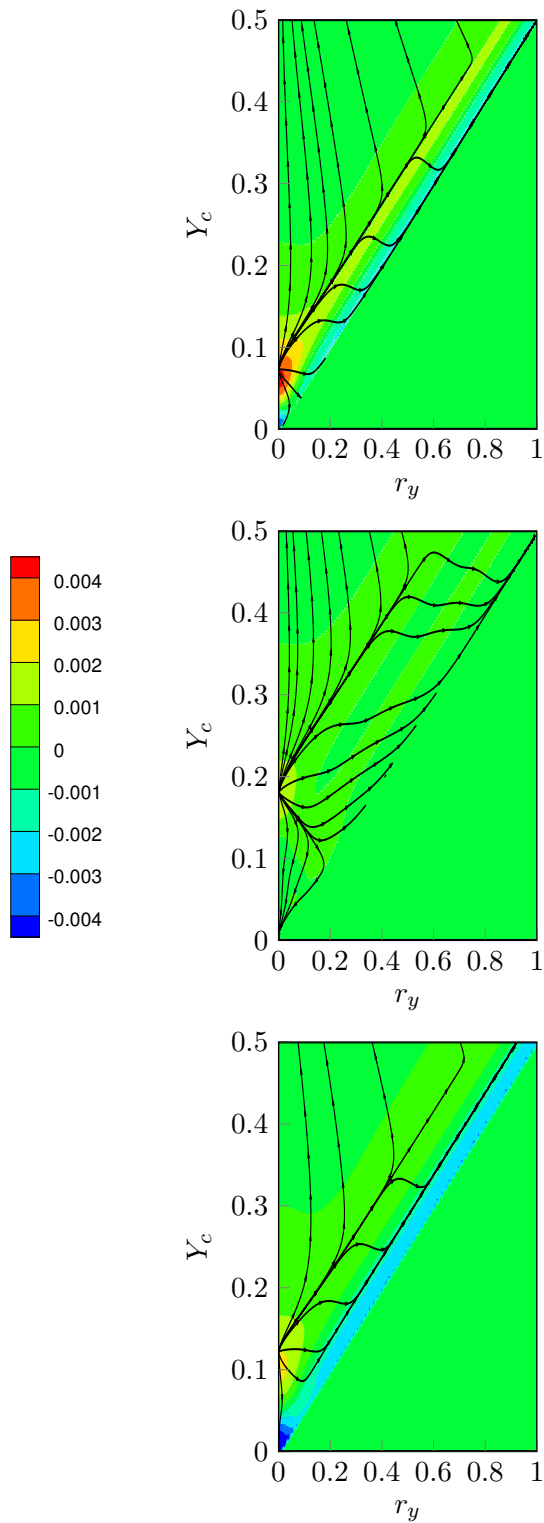
Figure 6.11: Contours of the source term of the GKE on a slice placed at $r_z^+ = 40$ in the plane (r_y, Y_c). Starting from the top: REF case, BF20 case and TW1 case. Streamlines integrates vectors components $\left(\phi_{r_x}, \phi_{r_y}, \phi_c\right)$. Values on the axes are in power units.

Chapter 7

Conclusions and future developments

This work describes a new, efficient tool for the analysis of the Generalized Kolmogorov Equation (GKE) in the entire physical-scale space (r_x, r_y, r_z, Y_c). Good performances have been reached thanks to the combined use of statistical symmetries, a memory-saving implementation and a parallelization strategy, achieving more than two order of magnitudes of speed-up compared to the existing reference implementation.

The tool has been used to understand how skin-friction drag reduction techniques affect the complex energy transfer phenomena. A DNS database for turbulent channel flow has been built on purpose with a reference channel flow and two active drag reduction techniques: damping of the near-wall spanwise fluctuations and streamwise travelling waves of spanwise wall velocity. Spatial resolution and other discretization parameters have been chosen on the basis of strict requirements, beyond the standards for such turbulent channel flow simulations. The simulations have been run according to the Constant Power Input (CPI) strategy, in order to keep the power input to the system unchanged.

The Turbulent Kinetic Energy (TKE) and the Mean Kinetic Energy (MKE) budget equations solved on this database proved that the peak of the source term of the TKE is shifted away from the channel wall by the drag reduction techniques, supporting an alternative interpretation of the damping of the the near-wall spanwise fluctuations as a virtual displacement of the wall. Streamwise travelling waves have been shown to create an high dissipation flux near the wall due to the presence of Generalized Stokes Layer (GSL). Looking at the integral MKE and TKE budget equations, the energy box representation allowed us to describe relative changes from a global perspective. On the other hand, an expanded view made possible by the GKE allowed more details to emerge and more physical insight on the drag reduction physics to be attained. In the reference channel flow, the presence of a direct and inverse energy cascade has been confirmed. For the first time, the GKE analysis has been then applied to drag reduction cases, where the source peak is found to shift away from the wall. However, differences have been highlighted between the two drag reduction techniques. For the near-wall damping

of spanwise velocity fluctuations, the slope of the divergence line is tilted towards smaller spanwise separations and a plateau at the end of the inverse energy cascade is observed. For travelling waves of spanwise wall velocity, the slope remains unchanged while the fluxes departing from it have a different behaviour, moving towards larger spanwise structures before ending up into a strong sink near the wall. The analysis in (r_x, r_y, Y_c) space confirmed our observations made in the space (r_x, r_z, Y_c).

Appendix A

Expansion of the terms

In following calculation consider velocity difference vector as:

$$\langle \delta u_i \rangle = \langle u_{i,iy2} \left(\boldsymbol{x} + \boldsymbol{\Delta x} \right) - u_{i,iy1}(\boldsymbol{x}) \rangle \tag{A.1}$$

A.1 Source term

$$s = -2 \langle \delta u \delta v \rangle \left(\frac{dU}{dY_c} \right)^* - 4 \langle \epsilon^* \rangle \tag{A.2}$$

$$\begin{aligned}
\langle \delta u \delta v \rangle &= \langle \left[u_{iy2} \left(\boldsymbol{x} + \boldsymbol{\Delta x} \right) - u_{iy1}(\boldsymbol{x}) \right] \left[v_{iy2} \left(\boldsymbol{x} + \boldsymbol{\Delta x} \right) - v_{iy1}(\boldsymbol{x}) \right] \rangle \\
&= \langle u_{iy2} \left(\boldsymbol{x} + \boldsymbol{\Delta x} \right) v_{iy2} \left(\boldsymbol{x} + \boldsymbol{\Delta x} \right) \rangle - \langle u_{iy2} \left(\boldsymbol{x} + \boldsymbol{\Delta x} \right) v_{iy1} \left(\boldsymbol{x} \right) \rangle + \\
&\quad - \langle u_{iy1} \left(\boldsymbol{x} \right) v_{iy2} \left(\boldsymbol{x} + \boldsymbol{\Delta x} \right) \rangle + \langle u_{iy1}(\boldsymbol{x}) v_{iy1}(\boldsymbol{x}) \rangle
\end{aligned} \tag{A.3}$$

Applying variable substitution $\tilde{\boldsymbol{x}} = \boldsymbol{x} + \boldsymbol{\Delta x}$ for the second term of eq. (A.3), it trasforms in:

$$\langle u_{iy2} \left(\boldsymbol{x} + \boldsymbol{\Delta x} \right) v_{iy1} \left(\boldsymbol{x} \right) \rangle = \langle u_{iy2} \left(\tilde{\boldsymbol{x}} \right) v_{iy1} \left(\tilde{\boldsymbol{x}} - \boldsymbol{\Delta x} \right) \rangle \tag{A.4}$$

$$\left(\frac{dU}{dY_c} \right)^* = \frac{1}{2} \left(\frac{dU}{dy_1} + \frac{dU}{dy_2} \right) \tag{A.5}$$

Pseudo dissipation is not decomposed in sipler terms.

A.2 Scale fluxes

$$\boldsymbol{\Phi_r} = \left(\Phi_{r_x}, \Phi_{r_y}, \Phi_{r_z} \right) = \underbrace{\langle \delta u^2 \delta \mathbf{u} \rangle}_{turbulent} - \underbrace{2\nu \nabla_r \langle \delta u^2 \rangle}_{viscous} + \underbrace{\langle \delta u^2 \delta \boldsymbol{U} \rangle}_{mean} \tag{A.6}$$

A.2.1 Turbulent term

$$\left\langle \delta u^2 \delta \boldsymbol{u} \right\rangle = \left\langle \left(\delta u \delta u + \delta v \delta v + \delta w \delta w \right) \delta u_i \right\rangle \qquad i = 1..3 \qquad \text{(A.7)}$$

Three components of turbulent part of scale fluxes are:

- $\phi_{rx} \to \left\langle \left(\delta u \delta u + \delta v \delta v + \delta w \delta w \right) \delta u \right\rangle$

- $\phi_{ry} \to \left\langle \left(\delta u \delta u + \delta v \delta v + \delta w \delta w \right) \delta v \right\rangle$

- $\phi_{rz} \to \left\langle \left(\delta u \delta u + \delta v \delta v + \delta w \delta w \right) \delta w \right\rangle$

ϕ_{r_x}

$$
\begin{aligned}
\left\langle \delta u^2 \delta u \right\rangle = &\left\langle \left(\delta u \delta u + \delta v \delta v + \delta w \delta w \right) \delta u \right\rangle = \\
= &\Big\langle \left(u_{iy2} \left(\boldsymbol{x} + \boldsymbol{\Delta x} \right) - u_{iy1}(\boldsymbol{x}) \right)^2 \left(u_{iy2} \left(\boldsymbol{x} + \boldsymbol{\Delta x} \right) - u_{iy1}(\boldsymbol{x}) \right) + \\
&+ \left(v_{iy2} \left(\boldsymbol{x} + \boldsymbol{\Delta x} \right) - v_{iy1}(\boldsymbol{x}) \right)^2 \left(u_{iy2} \left(\boldsymbol{x} + \boldsymbol{\Delta x} \right) - u_{iy1}(\boldsymbol{x}) \right) + \\
&+ \left(w_{iy2} \left(\boldsymbol{x} + \boldsymbol{\Delta x} \right) - w_{iy1}(\boldsymbol{x}) \right)^2 \left(u_{iy2} \left(\boldsymbol{x} + \boldsymbol{\Delta x} \right) - u_{iy1}(\boldsymbol{x}) \right) \Big\rangle = \\
= &\left\langle u_{iy2} \left(\boldsymbol{x} + \boldsymbol{\Delta x} \right) u_{iy2} \left(\boldsymbol{x} + \boldsymbol{\Delta x} \right) u_{iy2} \left(\boldsymbol{x} + \boldsymbol{\Delta x} \right) \right\rangle + \\
&- \left\langle u_{iy2} \left(\boldsymbol{x} + \boldsymbol{\Delta x} \right) u_{iy2} \left(\boldsymbol{x} + \boldsymbol{\Delta x} \right) u_{iy1}(\boldsymbol{x}) \right\rangle + \\
&- 2 \left\langle u_{iy2} \left(\boldsymbol{x} + \boldsymbol{\Delta x} \right) u_{iy1}(\boldsymbol{x}) u_{iy2} \left(\boldsymbol{x} + \boldsymbol{\Delta x} \right) \right\rangle + \\
&+ 2 \left\langle u_{iy2} \left(\boldsymbol{x} + \boldsymbol{\Delta x} \right) u_{iy1}(\boldsymbol{x}) u_{iy1}(\boldsymbol{x}) \right\rangle + \\
&+ \left\langle u_{iy1}(\boldsymbol{x}) u_{iy1}(\boldsymbol{x}) u_{iy2} \left(\boldsymbol{x} + \boldsymbol{\Delta x} \right) \right\rangle + \\
&- \left\langle u_{iy1}(\boldsymbol{x}) u_{iy1}(\boldsymbol{x}) u_{iy1}(\boldsymbol{x}) \right\rangle + \\
&+ \left\langle v_{iy2} \left(\boldsymbol{x} + \boldsymbol{\Delta x} \right) v_{iy2} \left(\boldsymbol{x} + \boldsymbol{\Delta x} \right) u_{iy2} \left(\boldsymbol{x} + \boldsymbol{\Delta x} \right) \right\rangle + \\
&- \left\langle v_{iy2} \left(\boldsymbol{x} + \boldsymbol{\Delta x} \right) v_{iy2}(\boldsymbol{x} + \boldsymbol{\Delta x}) u_{iy1}(\boldsymbol{x}) \right\rangle + \\
&- 2 \left\langle v_{iy2} \left(\boldsymbol{x} + \boldsymbol{\Delta x} \right) v_{iy1}(\boldsymbol{x}) u_{iy2} \left(\boldsymbol{x} + \boldsymbol{\Delta x} \right) \right\rangle + \\
&+ 2 \left\langle v_{iy2} \left(\boldsymbol{x} + \boldsymbol{\Delta x} \right) v_{iy1}(\boldsymbol{x}) u_{iy1}(\boldsymbol{x}) \right\rangle + \\
&+ \left\langle v_{iy1}(\boldsymbol{x}) v_{iy1}(\boldsymbol{x}) u_{iy2} \left(\boldsymbol{x} + \boldsymbol{\Delta x} \right) \right\rangle + \\
&- \left\langle v_{iy1}(\boldsymbol{x}) v_{iy1}(\boldsymbol{x}) u_{iy1}(\boldsymbol{x}) \right\rangle + \\
&+ \left\langle w_{iy2} \left(\boldsymbol{x} + \boldsymbol{\Delta x} \right) w_{iy2} \left(\boldsymbol{x} + \boldsymbol{\Delta x} \right) u_{iy2} \left(\boldsymbol{x} + \boldsymbol{\Delta x} \right) \right\rangle + \\
&- \left\langle w_{iy2} \left(\boldsymbol{x} + \boldsymbol{\Delta x} \right) w_{iy2}(\boldsymbol{x} + \boldsymbol{\Delta x}) u_{iy1}(\boldsymbol{x}) \right\rangle + \\
&- 2 \left\langle w_{iy2} \left(\boldsymbol{x} + \boldsymbol{\Delta x} \right) w_{iy1}(\boldsymbol{x}) u_{iy2} \left(\boldsymbol{x} + \boldsymbol{\Delta x} \right) \right\rangle + \\
&+ 2 \left\langle w_{iy2} \left(\boldsymbol{x} + \boldsymbol{\Delta x} \right) w_{iy1}(\boldsymbol{x}) u_{iy1}(\boldsymbol{x}) \right\rangle + \\
&+ \left\langle w_{iy1}(\boldsymbol{x}) w_{iy1}(\boldsymbol{x}) u_{iy2} \left(\boldsymbol{x} + \boldsymbol{\Delta x} \right) \right\rangle + \\
&- \left\langle w_{iy1}(\boldsymbol{x}) w_{iy1}(\boldsymbol{x}) u_{iy1}(\boldsymbol{x}) \right\rangle
\end{aligned}
\tag{A.8}
$$

ϕ_{r_y}

$$
\begin{aligned}
\left\langle \delta u^2 \delta v \right\rangle = \left\langle \left(\delta u \delta u + \delta v \delta v + \delta w \delta w \right) \delta v \right\rangle = \\
= \Big\langle \left(u_{iy2} \left(\boldsymbol{x} + \boldsymbol{\Delta x} \right) - u_{iy1}(\boldsymbol{x}) \right)^2 \left(v_{iy2} \left(\boldsymbol{x} + \boldsymbol{\Delta x} \right) - v_{iy1}(\boldsymbol{x}) \right) + \\
+ \left(v_{iy2} \left(\boldsymbol{x} + \boldsymbol{\Delta x} \right) - v_{iy1}(\boldsymbol{x}) \right)^2 \left(v_{iy2} \left(\boldsymbol{x} + \boldsymbol{\Delta x} \right) - v_{iy1}(\boldsymbol{x}) \right) + \\
+ \left(w_{iy2} \left(\boldsymbol{x} + \boldsymbol{\Delta x} \right) - w_{iy1}(\boldsymbol{x}) \right)^2 \left(v_{iy2} \left(\boldsymbol{x} + \boldsymbol{\Delta x} \right) - v_{iy1}(\boldsymbol{x}) \right) \Big\rangle = \\
= \left\langle u_{iy2} \left(\boldsymbol{x} + \boldsymbol{\Delta x} \right) u_{iy2} \left(\boldsymbol{x} + \boldsymbol{\Delta x} \right) v_{iy2} \left(\boldsymbol{x} + \boldsymbol{\Delta x} \right) \right\rangle + \\
- \left\langle u_{iy2} \left(\boldsymbol{x} + \boldsymbol{\Delta x} \right) u_{iy2} \left(\boldsymbol{x} + \boldsymbol{\Delta x} \right) v_{iy1}(\boldsymbol{x}) \right\rangle + \\
- 2 \left\langle u_{iy2} \left(\boldsymbol{x} + \boldsymbol{\Delta x} \right) u_{iy1}(\boldsymbol{x}) v_{iy2} \left(\boldsymbol{x} + \boldsymbol{\Delta x} \right) \right\rangle + \\
+ 2 \left\langle u_{iy2} \left(\boldsymbol{x} + \boldsymbol{\Delta x} \right) u_{iy1}(\boldsymbol{x}) v_{iy1}(\boldsymbol{x}) \right\rangle + \\
+ \left\langle u_{iy1}(\boldsymbol{x}) u_{iy1}(\boldsymbol{x}) v_{iy2} \left(\boldsymbol{x} + \boldsymbol{\Delta x} \right) \right\rangle + \\
- \left\langle u_{iy1}(\boldsymbol{x}) u_{iy1}(\boldsymbol{x}) v_{iy1}(\boldsymbol{x}) \right\rangle + \\
+ \left\langle v_{iy2} \left(\boldsymbol{x} + \boldsymbol{\Delta x} \right) v_{iy2} \left(\boldsymbol{x} + \boldsymbol{\Delta x} \right) v_{iy2} \left(\boldsymbol{x} + \boldsymbol{\Delta x} \right) \right\rangle + \\
- \left\langle v_{iy2} \left(\boldsymbol{x} + \boldsymbol{\Delta x} \right) v_{iy2}(\boldsymbol{x} + \boldsymbol{\Delta x}) v_{iy1}(\boldsymbol{x}) \right\rangle + \\
- 2 \left\langle v_{iy2} \left(\boldsymbol{x} + \boldsymbol{\Delta x} \right) v_{iy1}(\boldsymbol{x}) v_{iy2} \left(\boldsymbol{x} + \boldsymbol{\Delta x} \right) \right\rangle + \\
+ 2 \left\langle v_{iy2} \left(\boldsymbol{x} + \boldsymbol{\Delta x} \right) v_{iy1}(\boldsymbol{x}) v_{iy1}(\boldsymbol{x}) \right\rangle + \\
+ \left\langle v_{iy1}(\boldsymbol{x}) v_{iy1}(\boldsymbol{x}) v_{iy2} \left(\boldsymbol{x} + \boldsymbol{\Delta x} \right) \right\rangle + \\
- \left\langle v_{iy1}(\boldsymbol{x}) v_{iy1}(\boldsymbol{x}) v_{iy1}(\boldsymbol{x}) \right\rangle + \\
+ \left\langle w_{iy2} \left(\boldsymbol{x} + \boldsymbol{\Delta x} \right) w_{iy2} \left(\boldsymbol{x} + \boldsymbol{\Delta x} \right) v_{iy2} \left(\boldsymbol{x} + \boldsymbol{\Delta x} \right) \right\rangle + \\
- \left\langle w_{iy2} \left(\boldsymbol{x} + \boldsymbol{\Delta x} \right) w_{iy2}(\boldsymbol{x} + \boldsymbol{\Delta x}) v_{iy1}(\boldsymbol{x}) \right\rangle + \\
- 2 \left\langle w_{iy2} \left(\boldsymbol{x} + \boldsymbol{\Delta x} \right) w_{iy1}(\boldsymbol{x}) v_{iy2} \left(\boldsymbol{x} + \boldsymbol{\Delta x} \right) \right\rangle + \\
+ 2 \left\langle w_{iy2} \left(\boldsymbol{x} + \boldsymbol{\Delta x} \right) w_{iy1}(\boldsymbol{x}) v_{iy1}(\boldsymbol{x}) \right\rangle + \\
+ \left\langle w_{iy1}(\boldsymbol{x}) w_{iy1}(\boldsymbol{x}) v_{iy2} \left(\boldsymbol{x} + \boldsymbol{\Delta x} \right) \right\rangle + \\
- \left\langle w_{iy1}(\boldsymbol{x}) w_{iy1}(\boldsymbol{x}) v_{iy1}(\boldsymbol{x}) \right\rangle
\end{aligned}
\tag{A.9}
$$

ϕ_{r_z}

$$
\begin{aligned}
\langle \delta u^2 \delta w \rangle &= \langle (\delta u \delta u + \delta v \delta v + \delta w \delta w) \, \delta w \rangle = \\
&= \Big\langle \left(u_{iy2} \left(\boldsymbol{x} + \boldsymbol{\Delta x} \right) - u_{iy1}(\boldsymbol{x}) \right)^2 \left(w_{iy2} \left(\boldsymbol{x} + \boldsymbol{\Delta x} \right) - w_{iy1}(\boldsymbol{x}) \right) + \\
&+ \left(v_{iy2} \left(\boldsymbol{x} + \boldsymbol{\Delta x} \right) - v_{iy1}(\boldsymbol{x}) \right)^2 \left(w_{iy2} \left(\boldsymbol{x} + \boldsymbol{\Delta x} \right) - w_{iy1}(\boldsymbol{x}) \right) + \\
&+ \left(w_{iy2} \left(\boldsymbol{x} + \boldsymbol{\Delta x} \right) - w_{iy1}(\boldsymbol{x}) \right)^2 \left(w_{iy2} \left(\boldsymbol{x} + \boldsymbol{\Delta x} \right) - w_{iy1}(\boldsymbol{x}) \right) \Big\rangle = \\
&= \langle u_{iy2} \left(\boldsymbol{x} + \boldsymbol{\Delta x} \right) u_{iy2} \left(\boldsymbol{x} + \boldsymbol{\Delta x} \right) w_{iy2} \left(\boldsymbol{x} + \boldsymbol{\Delta x} \right) \rangle + \\
&- \langle u_{iy2} \left(\boldsymbol{x} + \boldsymbol{\Delta x} \right) u_{iy2} \left(\boldsymbol{x} + \boldsymbol{\Delta x} \right) w_{iy1}(\boldsymbol{x}) \rangle + \\
&- 2 \langle u_{iy2} \left(\boldsymbol{x} + \boldsymbol{\Delta x} \right) u_{iy1}(\boldsymbol{x}) w_{iy2} \left(\boldsymbol{x} + \boldsymbol{\Delta x} \right) \rangle + \\
&+ 2 \langle u_{iy2} \left(\boldsymbol{x} + \boldsymbol{\Delta x} \right) u_{iy1}(\boldsymbol{x}) w_{iy1}(\boldsymbol{x}) \rangle + \\
&+ \langle u_{iy1}(\boldsymbol{x}) u_{iy1}(\boldsymbol{x}) w_{iy2} \left(\boldsymbol{x} + \boldsymbol{\Delta x} \right) \rangle + \\
&- \langle u_{iy1}(\boldsymbol{x}) u_{iy1}(\boldsymbol{x}) w_{iy1}(\boldsymbol{x}) \rangle + \\
&+ \langle v_{iy2} \left(\boldsymbol{x} + \boldsymbol{\Delta x} \right) v_{iy2} \left(\boldsymbol{x} + \boldsymbol{\Delta x} \right) w_{iy2} \left(\boldsymbol{x} + \boldsymbol{\Delta x} \right) \rangle + \\
&- \langle v_{iy2} \left(\boldsymbol{x} + \boldsymbol{\Delta x} \right) v_{iy2}(\, \boldsymbol{x} + \boldsymbol{\Delta x} \,) w_{iy1}(\boldsymbol{x}) \rangle + \\
&- 2 \langle v_{iy2} \left(\boldsymbol{x} + \boldsymbol{\Delta x} \right) v_{iy1}(\boldsymbol{x}) w_{iy2} \left(\boldsymbol{x} + \boldsymbol{\Delta x} \right) \rangle + \\
&+ 2 \langle v_{iy2} \left(\boldsymbol{x} + \boldsymbol{\Delta x} \right) v_{iy1}(\boldsymbol{x}) w_{iy1}(\boldsymbol{x}) \rangle + \\
&+ \langle v_{iy1}(\boldsymbol{x}) v_{iy1}(\boldsymbol{x}) w_{iy2} \left(\boldsymbol{x} + \boldsymbol{\Delta x} \right) \rangle + \\
&- \langle v_{iy1}(\boldsymbol{x}) v_{iy1}(\boldsymbol{x}) w_{iy1}(\boldsymbol{x}) \rangle + \\
&+ \langle w_{iy2} \left(\boldsymbol{x} + \boldsymbol{\Delta x} \right) w_{iy2} \left(\boldsymbol{x} + \boldsymbol{\Delta x} \right) w_{iy2} \left(\boldsymbol{x} + \boldsymbol{\Delta x} \right) \rangle + \\
&- \langle w_{iy2} \left(\boldsymbol{x} + \boldsymbol{\Delta x} \right) w_{iy2}(\, \boldsymbol{x} + \boldsymbol{\Delta x} \,) w_{iy1}(\boldsymbol{x}) \rangle + \\
&- 2 \langle w_{iy2} \left(\boldsymbol{x} + \boldsymbol{\Delta x} \right) w_{iy1}(\boldsymbol{x}) w_{iy2} \left(\boldsymbol{x} + \boldsymbol{\Delta x} \right) \rangle + \\
&+ 2 \langle w_{iy2} \left(\boldsymbol{x} + \boldsymbol{\Delta x} \right) w_{iy1}(\boldsymbol{x}) w_{iy1}(\boldsymbol{x}) \rangle + \\
&+ \langle w_{iy1}(\boldsymbol{x}) w_{iy1}(\boldsymbol{x}) w_{iy2} \left(\boldsymbol{x} + \boldsymbol{\Delta x} \right) \rangle + \\
&- \langle w_{iy1}(\boldsymbol{x}) w_{iy1}(\boldsymbol{x}) w_{iy1}(\boldsymbol{x}) \rangle
\end{aligned} \tag{A.10}
$$

A.2.2   Mean term

$$
\langle \delta u^2 \delta U_i \rangle = \langle (\delta u \delta u + \delta v \delta v + \delta w \delta w) \, \delta U_i \rangle \tag{A.11}
$$

- $\phi_{rx} \rightarrow \langle (\delta u \delta u + \delta v \delta v + \delta w \delta w) \, \delta U \rangle$

- $\phi_{ry} \rightarrow \langle (\delta u \delta u + \delta v \delta v + \delta w \delta w) \, \delta V \rangle$

- $\phi_{rz} \rightarrow \langle (\delta u \delta u + \delta v \delta v + \delta w \delta w) \, \delta W \rangle$

ϕ_{rx}

$$\langle \delta u^2 \delta U \rangle = \langle (\delta u \delta u + \delta v \delta v + \delta w \delta w) \, \delta U \rangle =$$
$$= \Big\langle (u_{iy2} \, (\boldsymbol{x} + \boldsymbol{\Delta x}) - u_{iy1}(\boldsymbol{x}))^2 \, (U_{iy2} \, (\boldsymbol{x} + \boldsymbol{\Delta x}) - U_{iy1}(\boldsymbol{x})) +$$
$$+ \, (v_{iy2} \, (\boldsymbol{x} + \boldsymbol{\Delta x}) - v_{iy1}(\boldsymbol{x}))^2 \, (U_{iy2} \, (\boldsymbol{x} + \boldsymbol{\Delta x}) - U_{iy1}(\boldsymbol{x})) + \qquad \text{(A.12)}$$
$$+ \, (w_{iy2} \, (\boldsymbol{x} + \boldsymbol{\Delta x}) - w_{iy1}(\boldsymbol{x}))^2 \, (U_{iy2} \, (\boldsymbol{x} + \boldsymbol{\Delta x}) - U_{iy1}(\boldsymbol{x})) \Big\rangle$$

ϕ_{r_y}

$$\langle \delta u^2 \delta V \rangle = \langle (\delta u \delta u + \delta v \delta v + \delta w \delta w) \, \delta V \rangle =$$
$$= \Big\langle (u_{iy2} \, (\boldsymbol{x} + \boldsymbol{\Delta x}) - u_{iy1}(\boldsymbol{x}))^2 \, (V_{iy2} \, (\boldsymbol{x} + \boldsymbol{\Delta x}) - V_{iy1}(\boldsymbol{x})) +$$
$$+ \, (v_{iy2} \, (\boldsymbol{x} + \boldsymbol{\Delta x}) - v_{iy1}(\boldsymbol{x}))^2 \, (V_{iy2} \, (\boldsymbol{x} + \boldsymbol{\Delta x}) - V_{iy1}(\boldsymbol{x})) + \qquad \text{(A.13)}$$
$$+ \, (w_{iy2} \, (\boldsymbol{x} + \boldsymbol{\Delta x}) - w_{iy1}(\boldsymbol{x}))^2 \, (V_{iy2} \, (\boldsymbol{x} + \boldsymbol{\Delta x}) - V_{iy1}(\boldsymbol{x})) \Big\rangle$$

ϕ_{r_z}

$$\langle \delta u^2 \delta W \rangle = \langle (\delta u \delta u + \delta v \delta v + \delta w \delta w) \, \delta W \rangle =$$
$$= \Big\langle (u_{iy2} \, (\boldsymbol{x} + \boldsymbol{\Delta x}) - u_{iy1}(\boldsymbol{x}))^2 \, (W_{iy2} \, (\boldsymbol{x} + \boldsymbol{\Delta x}) - W_{iy1}(\boldsymbol{x})) +$$
$$+ \, (v_{iy2} \, (\boldsymbol{x} + \boldsymbol{\Delta x}) - v_{iy1}(\boldsymbol{x}))^2 \, (W_{iy2} \, (\boldsymbol{x} + \boldsymbol{\Delta x}) - W_{iy1}(\boldsymbol{x})) + \qquad \text{(A.14)}$$
$$+ \, (w_{iy2} \, (\boldsymbol{x} + \boldsymbol{\Delta x}) - w_{iy1}(\boldsymbol{x}))^2 \, (W_{iy2} \, (\boldsymbol{x} + \boldsymbol{\Delta x}) - W_{iy1}(\boldsymbol{x})) \Big\rangle$$

A.2.3   Viscous term

$$- 2\nu \nabla_r \left\langle \delta u^2 \right\rangle = -2\nu \nabla_r \left\langle \delta u \delta u + \delta v \delta v + \delta w \delta w \right\rangle \qquad \text{(A.15)}$$

- $\phi_{rx} \rightarrow -2\nu \frac{\partial}{\partial r_x} \left\langle (\delta u \delta u + \delta v \delta v + \delta w \delta w) \right\rangle$

- $\phi_{ry} \rightarrow -2\nu \frac{\partial}{\partial r_y} \left\langle (\delta u \delta u + \delta v \delta v + \delta w \delta w) \right\rangle$

- $\phi_{rz} \rightarrow -2\nu \frac{\partial}{\partial r_z} \left\langle (\delta u \delta u + \delta v \delta v + \delta w \delta w) \right\rangle$

Derivative in homogeneous direction are computed in the Fourier Space, whereas for wall-normal separation, derivative are computed through a five point molecule finite difference method.

A.3   Space flux

$$\boldsymbol{\Phi_c} = \underbrace{\left\langle \delta u^2 \delta v^* \right\rangle}_{turbulent} + \underbrace{\frac{2}{\rho} \left\langle \delta p \delta v \right\rangle}_{pressure} - \underbrace{\frac{\nu}{2} \frac{d \left\langle \delta u^2 \right\rangle}{dY_c}}_{viscous} \tag{A.16}$$

A.3.1   Turbulent term

$$\left\langle (\delta u \delta u + \delta v \delta v + \delta w \delta w) \frac{v_{iy2}\left(\boldsymbol{x} + \boldsymbol{\Delta x}\right) + v_{iy1}(\boldsymbol{x})}{2} \right\rangle \tag{A.17}$$

$$\left\langle \delta u \delta u v^* \right\rangle =$$
$$\left\langle (u_{iy2}\left(\boldsymbol{x} + \boldsymbol{\Delta x}\right) - u_{iy1}(\boldsymbol{x})) (u_{iy2}\left(\boldsymbol{x} + \boldsymbol{\Delta x}\right) - u_{iy1}(\boldsymbol{x})) \frac{v_{iy2}\left(\boldsymbol{x} + \boldsymbol{\Delta x}\right) + v_{iy1}(\boldsymbol{x})}{2} \right\rangle \tag{A.18}$$

$$\left\langle \delta u \delta u v^* \right\rangle =$$
$$= \frac{1}{2} \left\langle u_{iy2}(\boldsymbol{x} + \boldsymbol{\Delta x}) u_{iy2}(\boldsymbol{x} + \boldsymbol{\Delta x}) v_{iy2}(\boldsymbol{x} + \boldsymbol{\Delta x}) \right\rangle +$$
$$+ \frac{1}{2} \left\langle u_{iy2}(\boldsymbol{x} + \boldsymbol{\Delta x}) u_{iy2}(\boldsymbol{x} + \boldsymbol{\Delta x}) v_{iy1}(\boldsymbol{x}) \right\rangle +$$
$$- \left\langle u_{iy2}(\boldsymbol{x} + \boldsymbol{\Delta x}) u_{iy1}(\boldsymbol{x}) v_{iy2}(\boldsymbol{x} + \boldsymbol{\Delta x}) \right\rangle +$$
$$- \left\langle u_{iy2}(\boldsymbol{x} + \boldsymbol{\Delta x}) u_{iy1}(\boldsymbol{x}) v_{iy1}(\boldsymbol{x}) \right\rangle + \tag{A.19}$$
$$+ \frac{1}{2} \left\langle u_{iy1}(\boldsymbol{x}) u_{iy1}(\boldsymbol{x}) v_{iy2}(\boldsymbol{x} + \boldsymbol{\Delta x}) \right\rangle +$$
$$+ \frac{1}{2} \left\langle u_{iy1}(\boldsymbol{x}) u_{iy1}(\boldsymbol{x}) v_{iy1}(\boldsymbol{x}) \right\rangle$$

$$\left\langle \delta v \delta v v^* \right\rangle =$$
$$\left\langle (v_{iy2}\left(\boldsymbol{x} + \boldsymbol{\Delta x}\right) - v_{iy1}(\boldsymbol{x})) (v_{iy2}\left(\boldsymbol{x} + \boldsymbol{\Delta x}\right) - v_{iy1}(\boldsymbol{x})) \frac{v_{iy2}\left(\boldsymbol{x} + \boldsymbol{\Delta x}\right) + v_{iy1}(\boldsymbol{x})}{2} \right\rangle \tag{A.20}$$

$$\left\langle \delta v \delta v v^* \right\rangle =$$
$$= \frac{1}{2} \left\langle v_{iy2}(\boldsymbol{x} + \boldsymbol{\Delta x}) v_{iy2}(\boldsymbol{x} + \boldsymbol{\Delta x}) v_{iy2}(\boldsymbol{x} + \boldsymbol{\Delta x}) \right\rangle +$$
$$+ \frac{1}{2} \left\langle v_{iy2}(\boldsymbol{x} + \boldsymbol{\Delta x}) v_{iy2}(\boldsymbol{x} + \boldsymbol{\Delta x}) v_{iy1}(\boldsymbol{x}) \right\rangle +$$
$$- \left\langle v_{iy2}(\boldsymbol{x} + \boldsymbol{\Delta x}) v_{iy1}(\boldsymbol{x}) v_{iy2}(\boldsymbol{x} + \boldsymbol{\Delta x}) \right\rangle +$$
$$- \left\langle v_{iy2}(\boldsymbol{x} + \boldsymbol{\Delta x}) v_{iy1}(\boldsymbol{x}) v_{iy1}(\boldsymbol{x}) \right\rangle + \tag{A.21}$$
$$+ \frac{1}{2} \left\langle v_{iy1}(\boldsymbol{x}) v_{iy1}(\boldsymbol{x}) v_{iy2}(\boldsymbol{x} + \boldsymbol{\Delta x}) \right\rangle +$$
$$+ \frac{1}{2} \left\langle v_{iy1}(\boldsymbol{x}) v_{iy1}(\boldsymbol{x}) v_{iy1}(\boldsymbol{x}) \right\rangle$$

$$\langle \delta w \delta w v^* \rangle =$$
$$\left\langle \left(w_{iy2} \left(\boldsymbol{x} + \boldsymbol{\Delta x} \right) - w_{iy1}(\boldsymbol{x}) \right) \left(w_{iy2} \left(\boldsymbol{x} + \boldsymbol{\Delta x} \right) - w_{iy1}(\boldsymbol{x}) \right) \frac{v_{iy2} \left(\boldsymbol{x} + \boldsymbol{\Delta x} \right) + v_{iy1}(\boldsymbol{x})}{2} \right\rangle$$

$$(A.22)$$

$$\langle \delta v \delta v v^* \rangle =$$
$$= \frac{1}{2} \left\langle w_{iy2}(\boldsymbol{x} + \boldsymbol{\Delta x}) w_{iy2}(\boldsymbol{x} + \boldsymbol{\Delta x}) v_{iy2}(\boldsymbol{x} + \boldsymbol{\Delta x}) \right\rangle +$$
$$+ \frac{1}{2} \left\langle w_{iy2}(\boldsymbol{x} + \boldsymbol{\Delta x}) w_{iy2}(\boldsymbol{x} + \boldsymbol{\Delta x}) v_{iy1}(\boldsymbol{x}) \right\rangle +$$
$$- \left\langle w_{iy2}(\boldsymbol{x} + \boldsymbol{\Delta x}) w_{iy1}(\boldsymbol{x}) v_{iy2}(\boldsymbol{x} + \boldsymbol{\Delta x}) \right\rangle +$$
$$- \left\langle w_{iy2}(\boldsymbol{x} + \boldsymbol{\Delta x}) w_{iy1}(\boldsymbol{x}) v_{iy1}(\boldsymbol{x}) \right\rangle + \qquad (A.23)$$
$$+ \frac{1}{2} \left\langle w_{iy1}(\boldsymbol{x}) w_{iy1}(\boldsymbol{x}) v_{iy2}(\boldsymbol{x} + \boldsymbol{\Delta x}) \right\rangle +$$
$$+ \frac{1}{2} \left\langle w_{iy1}(\boldsymbol{x}) w_{iy1}(\boldsymbol{x}) v_{iy1}(\boldsymbol{x}) \right\rangle$$

A.3.2 Pressure term

$$\frac{2}{\rho} =$$
$$= \frac{2}{\rho} \left\langle \left(p_{iy2}(\boldsymbol{x} + \boldsymbol{\Delta x}) - p_{iy1}(\boldsymbol{x}) \right) \left(v_{iy_2}(\boldsymbol{x} + \boldsymbol{\Delta x}) - v_{iy1} \right) \right\rangle =$$
$$= \frac{2}{\rho} \left[\left\langle p_{iy2}(\boldsymbol{x} + \boldsymbol{\Delta x}) v_{iy2}(\boldsymbol{x} + \boldsymbol{\Delta x}) \right\rangle + \qquad (A.24)$$
$$- \left\langle p_{iy2}(\boldsymbol{x} + \boldsymbol{\Delta x}) v_{iy1}(\boldsymbol{x}) \right\rangle - \left\langle p_{iy1}(\boldsymbol{x}) v_{iy2}(\boldsymbol{x} + \boldsymbol{\Delta x}) \right\rangle +$$
$$+ \left\langle p_{iy1}(\boldsymbol{x}) v_{iy1}(\boldsymbol{x}) \right\rangle \right]$$

A.3.3 Viscous term

$$-\frac{\nu}{2} \frac{\partial \langle \delta u^2 \rangle}{\partial Y_c} = -\frac{\nu}{2} \left[\frac{1}{2} \left(\frac{\partial}{\partial y_2} \langle \delta u^2 \rangle + \frac{\partial}{\partial y_1} \langle \delta u^2 \rangle \right) \right] \qquad (A.25)$$

Appendix B

TKE and MKE: Residuals and further results

B.1 TKE and MKE budget

B.1.1 Reference channel flow
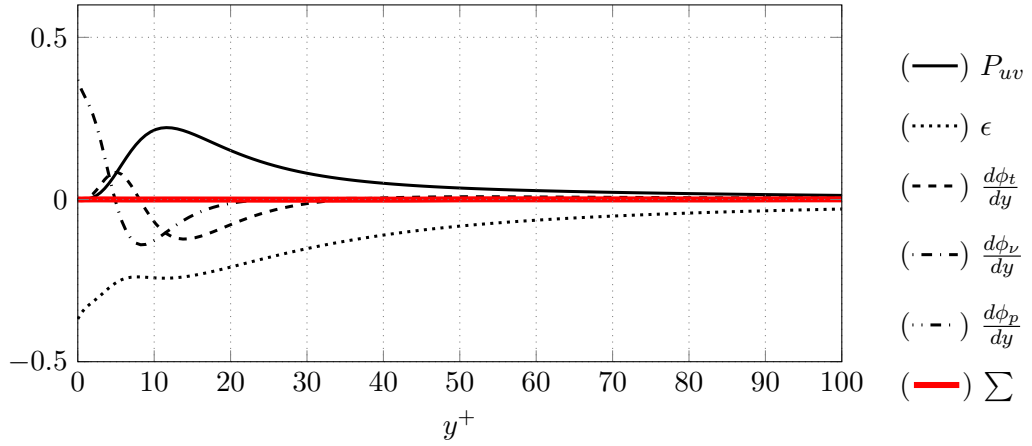
Figure B.1: Terms of the TKE budget equation for the reference channel flow (REF with $Re_\Pi = 6500$ and $Re_\tau = 199.7$) with respect to the wall-normal direction. Both the magnitude of the terms and the wall-normal direction are in viscous units. In the plot: production term (P_{uv}), pseudo-dissipation (ϵ), derivative of the turbulent transport term($\frac{d\phi_t}{dy}$), derivative of the viscous diffusion term ($\frac{d\phi_\nu}{dy}$), derivative of the pressure transport term ($\frac{d\phi_p}{dy}$) and residual ($\sum$).
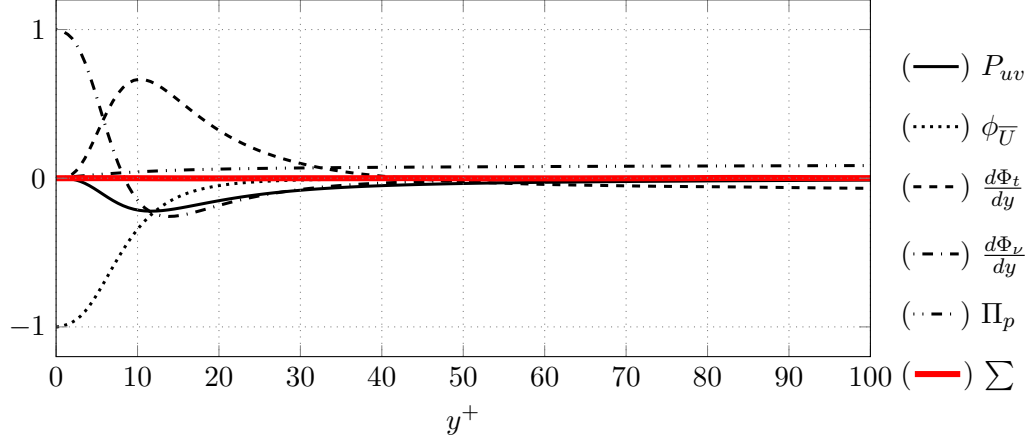
Figure B.2: Terms of the MKE budget equation for the reference channel flow (REF with $Re_\Pi = 6500$ and $Re_\tau = 199.7$) with respect to the wall-normal direction. Both the magnitude of terms and the wall-normal direction are in viscous units. In the plot: production term (P_{uv}), mean flow dissipation ($\Phi_{\overline{U}}$), derivative of the turbulent transport term ($\frac{d\Phi_t}{dy}$), derivative of the viscous diffusion term ($\frac{d\Phi_\nu}{dy}$), pumping term (Π_p) and residual ($\sum$).
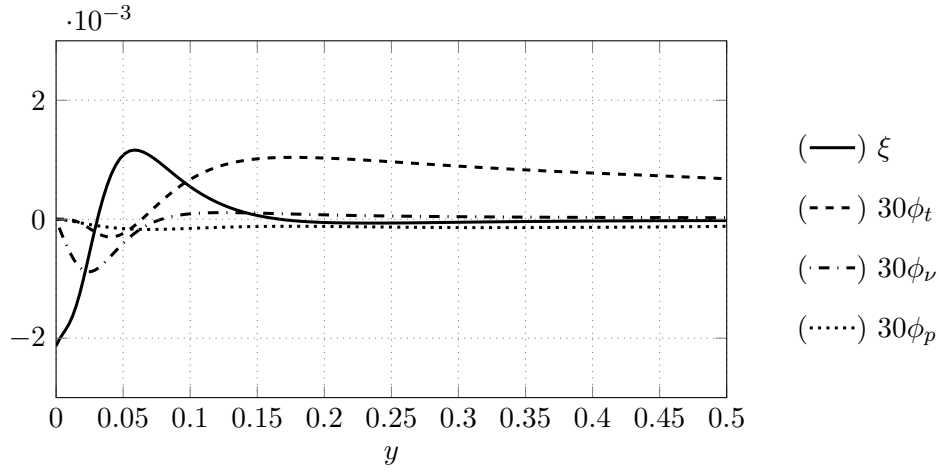
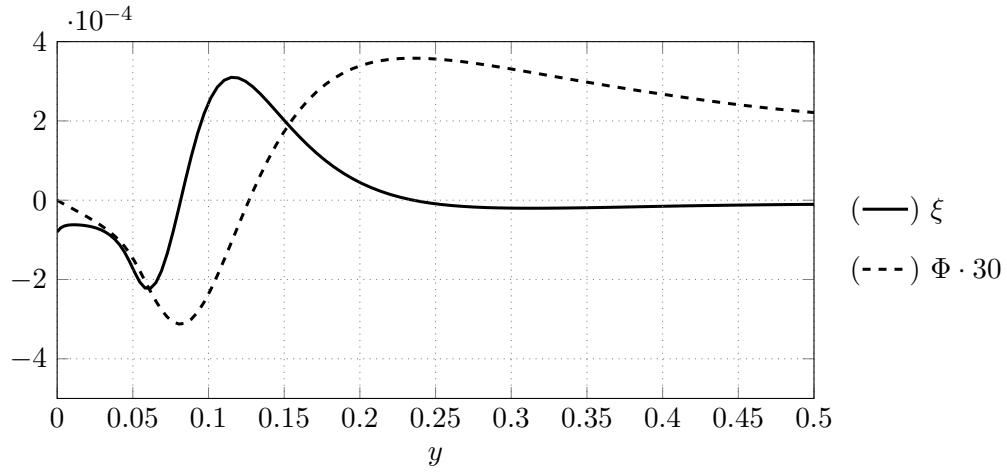**Figure B.3:** Source and fluxes terms of the TKE budget equation for the reference channel flow (REF with $Re_\Pi = 6500$ and $Re_\tau = 199.7$) with respect to the wall-normal direction. Both the magnitude of the terms and the wall-normal direction are in power units, therefore in Π units. In the plot: source term (ξ), turbulent transport term (ϕ_t), pressure transport term (ϕ_p), viscous diffusion term (ϕ_ν).
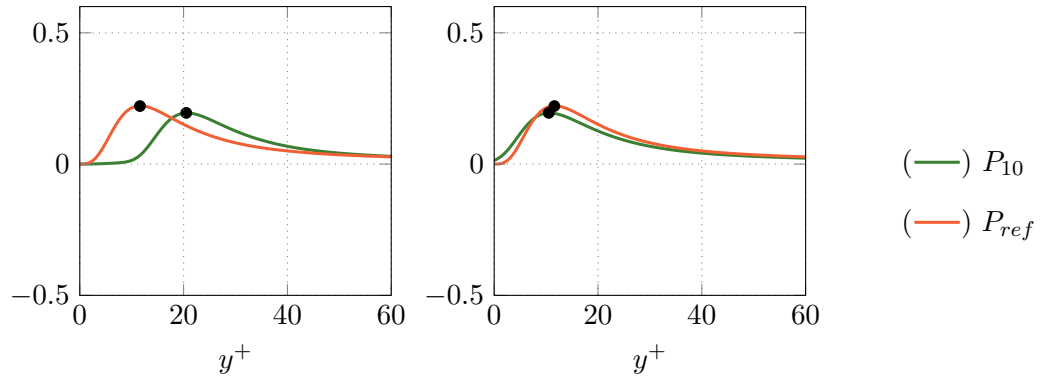
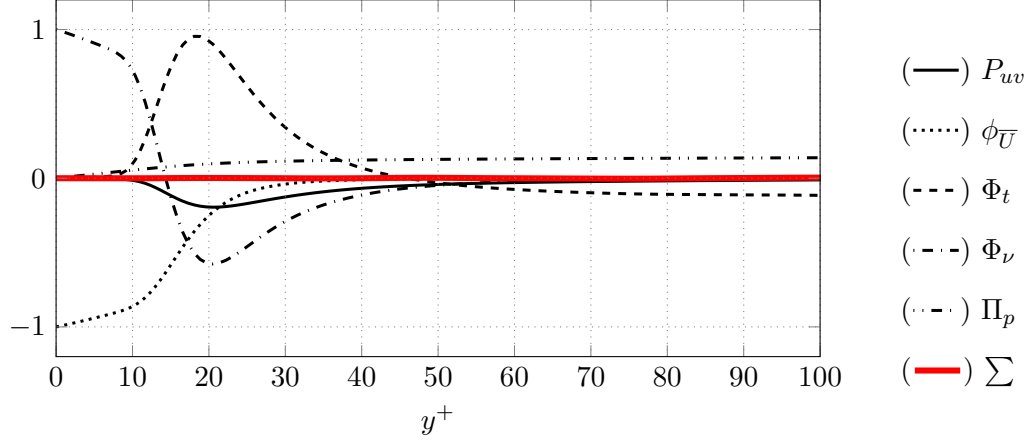### B.1.2 Damping of the near-wall spanwise fluctuations (BF20)
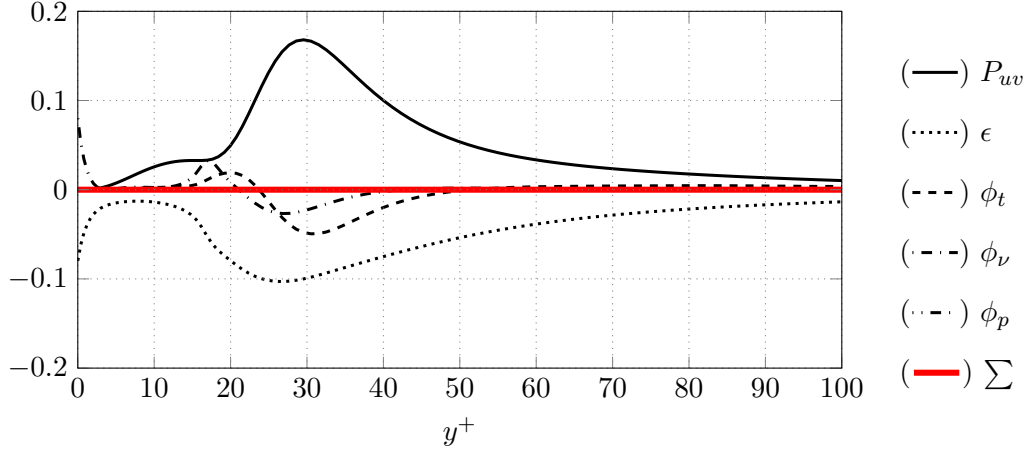
Figure B.4: Terms of the TKE budget equation for the channel flow with damping of the near-wall spanwise fluctuations drag reduction strategy (BF20 of table 3.2 with $Re_\Pi = 6500$ and $Re_\tau = 166.73$) with respect to the wall-normal direction. Both the magnitude of the terms and the wall-normal direction are in viscous units. In the plot: production term (P_{uv}), pseudo-dissipation (ϵ), derivative of the turbulent transport ($\frac{d\phi_t}{dy}$), of the viscous diffusion ($\frac{d\phi_\nu}{dy}$), of the pressure transport ($\frac{d\phi_p}{dy}$) terms and residual ($\sum$).
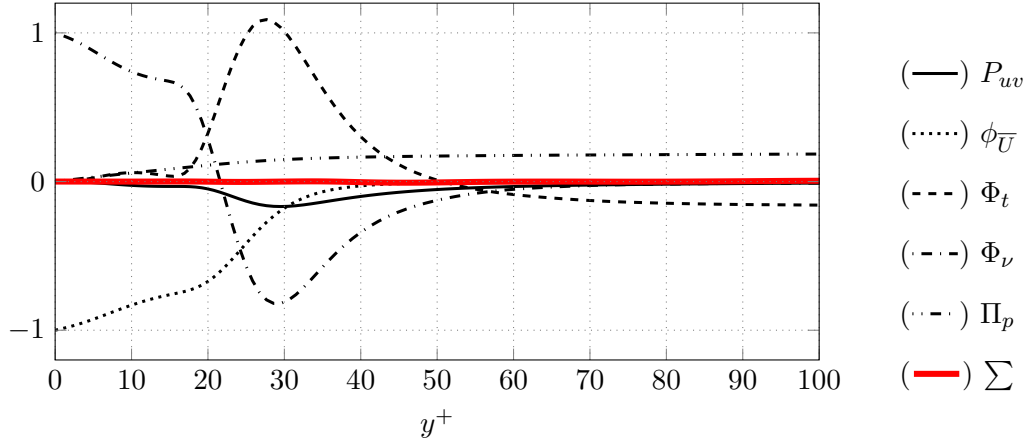
Figure B.5: Terms of the MKE budget equation for the channel flow with damping of the near-wall spanwise fluctuations drag reduction strategy (BF20 of table 3.2 with $Re_\Pi = 6500$ and $Re_\tau = 166.73$) with respect to the wall-normal direction. Both the magnitude of terms and the wall-normal direction are in viscous units. In the plot: production term (P_{uv}), mean flow dissipation ($\Phi_{\overline{U}}$), derivative of turbulent transport term ($\frac{d\Phi_t}{dy}$), derivative of the viscous diffusion term ($\frac{d\Phi_\nu}{dy}$), pumping term (Π_p) and residual ($\sum$).
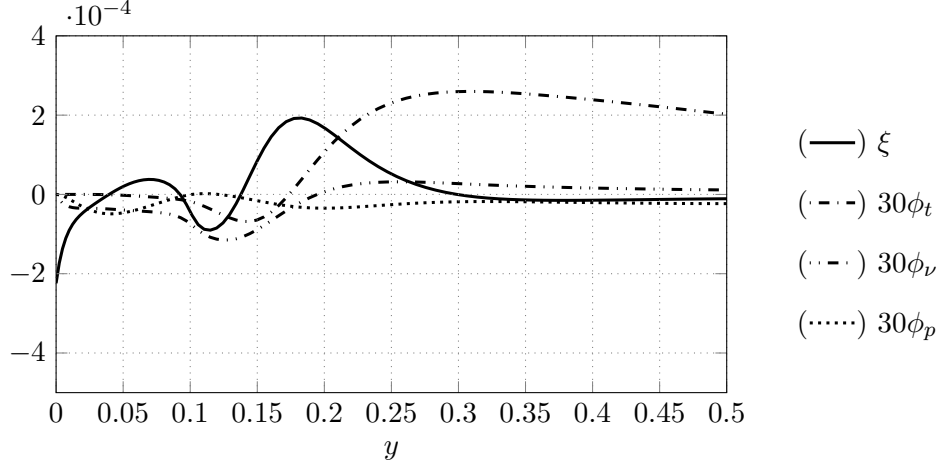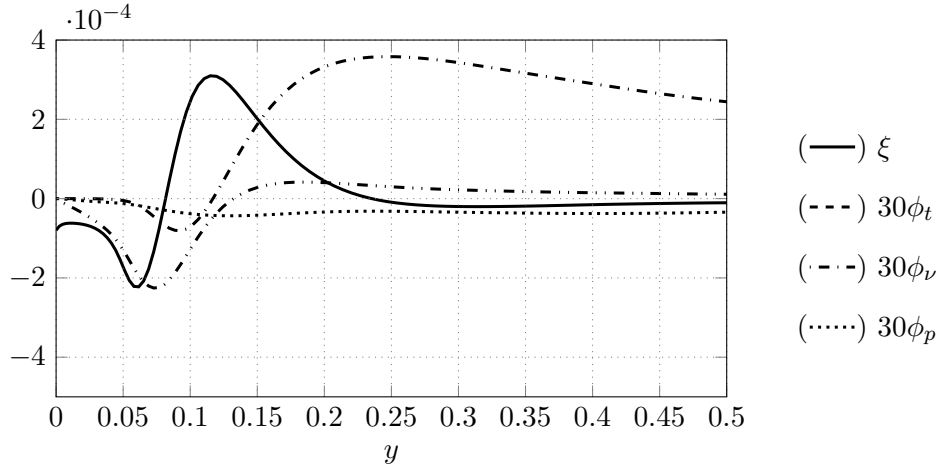
Figure B.6: Source and fluxes terms of the TKE budget equation for the channel flow with damping of the near-wall spanwise fluctuations drag reduction strategy (BF20 of table 3.2 with $Re_\Pi = 6500$ and $Re_\tau = 166.73$) with respect to the wall-normal direction. Both the magnitude of the terms and the wall-normal direction are in power units, therefore in Π units. In the plot: the source term (ξ), the turbulent transport term (ϕ_t), the pressure transport term (ϕ_p), viscous diffusion term(ϕ_ν).

### B.1.3   Damping of the near-wall spanwise fluctuations (BF10)
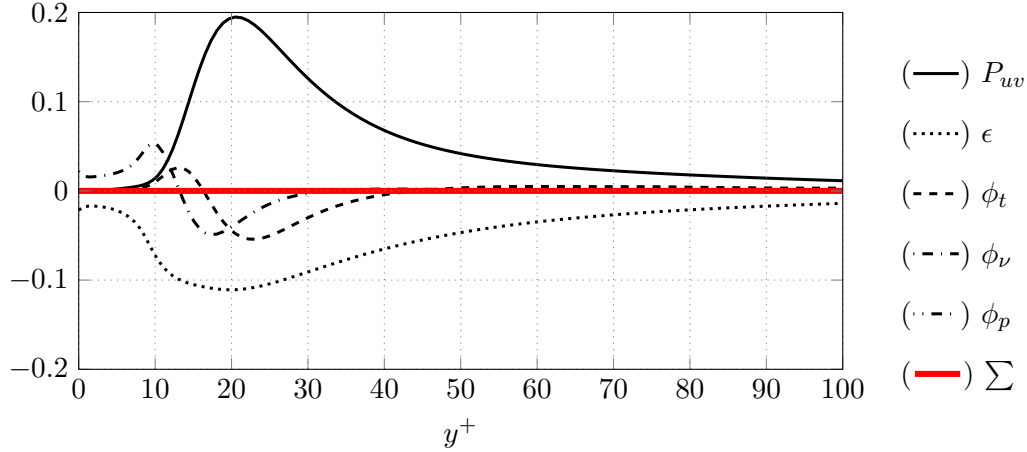
Figure B.7: Terms of the TKE budget equation of the channel flow with damping of the near-wall spanwise fluctuations drag reduction strategy (BF10 of table 3.2 with $Re_\Pi = 6500$ and $Re_\tau = 178.34$) with respect to the wall-normal direction. Both the magnitude of the terms and the wall-normal direction are in viscous units. In the plot: production term (P_{uv}), pseudo-dissipation (ϵ), derivative of the turbulent transport ($\frac{d\phi_t}{dy}$), of the viscous diffusion ($\frac{d\phi_\nu}{dy}$), of the pressure transport ($\frac{d\phi_p}{dy}$) terms and residual ($\sum$).

Figure B.8: Source and global flux terms of the TKE budget equation for the channel flow with damping of the near-wall spanwise fluctuations drag reduction strategy (BF10 of table 3.2 with $Re_\Pi = 6500$ and $Re_\tau = 178.34$) with respect to the wall-normal direction. Both the magnitude of terms and the wall-normal direction are in power units, therefore in Π units.

Figure B.9: Production term of the reference channel flow (REF) and of the channel flow with damping of the near-wall spanwise fluctuations drag reduction strategy (BF10 of table 3.2) in viscous units. On the right: the production profile of drag reduction case is shifted of 10 viscous units towards the wall. With a black mark maximum of the production term is stressed.

Figure B.10: Terms of the TKE budget equation of the channel flow with damping of the near-wall spanwise fluctuations drag reduction strategy (BF10 of table 3.2 with $Re_\Pi = 6500$ and $Re_\tau = 178.34$) with respect to the wall-normal direction. Both the magnitude of the terms and the wall-normal direction are in viscous units. In the plot: production term (P_{uv}), mean flow dissipation ($\Phi_{\overline{U}}$), derivative of the turbulent transport term ($\frac{d\Phi_t}{dy}$), derivative of the viscous diffusion term ($\frac{d\Phi_\nu}{dy}$), pumping term (Π_p) and residual ($\sum$).

Figure B.11: Source and fluxes terms of the TKE Budget equation for the channel flow with damping of the near-wall spanwise fluctuations drag reduction strategy (BF10 of table 3.2 with $Re_\Pi = 6500$ and $Re_\tau = 178.34$) with respect to the wall-normal direction. Both the magnitude of the terms and the wall-normal direction are in power units, therefore in Π units. In the plot: source term (ξ), turbulent transport (ϕ_t), pressure transport (ϕ_p), viscous diffusion (ϕ_ν).

B.1.4 Streamwise travelling waves of spanwise wall velocity (TW1)
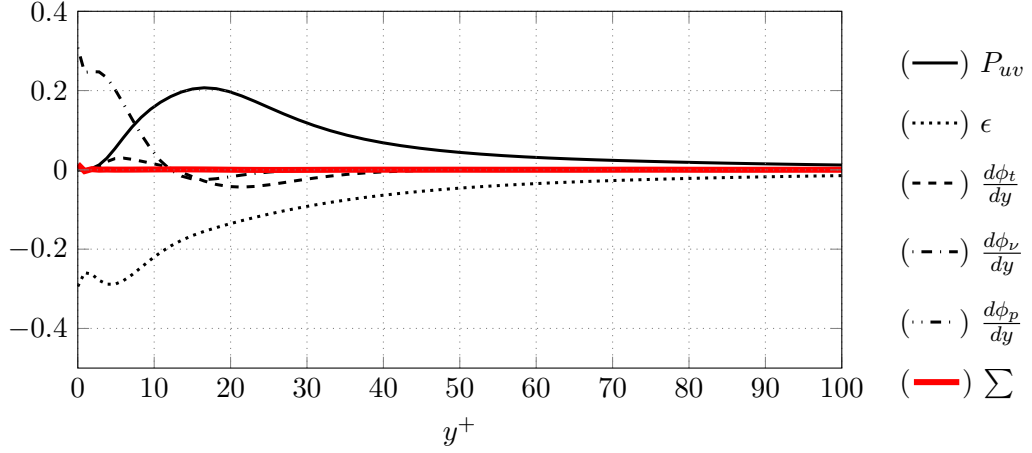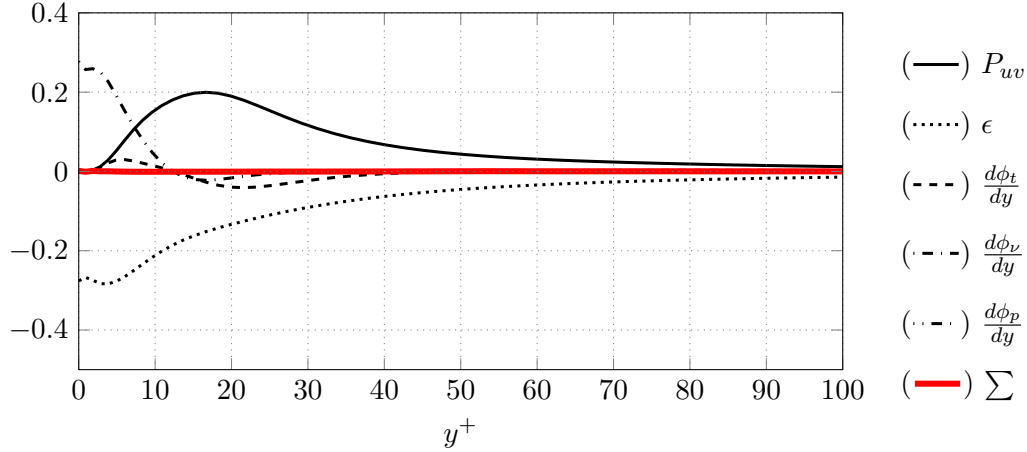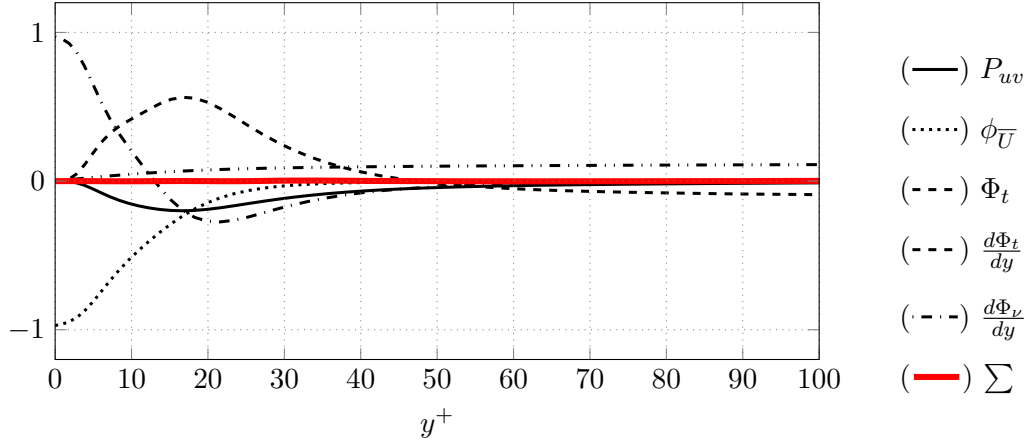

Figure B.12: Terms of the TKE budget equation for the channel flow with streamwise travelling waves of spanwise wall velocity (TW1 of table 3.3 with $Re_\Pi = 6500$, $Re_\tau = 186.48$) with respect to the wall-normal direction. Both magnitude of the terms and the wall-normal direction are in viscous units. In the plot: production term (P_{uv}), pseudo-dissipation (ϵ), derivative of the turbulent transport term ($\frac{d\phi_t}{dy}$), of the viscous diffusion ($\frac{d\phi_\nu}{dy}$), of the pressure transport ($\frac{d\phi_p}{dy}$) terms, residual ($\sum$).
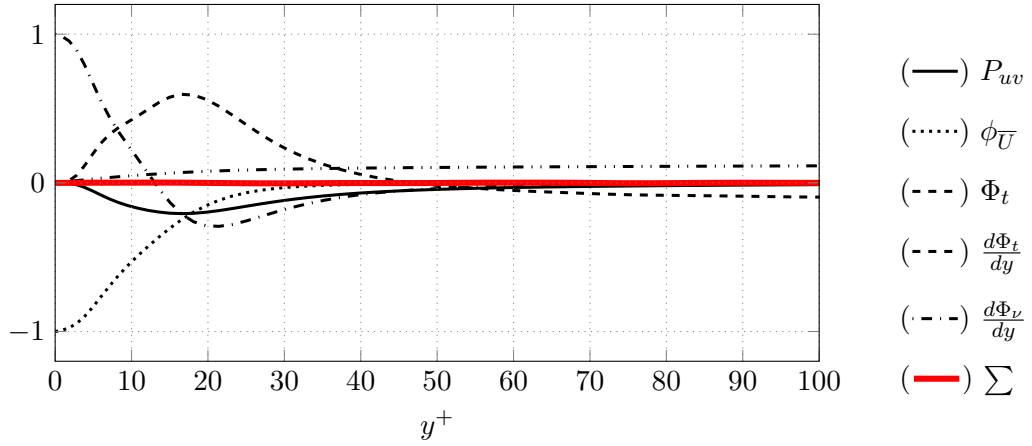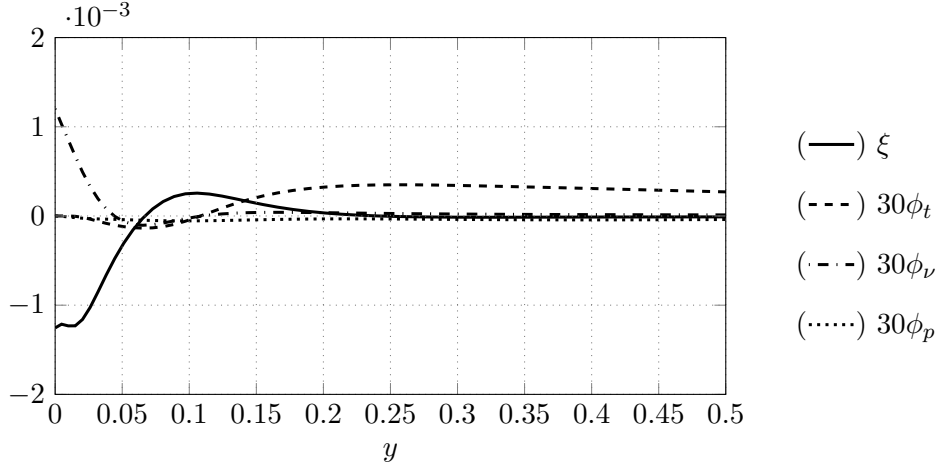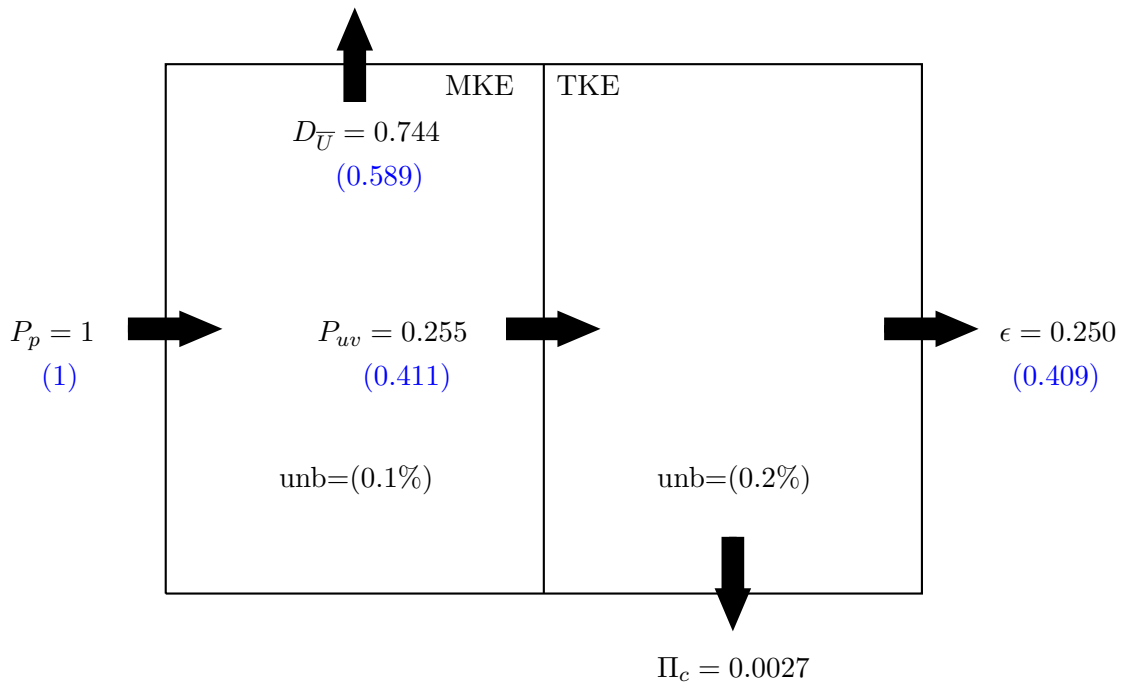

Figure B.13: Terms of the MKE budget equation for the channel flow with streamwise travelling waves of spanwise wall velocity (TW1 of table 3.3 with $Re_\Pi = 6500$, $Re_\tau = 186.48$) with respect to the wall-normal direction. Both the magnitude of the terms and the wall-normal direction are in viscous units. In the plot: (P_{uv}), the mean flow dissipation ($\Phi_{\overline{U}}$), the derivative of the turbulent transport term ($\frac{d\Phi_t}{dy}$), the derivative of the viscous diffusion term($\frac{d\Phi_\nu}{dy}$), pumping term (Π_p) and residual ($\sum$).
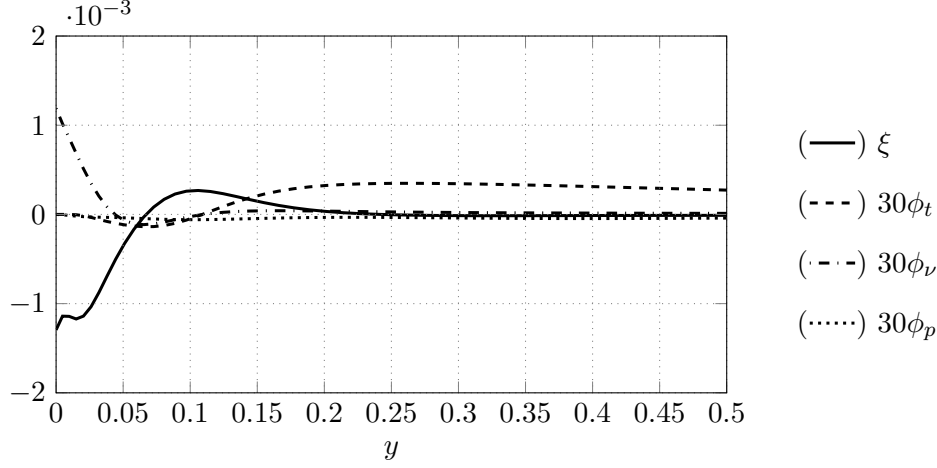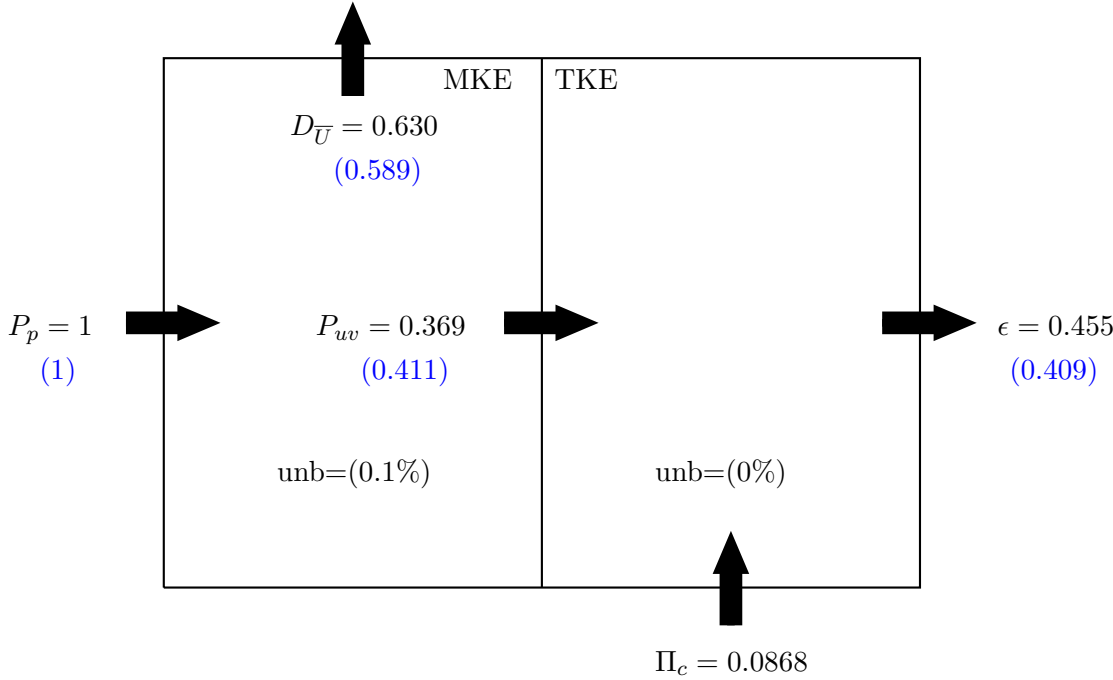
Figure B.14: Source and fluxes of the TKE budget equation for the channel flow with streamwise travelling waves of spanwise wall velocity (TW1 of table 3.3 with $Re_\Pi = 6500$, $Re_\tau = 186.48$) with respect to the wall-normal direction. Both the magnitude of the terms and the wall-normal direction are in power units, therefore in Π units. In the plot: source term (ξ), turbulent transport (ϕ_t), pressure transport (ϕ_p), viscous diffusion (ϕ_ν).

B.1.5 Streamwise travelling waves of spanwise wall velocity (TW2)

Figure B.15: Terms of the TKE budget equation of the channel flow with streamwise travelling waves of spanwise wall velocity (TW2 of table 3.3 with $Re_\Pi = 6500$, $Re_\tau = 187.96$) with respect to the wall-normal direction. Both the magnitude of the terms and the wall-normal direction are in viscous units. In the plot: production term (P_{uv}), pseudo-dissipation (ϵ), derivative of the turbulent transport ($\frac{d\phi_t}{dy}$), of the viscous diffusion ($\frac{d\phi_\nu}{dy}$), of the pressure transport ($\frac{d\phi_p}{dy}$) terms, residual ($\sum$).

Figure B.16: Terms of the MKE budget equation of the channel flow with streamwise travelling waves of spanwise wall velocity (TW2 of table 3.3 with $Re_\Pi = 6500$, $Re_\tau = 187.96$) with respect to the wall-normal direction. Both the magnitude of the terms and the wall-normal direction are in viscous units. In the plot: (P_{uv}), mean flow dissipation ($\Phi_{\overline{U}}$), derivative of the turbulent transport term ($\frac{d\Phi_t}{dy}$), derivative of the viscous diffusion term ($\frac{d\Phi_\nu}{dy}$), pumping term (Π_p) and residual ($\sum$).

Figure B.17: Source and fluxes terms of the TKE budget equation for the channel flow with streamwise travelling waves of spanwise wall velocity (TW2 of table 3.3 with $Re_\Pi = 6500$, $Re_\tau = 187.96$) with respect to the wall-normal direction. Both magnitude of the terms and the wall-normal direction are in power units, therefore in Π units. In the plot: source term (ξ), turbulent transport (ϕ_t), pressure transport (ϕ_p), viscous diffusion (ϕ_ν).

B.2   Energy boxes

Figure B.18: Energy box representation for the channel flow with damping layer of the spanwise wall fluctuations (BF10,$Re_\Pi = 6500$, $Re_\tau = 178.34$). Unbalance is due to terms neglected from the budgets. All values are normalized with respect to pumping power, since all simulation of the database are run with a CPI strategy. In blue values for the reference channel flow.

Figure B.19: Energy box representation for the channel flow with streamwise travelling waves of spanwise wall velocity (TW2,$Re_\Pi = 6500$, $Re_\tau = 187.96$). Unbalance is due to terms neglected from the budgets. All values are normalized with respect to pumping power, since all simulation of the database are run with a CPI strategy. In blue values for the reference channel flow.

Appendix C

GKE: residuals and further results

In this chapter will be presented residuals of the GKE for each case analyzed through the new tool.

C.1 Reference channel flow (REF)
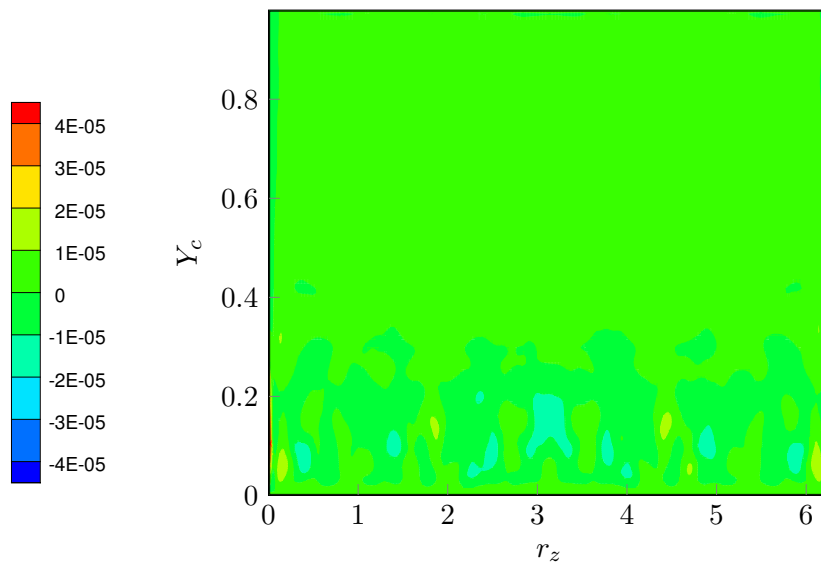
Figure C.1: Residual of the GKE equation applied to the reference channel flow case (REF) in the plane for which $r_y = 0$ and $r_x = 0$. axes are in power units.
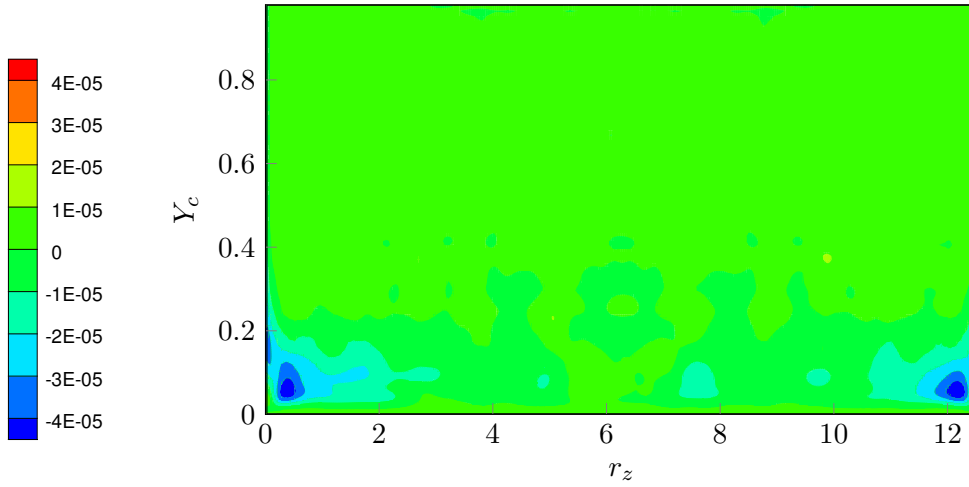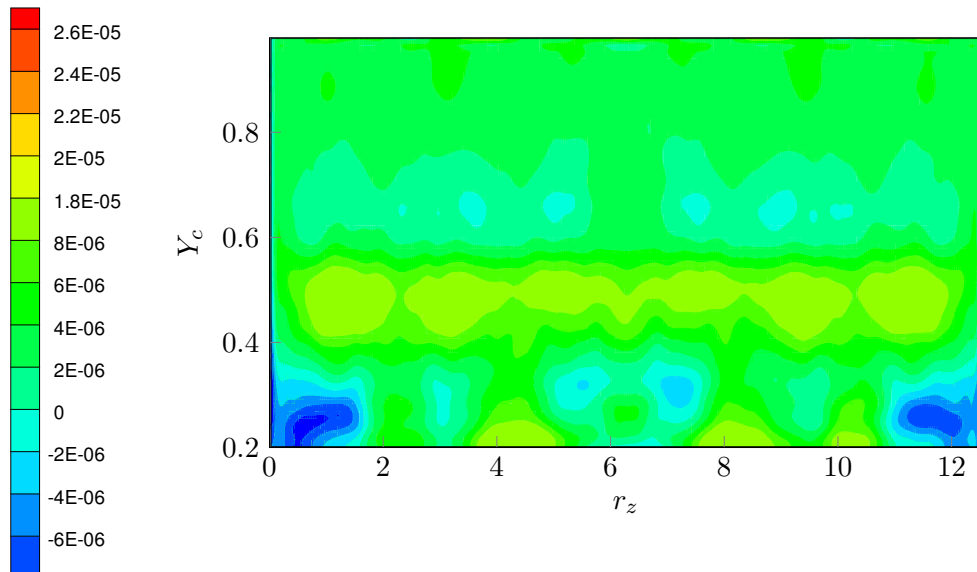
Figure C.2: Residual of the GKE applied to the reference channel flow case (REF) in the plane for which $r_y = 0$ and $r_z = 0$. axes are in power units.

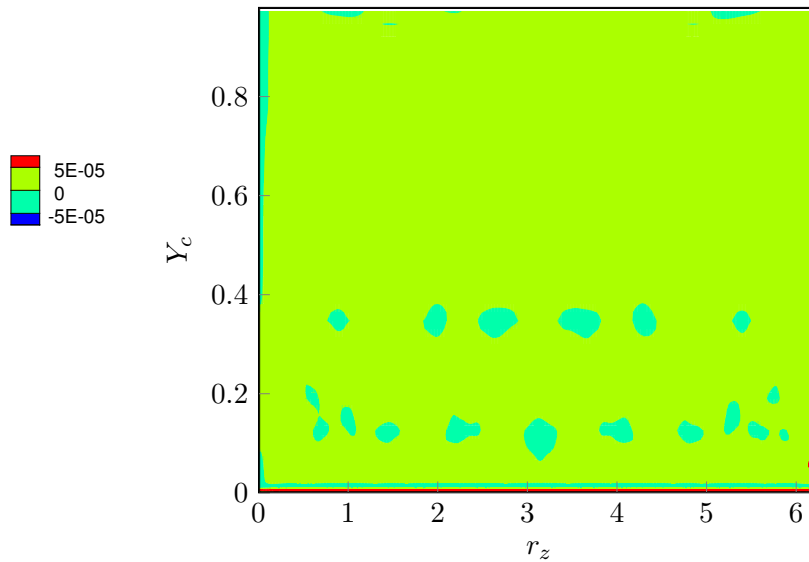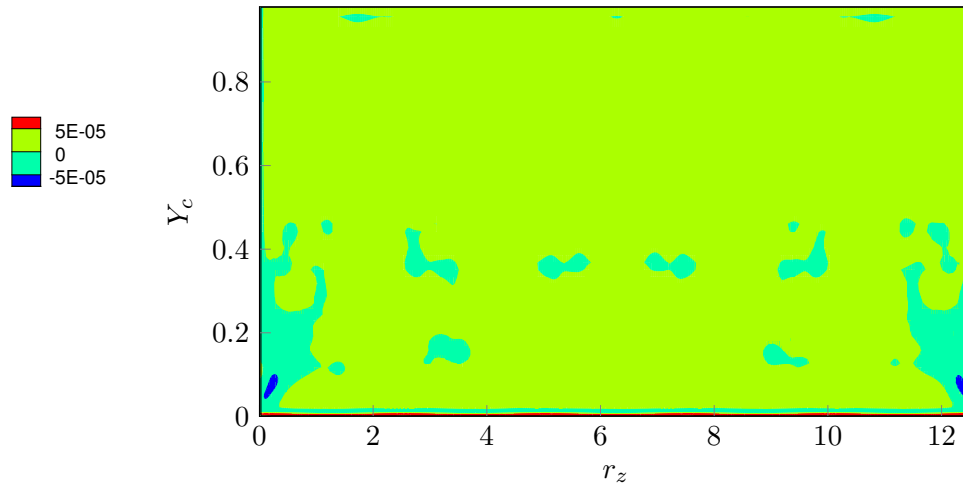## C.2 Damping of the near-wall spanwise fluctuations (BF20)
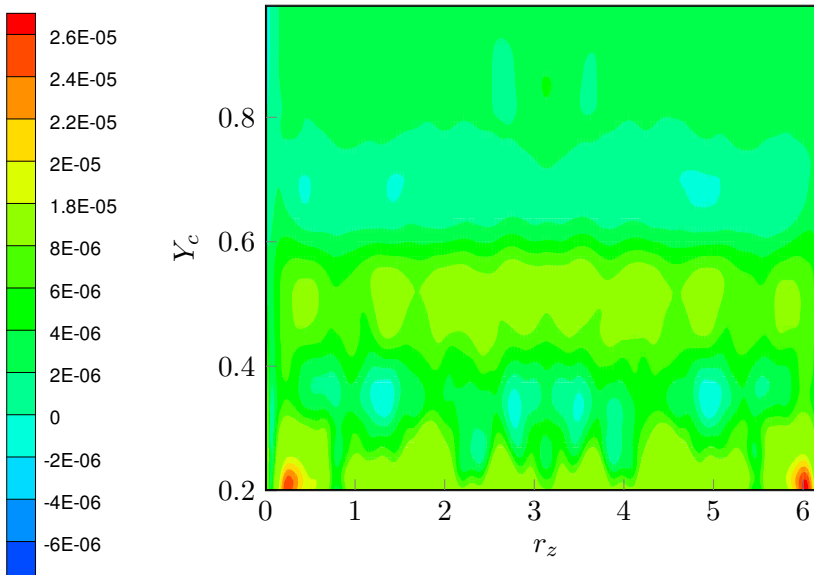
Figure C.3: Residual of the GKE applied to the reference channel flow case with damping of the near-wall spanwise fluctuations (BF20) in the plane for which $r_y = 0$ and $r_x = 0$. axes are in power units.

Figure C.4: Residual of the GKE applied to the reference channel flow case with damping of the near-wall spanwise fluctuations (BF20) in the plane for which $r_y = 0$ and $r_z = 0$. axes are in power units.

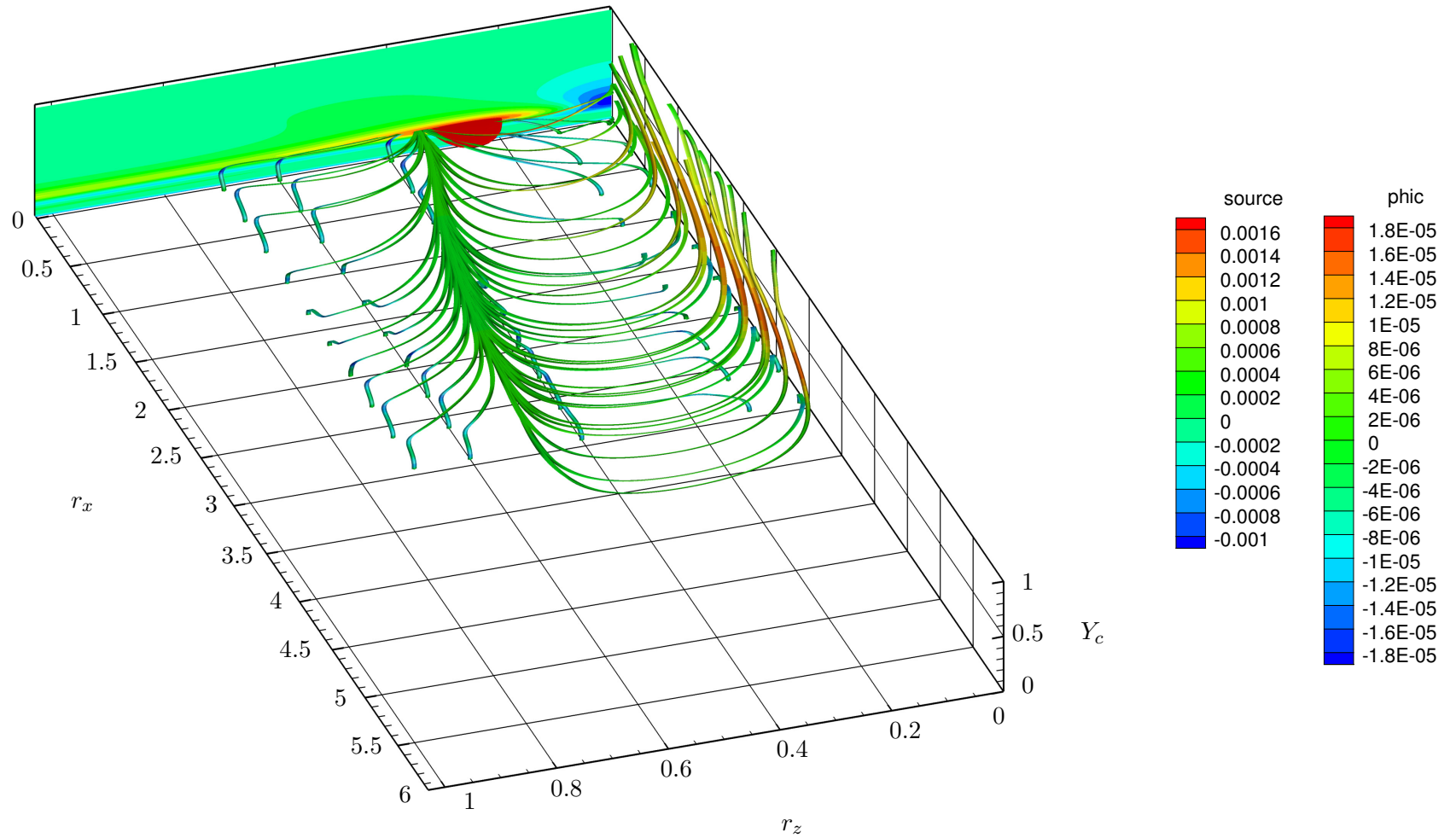## C.3   Streamwise travelling waves of spanwise wall velocity (TW1)

Figure C.5: Residual of the GKE applied to the reference channel flow case with streamwise travelling wave of spanwise wall velocity (TW1) in the plane for which $r_y = 0$ and $r_x = 0$. axes are in power units.

Figure C.6: Residual of the GKE applied to the reference channel flow case with streamwise travelling wave of spanwise wall velocity (TW1) in the plane for which $r_y = 0$ and $r_z = 0$. axes are in power units.

C.4   Further results

Figure C.7: Results for the GKE analysis of the turbulent channel flow with damping layer of the near-wall spanwise fluctuations (BF20) at $Re_\Pi = 6500$, in the space (r_x, r_z, Y_c) and at $r_y = 0$. Volume streamlines represent the reduced flux vector field $(\phi_{r_x}, \phi_{r_z}, \phi_c)$ and the colour code indicates the magnitude of the physical flux ϕ_c. The contours at separation $r_x = 0$ represent the source term of the GKE in the same plane.
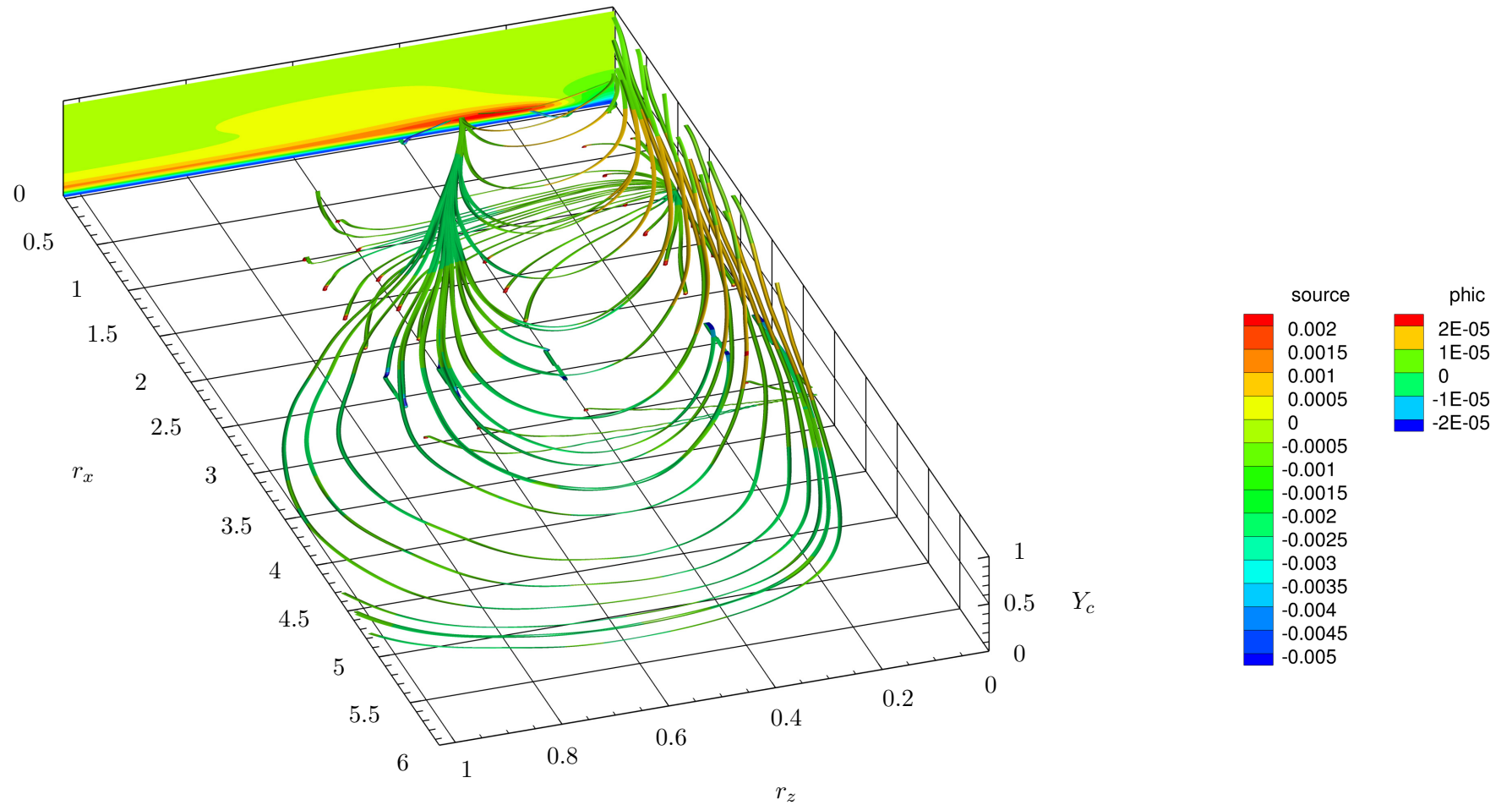
Figure C.8: Results for the GKE analysis of a turbulent channel flow with streamwise travelling waves of spanwise wall velocity (TW1) at $Re_{\Pi} = 6500$, in the space (r_x, r_z, Y_c) and at $r_y = 0$. The volume streamlines represent the reduced flux vector field $(\phi_{r_x}, \phi_{r_z}, \phi_c)$ and the colour code indicates magnitude of the physical flux ϕ_c. Contours at separation $r_x = 0$ represent the source term of the GKE in the same plane.

Ringraziamenti

Bibliography

[1] P. Davidson, Y. Kaneda, K. Moffatt, and K. Sreenivasan, *A Voyage Through Turbulence*. Cambridge University Press, 2011.

[2] U. Frisch and A. N. Kolmogorov, *Turbulence: The Legacy of A. N. Kolmogorov*. Cambridge University Press, 1995.

[3] S. Pope, *Turbulent Flows*. Cambridge University Press, 2000.

[4] M. S. Acarlar and C. R. Smith, "A study of hairpin vortices in a laminar boundary layer. part 2. hairpin vortices generated by fluid injection," *Journal of Fluid Mechanics*, vol. 175, pp. 43–83, 002 1987.

[5] D. Gatti and M. Quadrio, "Reynolds-number dependence of turbulent skin-friction drag reduction induced by spanwise forcing," *Journal of Fluid Mechanics*, vol. 802, pp. 553–582, 2016.

[6] D. Gatti, B. Fronhapfel, A. Cimarelli, M. Quadrio, and H. Y, "Study of energetics in drag-reduced turbulent channels," in *ITI Bertinoro*, 2016.

[7] O. Reynolds, "An experimental investigation of the circumstances which determine whether the motion of water shall be direct or sinuous, and of the law of resistance in parallel channels.," *Proceedings of the royal society of London*, vol. 35, no. 224-226, pp. 84–99, 1883.

[8] M. Quadrio, "Drag reduction in turbulent boundary layers by in-plane wall motion," *Philosophical Transactions of the Royal Society of London A: Mathematical, Physical and Engineering Sciences*, vol. 369, no. 1940, pp. 1428–1442, 2011.

[9] S.-i. Satake and N. Kasagi, "Turbulence control with wall-adjacent thin layer damping spanwise velocity fluctuations," *International Journal of Heat and Fluid Flow*, vol. 17, no. 3, pp. 343 – 352, 1996.

[10] B. Frohnapfel, Y. Hasegawa, and M. Quadrio, "Money versus time: evaluation of flow control in terms of energy consumption and convenience," *Journal of Fluid Mechanics*, vol. 700, pp. 406–418, 006 2012.

[11] N. Marati, C. M. Casciola, and R. Piva, "Energy cascade and spatial fluxes in wall turbulence," *Journal of Fluid Mechanics*, vol. 521, pp. 191–215, 2004.

[12] A. N. Kolmogorov, "The local structure of turbulence in incompressible viscous fluid for very large reynolds numbers," in *Dokl. Akad. Nauk SSSR*, vol. 30, pp. 301–305, JSTOR, 1941.

[13] A. N. Kolmogorov, "A refinement of previous hypotheses concerning the local structure of turbulence in a viscous incompressible fluid at high reynolds number," *Journal of Fluid Mechanics*, vol. 13, no. 01, pp. 82–85, 1962.

[14] S. G. Saddoughi and S. V. Veeravalli, "Local isotropy in turbulent boundary layers at high reynolds number," *Journal of Fluid Mechanics*, vol. 268, pp. 333–372, 1994.

[15] H. Eckelmann, "The structure of the viscous sublayer and the adjacent wall region in a turbulent channel flow," *Journal of Fluid Mechanics*, vol. 65, no. 03, pp. 439–459, 1974.

[16] J. Kim, P. Moin, and R. Moser, "Turbulence statistics in fully developed channel flow at low reynolds number," *Journal of Fluid Mechanics*, vol. 177, pp. 133–166, 04 1987.

[17] N. Mansour, J. Kim, and P. Moin, "Reynolds-stress and dissipation-rate budgets in a turbulent channel flow," *Journal of Fluid Mechanics*, vol. 194, pp. 15–44, 1988.

[18] R. J. Hill, "Exact second-order structure-function relationships," *Journal of Fluid Mechanics*, vol. 468, pp. 317–326, 2002.

[19] A. Cimarelli, E. De Angelis, and C. M. Casciola, "Paths of energy in turbulent channel flows," *Journal of Fluid Mechanics*, vol. 715, pp. 436–451, 2013.

[20] A. Cimarelli, E. De Angelis, J. Jimenez, and C. M. Casciola, "Cascades and wall-normal fluxes in turbulent channel flows," *Journal of Fluid Mechanics*, vol. 796, pp. 417–436, 2016.

[21] M. Quadrio and P. Ricco, "The laminar generalized stokes layer and turbulent drag reduction," *Journal of Fluid Mechanics*, vol. 667, pp. 135–157, 2011.

[22] Y. Hasegawa, M. Quadrio, and B. Frohnapfel, "Numerical simulation of turbulent duct flows with constant power input," *J. Fluid Mech.*, vol. 750, pp. 191–209, 2014.

[23] T. Von Kármán, "Mechanical similitude and turbulence," 1931.

[24] P. Ricco, C. Ottonelli, Y. Hasegawa, and M. Quadrio, "Changes in turbulent dissipation in a channel flow with oscillating walls," *Journal of Fluid Mechanics*, vol. 700, pp. 77–104, 2012.

[25] A. N. Kolmogorov, "Dissipation of energy in locally isotropic turbulence," in *Dokl. Akad. Nauk SSSR*, vol. 32, pp. 16–18, JSTOR, 1941.

[26] T. De Karman and L. Howarth, "On the statistical theory of isotropic turbulence," in *Proceedings of the Royal Society of London A: Mathematical, Physical and Engineering Sciences*, vol. 164, pp. 192–215, The Royal Society, 1938.

[27] R. J. Hill, "Equations relating structure functions of all orders," *Journal of Fluid Mechanics*, vol. 434, pp. 379–388, 2001.

[28] S. Robinson, "Coherent Motions In The Turbulent Boundary Layer," *Annual Review of Fluid Mechanics*, vol. 23, no. 1, pp. 601–639, 1991.

[29] W. Schoppa and F. Hussain, "Coherent structure generation in near-wall turbulence," *J. Fluid Mech.*, vol. 453, pp. 57–108, 2002.

[30] P. Luchini and M. Quadrio, "A low-cost parallel implementation of direct numerical simulation of wall turbulence," *J. Comput. Phys.*, vol. 211, pp. 551–571, Jan. 2006.

[31] Y. Suzuki and N. Kasagi, "Turbulent drag reduction mechanism above a riblet surface," *AIAA journal*, vol. 32, no. 9, pp. 1781–1790, 1994.

[32] B. Frohnapfel, Y. Hasegawa, and N. Kasagi, "Friction drag reduction through damping of the near-wall spanwise velocity fluctuation," *International Journal of Heat and Fluid Flow*, vol. 31, no. 3, pp. 434 – 441, 2010. Sixth International Symposium on Turbulence and Shear Flow Phenomena.

[33] M. Quadrio, P. Ricco, and C. Viotti, "Streamwise-travelling waves of spanwise wall velocity for turbulent drag reduction," *Journal of Fluid Mechanics*, vol. 627, pp. 161–178, 2009.

[34] W. Jung, N. Mangiavacchi, and R. Akhavan, "Suppression of turbulence in wall-bounded flows by high-frequency spanwise oscillations," *Physics of Fluids A: Fluid Dynamics*, vol. 4, no. 8, pp. 1605–1607, 1992.

[35] P. Ricco and M. Quadrio, "Wall-oscillation conditions for drag reduction in turbulent channel flow," *International Journal of Heat and Fluid Flow*, vol. 29, no. 4, pp. 891–902, 2008.

[36] A. Pozzi, *Applications of Padé Approximation Theory in Fluid Dynamics*. Series on advances in mathematics for applied sciences, World Scientific, 1994.

[37] A. Cimarelli, E. De Angelis, A. Talamelli, C. M. Casciola, and J. Jiménez, "The attached reverse and detached forward cascades in wall-turbulent flows," in *Journal of Physics: Conference Series*, vol. 506, p. 012005, IOP Publishing, 2014.

[38] A. Cimarelli and E. De Angelis, "The physics of energy transfer toward improved subgrid-scale models," *Physics of Fluids*, vol. 26, no. 5, p. 055103, 2014.

[39] W. Willmarth and S. Lu, "Structure of the reynolds stress near the wall," *Journal of Fluid Mechanics*, vol. 55, no. 01, pp. 65–92, 1972.

[40] J. M. Wallace, H. Eckelmann, and R. S. Brodkey, "The wall region in turbulent shear flow," *Journal of Fluid Mechanics*, vol. 54, no. 01, pp. 39–48, 1972.

[41] C. Smith and S. Metzler, "The characteristics of low-speed streaks in the near-wall region of a turbulent boundary layer," *Journal of Fluid Mechanics*, vol. 129, pp. 27–54, 1983.